THEORY OF DETONATION STRUCTURE FOR TWO-PHASE MATERIALS

BY

JOSEPH MICHAEL POWERS

B.S., University of Illinois, 1983
M. S., University of Illinois, 1985

THESIS

Submitted in partial fulfillment of the requirements
for the degree of Doctor of Philosophy in Mechanical Engineering
in the Graduate College of the
University of Illinois at Urbana-Champaign, 1988

Urbana, Illinois

UNIVERSITY OF ILLINOIS AT URBANA-CHAMPAIGN

THE GRADUATE COLLEGE

MAY 1988

WE HEREBY RECOMMEND THAT THE THESIS BY

JOSEPH MICHAEL POWERS

ENTITLED THEORY OF DETONATION STRUCTURE FOR TWO-PHASE MATERIALS

BE ACCEPTED IN PARTIAL FULFILLMENT OF THE REQUIREMENTS FOR

THE DEGREE OF DOCTOR OF PHILOSOPHY

D. Scott Stewart, Hans Kuhn
Director of Thesis Research

A. M. Clausing
Head of Department

Committee on Final Examination†

Hans Kuhn
Chairperson

D. S. Stewart

Roger A. Strehlow

J. Craig Dutton

† Required for doctor's degree but not for master's.

O-517

ABSTRACT

The structure of a two-phase steady detonation in a granulated solid propellant has been studied, and existence conditions for a one-dimensional, steady two-phase detonation have been predicted. Ordinary differential equations from continuum mixture theory have been solved numerically to determine steady wave structure. In the limiting case where there is no chemical reaction and no gas phase effects, the model describes inert compaction waves. The equations predict detonation structure when reaction and gas phase effects are included. In the limiting case where heat transfer and compaction effects are negligible, the model reduces to two ordinary differential equations which have a clear geometrical interpretation in a two-dimensional phase plane. The two-equation model predicts results which are quite similar to those of the full model which suggests that heat transfer and compaction are not important mechanisms in determining the detonation structure. It is found that strong and Chapman-Jouguet (CJ) detonation solutions with a leading gas phase shock and unshocked solid are admitted as are weak and CJ solutions with an unshocked gas and solid. The initial conditions determine which of these solutions is obtained. As for one-phase materials, the CJ wave speed is the speed of propagation predicted for an unsupported, one-dimensional, two-phase detonation. The model predicts that there is no physically admissible CJ structure below a critical value of initial bulk density. This result is not predicted from equilibrium end state analysis, and based on this result, it is concluded that it is essential to consider reaction zone structure.

ACKNOWLEDGMENTS

I would like to acknowledge the contributions of several people who assisted in various stages of preparation of this study. First, I would like to thank my co-advisors, Professor Herman Krier and Professor Scott Stewart, who each in their own way directed this study so as to be both theoretically sound and of value to the two-phase detonation community. The advise of both Professors Stewart and Krier in all aspects of the study has been instrumental in completing this thesis.

The assistance of several others is also appreciated. First, I would like to thank the remaining members of the examining committee, Professors Craig Dutton and Roger Strehlow, for their helpful suggestions. Professor Barry Butler, University of Iowa, by showing me the fundamentals of two-phase models and their numerical solution, gave my work a helpful start. I also thank Dr. Jim Jones, Los Alamos National Laboratory, who gave a suggestion concerning ODE solution techniques which proved to be of great value to this study. Suzanne Palmer assisted with some of the figures. Finally, I thank my parents, Leo and Mary Powers, for their support and encouragement.

This work was funded by the Air Force Office of Scientific Research and Los Alamos National Laboratory.

TABLE OF CONTENTS

LIST OF SYMBOLS

D	Steady Wave Speed
t	Time
x	Distance in Laboratory Frame
1	Subscript Denoting Gas Phase
2	Subscript Denoting Solid Phase
ρ	Density
ϕ	Volume Fraction
u	Velocity in Laboratory Frame
r	Solid Particle Radius
a	1) Burning Rate Coefficient, 2) Subscript Denoting Bulk Property
P	Pressure
m	Burning Rate Exponent
β	Drag Coefficient
e	Internal Energy
h	1) Heat Transfer Coefficient, 2) Function Specifying Volume Fraction Change, 3) Function Specifying Initial Porosity Distribution
T	Temperature
0	Subscript Denoting Initial Property
R	Gas Constant
b	Gas Phase Virial Coefficient
c_v	Specific Heat at Constant Volume
c	Sound Speed
γ_2	Tait Equation Parameter
s	1) Non-Ideal Solid Parameter, 2) Subscript Denoting Shocked State 3) Entropy
q	Chemical Energy
μ_c	Compaction Viscosity
π	Dimensionless Parameter
f	1) Static Pore Collapse Function, 2) Function Specifying Density Change
ξ	Distance in Steady Wave Frame
v	1) Velocity in Steady Wave Frame, 2) Specific Volume
$*$	Subscript Denoting Dimensionless Parameter
σ	Dimensionless Non-Ideal Solid Parameter
u_p	Piston Velocity

CJ	Subscript Denoting Chapman-Jouguet Condition
L	Reaction Zone Length
g	1) Function Specifying Sonic and Complete Reaction Singularities,
	2) Gravitational Acceleration
M	Mach Number
λ	Eigenvalue
δ	Switching Variable (= 0 or 1)
κ	Switching Variable (= 0 or 1)
c_s^+	Mass Transfer Function
α	Drag Coefficient
n	Number Density

I. INTRODUCTION

Predicting the behavior of combustion waves in mixtures of gas and reactive solid particles is an important and partially unsolved problem. Practical applications include the burning of damaged, granulated solid rocket propellants, detonation of granular explosives, burning of coal dust, and explosion of dust-air mixtures. Understanding these combustion processes could lead to more accurate design criteria for rockets, new tailored explosives, and improved safety criteria for environments where dust explosions are a hazard.

One way to gain understanding is to model these processes. A class of models which has the potential to describe these processes has been developed from two-phase continuum mixture theory. These models describe each phase as a continuum; distinct equations for the mass, momentum, and energy, and constitutive equations for both phases are written. The two phases are coupled through terms representing the transfer of mass, momentum, and energy from one phase to another. Models of these phase interaction processes are determined from experiments. In the models the phase interaction terms are constructed such that global conservation of mass, momentum, and energy is maintained. Regardless of the particular form of the two-phase equations, the idea of global conservation is a criterion which must be enforced.

Unsteady two-phase models have been widely used to study the problem of deflagration-to-detonation transition (DDT) in granulated solid propellants [1-21], which has been observed experimentally [22-24]. Similar unsteady models are used to study transient combustion in porous media [25-30]. By concentrating on unsteady solutions, many simple results available from the less-complicated two-phase steady theory have been overlooked. These results are found by solving the ordinary differential equations which define the steady two-phase detonation equilibrium end states and reaction zone structure. None of the previous steady two-phase studies [31-39] has adequately described the admissible end states and structure of a two-phase detonation. Only when steady detonation solutions are understood will it be possible to fully comprehend the implications of unsteady two-phase detonation theory.

A sketch of an envisioned two-phase steady detonation structure is shown in Figure 1.1. In this study the term "structure" refers to the spatial details of the detonation wave. Such details include the reaction zone length and the variation of pressure, temperature, etc. within the reaction zone.

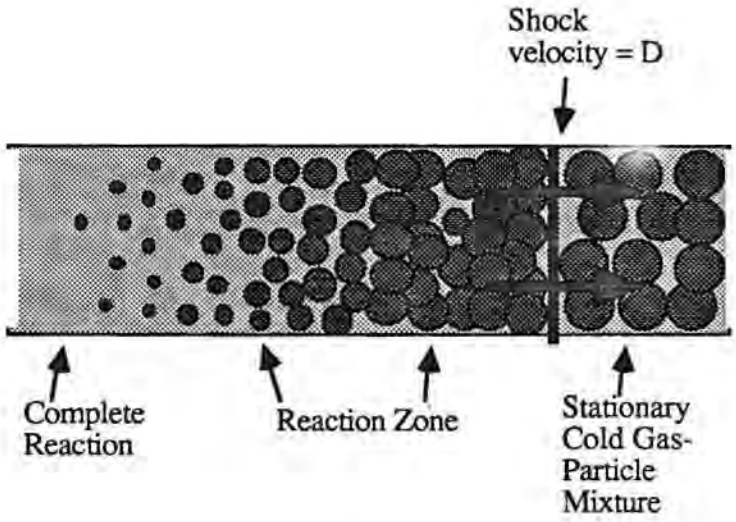

Figure 1.1 Hypothesized Two-Phase Steady Detonation

Drawing on the results of one-phase detonation theory, it is hypothesized that a two-phase detonation consists of a chemical reaction induced by a shock wave propagating into a mixture of reactive particles and inert gas. At the end of the reaction zone the particles are completely consumed; only inert gas remains. Important questions concerning such a detonation exist, for example,

1) *What is the speed of propagation of an unsupported two-phase detonation?*

2) *What are the potential two-phase detonation end states?*

3) *What is the structure of the two-phase reaction zone?*

4) *What is the nature of a shock wave in a two-phase material?*

5) *How is two-phase detonation theory related to and different from one-phase detonation theory?*

It is the goal of this work to use steady state analysis to answer these and other questions.

The steady equations are best studied using standard phase space techniques. In this work such techniques are used to study a general two-phase detonation model. In so doing, two-phase steady detonations have been studied in the same context as the extensive one-phase steady theory [40].

An outline of the two-phase detonation analysis of this work is now given. The unsteady model is first presented. Then the steady dimensionless form of this model is

shown, and a description is given of how the problem of determining two-phase detonation structure can be reduced to solving four coupled ordinary differential equations. In certain limits, two of these equations may be integrated, and the detonation structure problem is reduced to solving two ordinary differential equations in two unknowns. In these limits the detonation structure has a clear geometrical interpretation in the two-dimensional phase plane. Both two and four equation models are then used to predict examples of acceptable reaction zone structure and unacceptable, non-physical solutions. Parametric conditions are obtained for the existence of a steady, one-dimensional, two-phase detonation.

Two methods are used to restrict the available solutions: algebraic end state analysis and reaction zone structure analysis. Algebraic analysis of the equilibrium end states, described in detail in Ref. 41, identifies a minimum wave speed necessary for a steady solution. This wave speed is analogous to the well-known one-phase Chapman-Jouguet (CJ) wave speed. As in one-phase theory, the two-phase CJ wave speed is identified as the unique wave speed of an unsupported two-phase detonation. The available solutions are further restricted by considering the structure of the two-phase detonation wave. In particular, results from the structural analysis show that below a critical initial solid volume fraction, no steady two-phase detonation exists.

The behavior of integral curves near singular points identified by this analysis is crucial in understanding why structural analysis limits the class of available detonation solutions. Analysis of two-phase equations near singularities has not been emphasized in two-phase detonation theory or two-phase theory in general. This is argued by Bilicki, et al. [42] who write in a recent article concerning steady two-phase flow,

> *...the theory of singular points of systems of coupled, ordinary nonlinear differential equations--still largely unexploited in this field--is essential for clarity, for the proper management of computer codes and for the understanding of the phenomenon of choking* ***as predicted by the adopted mathematical model,*** *an impossible task when only numerical procedures are used.*
>
> *The kingpin of the analysis is the identification of the singular points of the basic system of equations and of the solution patterns that they imply. Such an analysis serves two purposes. First, it gives the analyst the ability to understand the physical characteristics of a class of flows without the need to produce complete solutions. Secondly, it gives valuable indications as to how to supplement computer codes because practically all numerical methods of solution become inadequate in the neighborhood of the singular points and are constitutionally incapable of locating them in the first place, which leads to numerical difficulties and incorrect interpretations. This has to do with the fact that the set of algebraic equations, which the computer code must solve at each step, becomes either impossible or indeterminate...and no longer solves the coupled differential equations of the model.*

The analysis presented here identifies two types of singular points, explained in detail below, which exist in most two-phase particle burning models based on continuum mixture theory. Near a singularity there is a zero in the denominator of the forcing functions of the governing differential equations. The consequences of these singularities are not straightforward and must be analyzed in detail.

One type of singularity occurs at the point of complete reaction. The complete reaction singularity arises in most particle-burning two-phase detonation models because the interphase transport terms used in the mass, momentum, and energy equations typically have a 1/r dependence where r is particle radius. When the particle radius approaches zero, a singularity exists. It is an open question as to whether this singularity gives rise to infinite gradients, infinite property values, or whether there is a balancing zero in the numerator to counteract the singularity. No work in the current two-phase detonation literature adequately addresses this issue. The results presented in this work account for the complete reaction singularity.

Another type of singularity occurs when the velocity of either phase relative to the wave front is locally sonic. In this work the term "sonic" is taken to mean that the velocity of an individual phase relative to the steady wave is equal to the local sound speed of that particular phase as predicted by the state equation for that particular phase. The term "sonic" in this work does not in any way refer to a mixture sound speed, nor is the idea of a mixture sound speed incorporated into any of the arguments developed in this work.

The sonic singularity arises naturally from the differential equations and has been extensively studied for one-phase systems. Here for the first time the importance of sonic conditions in two-phase detonation theory is shown: in general if a solid sonic condition is reached within the detonation structure, a physically acceptable steady two-phase detonation cannot exist. If a solid sonic condition is reached, it is predicted that all physical variables are double-valued functions of position; for instance at any point in the wave structure two distinct gas densities, solid temperatures, etc. are predicted. This condition is obviously not physical. Furthermore, when such a condition is reached the solution does not reach an equilibrium point; thus, no steady solution is predicted. This alone is a sufficient reason to reject solutions contain a solid sonic condition. In addition to the solid phase sonic singularity, imaginary gas phase properties are predicted if the solution includes a gas phase sonic point at a point of incomplete reaction.

The influence of the two-phase shock state on steady detonation structure is shown in this work. The shock wave, assumed to be inert, leaves the material in a state of higher pressure, temperature, and density than the ambient state. This serves to initiate chemical reaction which in turn releases energy to drive the shock wave. In this work mechanisms

which define the structure of a shock wave such as diffusive heat conduction and momentum transport are ignored. It is assumed that the length scales on which these processes are important are small in comparison with the reaction zone length scales. By ignoring the diffusive processes, the model equations become hyperbolic, and discontinuous shocks are admitted by the governing equations.

The shock state can be determined by an algebraic analysis. Any state admitted by the shock discontinuity equations can serve as an initial condition for the ordinary differential equations which define the reaction zone structure. It is shown that four classes of initial conditions are admitted for a given wave speed: 1) gas and solid at ambient conditions, 2) a shocked gas and shocked solid, 3) an unshocked gas and shocked solid, and 4) a shocked gas and unshocked solid. Any of these initial states has the potential to initiate a steady two-phase detonation. Examples are found of the first and fourth classes of two-phase detonation in this thesis. Previous work in two-phase detonation has not adequately shown whether the gas and solid are shocked or unshocked.

In addition to two-phase detonation structure, this study contains a discussion of inert compaction waves in granular materials. This discussion, including a review of compaction wave theory and experiments, is contained in Chapter 4 and is not germane to the subject of steady two-phase detonations. The results are predicted by the same equations used to predict two-phase detonations in the limit of no chemical reaction and a negligible gas phase. In Chapter 4 analysis is presented to describe the wave motion which results when a constant velocity piston strikes a granular material.

A sketch of an envisioned compaction wave is shown in Figure 1.2.

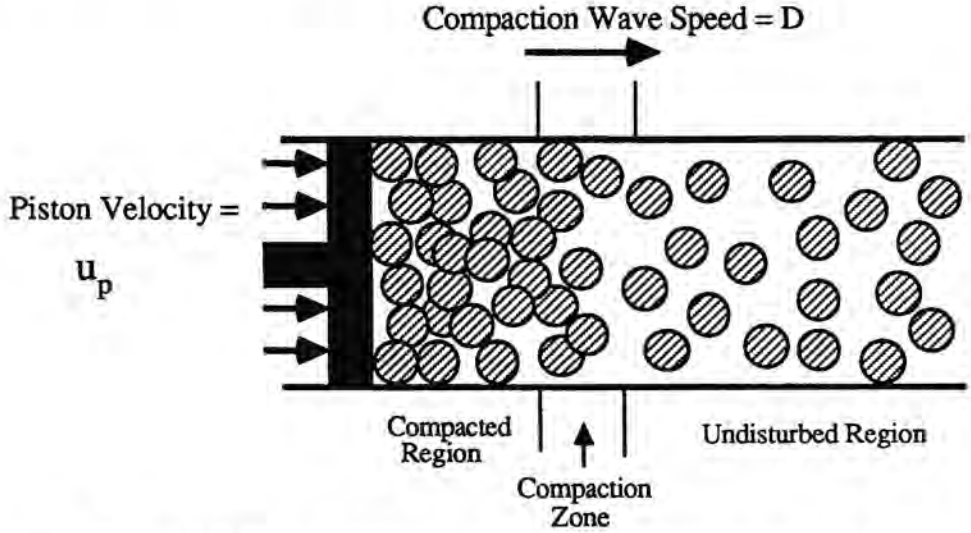

Figure 1.2 Sketch of Compaction Wave in Granular Material

A compaction wave is thought to be an important event in the process in the transition from deflagration to detonation (DDT). It is thought that a compaction process in which the granular material rearranges can give rise to local hot spots which could induce a detonation in the reactive material.

Much as for two-phase steady detonation analysis, the compaction wave analysis identifies equilibrium end states and compaction zone structure. It is shown that the problem of determining compaction zone structure can be reduced to solving one ordinary differential equation for one unknown, solid volume fraction. The results show a continuous dependence of compaction wave structure with supporting piston velocity; depending on the piston velocity, two broad classes of compaction zone structure exist. At low piston velocities the compaction wave travels at speeds less than the ambient solid sound speed. Such waves are called subsonic compaction waves. The structure is characterized by a smooth rise in pressure from the ambient to a higher pressure equal to the static pore collapse stress level. Subsonic compaction waves have been observed in experiment [43, 44] and predicted by Baer [45] and Powers, Stewart, and Krier [46]. Above a critical piston velocity the compaction wave travels at speeds greater than the ambient solid sound speed. A discontinuous shock wave leads a relaxation zone where the pressure adjusts to its equilibrium static pore collapse value. Such waves are called supersonic compaction waves. Supersonic compaction waves with leading shocks have not yet been observed nor predicted in previous studies.

The plan of this thesis is to first review the relevant literature in Chapter 2. The unsteady model is presented in Chapter 3. Steady inert compaction waves predicted by this model are discussed in Chapter 4 which is followed by a discussion of two-phase detonation equilibrium end states and structure in Chapter 5. Conclusions and recommendations are given in Chapter 6. Appendix A discusses the method of characteristics, and lists the characteristic directions and equations for one-dimensional, unsteady, two-phase reactive flow. Appendix B has a detailed discussion of state relations and demonstrates that the thermal and caloric state equations used in this study are compatible. Appendix C compares the momentum and energy equations of this study to other common forms of these equations and defends the choices made for this study. Two-phase CJ deflagration conditions are considered in Appendix D. Appendix E contains a detailed description of how to reduce the model to the simple two-equation model presented in Chapter 5. Appendix F gives a derivation of the number conservation equation. This equation holds that in the two-phase flow field, the number density of particles does not change.

II. REVIEW OF TWO-PHASE DETONATION THEORY

This chapter will briefly describe the literature which is relevant to the field of two-phase steady detonation theory. This includes works on the fundamentals of two-phase continuum mixture theory, basic one-phase detonation theory, and applications of these theories to combustion in porous media. As this thesis is primarily concerned with the details of modeling two-phase detonations using existing models and not with the experiments which provide the basis for these models, the experimental literature regarding two-phase detonations will not be reviewed. The interested reader is referred to Butler's thesis [47] for a thorough description. A review of compaction wave theory is found in Chapter 4.

The theory of two-phase flow is still under development, and there are many issues which remain unresolved. Drew [48] considers some of these issues in a recent review article. However, one need only look at the wide disparity in the forms of two-phase model equations expressed by various researchers to realize that the particular form of the equations is a matter of dispute. Thus in constructing a model, one looks for the most basic principles to use as a guide. In his description of two-phase theory from a continuum mechanics perspective, Truesdell [49] describes three metaphysical principles which can be used as a guide. They are:

1. *All properties of the mixture must be mathematical consequences of properties of the constituents.*

2. *So as to describe the motion of a constituent, we may in imagination isolate it from the rest of the mixture, provided we allow properly for the actions of the other constituents upon it.*

3. *The motion of the mixture is governed by the same equations as is a single body.*

Two-phase theory as applied to combustion in granular materials has been developed primarily through the work of Krier and co-workers [1, 7, 16, 17, 18, 20, 21], Kuo, Summerfield, and co-workers [29, 30, 37, 38], and more recently by Nunziato, Baer, and co-workers [2, 3, 4, 11, 13]. In addition, Nigmatulin's book [50], available in Russian and not reviewed by this author, is widely referred to in the Russian literature as a source for the governing equations of two-phase reactive flow. As opposed to the work of Kuo, et al., who consider only deflagrations, the work of Krier, et al., and Nunziato, et al., has been applied to the detonation of granular propellants and explosives. The extreme

conditions of a detonation (gas pressures are of the order of 10 GPa) force the adoption of a fully compressible solid phase state equation and a non-ideal gas phase state equation. These models use constitutive theory specially developed to describe the pore collapse which can be associated with detonations in these materials. There are only minor differences in the Krier and Nunziato model formulations; these are considered in detail in Chapter 3 and Appendix C.

To understand two-phase detonation theory, it is necessary to be familiar with some of the results of one-phase detonation theory. The best summary of these results is given in Fickett and Davis's book [40]. The one-phase concept most relevant to two-phase theory is that of a steady Zeldovich, von Neumann, Doering (ZND) detonation which terminates at a CJ point. The ZND theory is named for its developers who independently described the theory in the 1940's. The CJ analysis describes the equilibrium end states for a one-phase detonation, and the ZND analysis describes the structure of the detonation reaction zone.

Much of one-phase detonation theroy can be understood by considering the equilibrium end states. The CJ point is an equilibrium end state at which the gas velocity is sonic with respect to the wave front. Since this point is sonic, the theory predicts that any trailing rarefaction wave is unable to catch and disturb the steady wave. There is only one detonation wave speed which leaves the material in a CJ state. The equilibrium end state analysis of one-dimensional theory hypothesizes that this wave speed is the unique speed of propagation for an unsupported detonation wave. There are no equilibrium end states for wave speeds less than the CJ wave speed. For wave speeds greater than the CJ wave speed, two equilibrium states are predicted. They are classified on the basis of the equilbrium end state pressure: the solution which terminates at the higher pressure is called a strong solution, the other solution is called the weak solution. The strong end state is a subsonic state, and thus the strong detonation is susceptable to degradation from trailing rarefactions. To achieve a strong detonation, the theory predicts a supporting piston is necessary so that no rarefactions will exist. The weak end state is a supersonic state and thus does not require any piston support and is not ruled out by simple equilibrium end state analysis.

ZND theory considers the structure of a detonation wave which links the initial state to the equilibrium end state. A ZND detonation is described by an inert shock wave propagating into a reactive material. The shock wave leaves the material in a locally subsonic, high temperature state. The high temperature initiates an exothermic chemical reaction. Energy released by this chemical reaction is predicted to drive the detonation wave. For wave speeds greater than the CJ speed, the solution terminates at the strong point, a subsonic state which requires piston support to remain steady. For a CJ wave

speed the solution terminates at a sonic point and thus is able to propagate without piston support. The simple ZND theroy predicts that there is no path from the initial shock state to the weak solution point and thus rules out a weak detonation with a leading shock in the structure. Thus simple ZND theory predicts that the wave speed for an unsupported detonation is the CJ wave speed. There is, however, evidence, described in detail by Fickett and Davis, that weak solutions can be achieved. In general the weak detonations described by Fickett and Davis require special conditions to exist.

Fickett and Davis describe how ZND theory can be placed in the context of the general theory of systems of ordinary differential equations. Details of this theory can be found in standard texts [51, 52]. The theory describes how, given a set of ordinary differential equations, solutions link an initial state to an equilbrium end state and how other solutions do not have equilibrium states. Equilibrium states are defined at points where the forcing functions for each differential equation are simultaneously zero. Whether or not an equilibrium state is reached depends on the particular form of the differential equations. A solution which does not reach an equilibrium point is rejected as a steady solution by definition.

A shortcoming of most two-phase detonation studies is that little emphasis has been put on placing two-phase detonation theory in the context of one-phase detonation theory and the more general ordinary differential equation theory. Most work in two-phase detonation theory has concentrated solely on using numerical solution of the unsteady equations to predict the two-phase equivalent of a CJ detonation [1, 2]. A primary goal of these works has been to predict the deflagration-to-detonation transition (DDT) zone length rather than the character of the detonation itself. As such, there has been little discussion of the basic characteristics of a steady two-phase detonation. In these studies the definition of the two-phase CJ state is unclear. Reference is often made to the one-phase CJ results with the assumption that the one-phase CJ condition naturally must also apply to the two-phase detonation model. Also in these works no attempt has been made to describe conditions under which a two-phase strong or weak detonation can exist. Since these states can be predicted by one-phase theory, it is reasonable to suggest that two-phase equivalents may also exist. Detailed descriptions of the steady two-phase reaction zone structure have been generally ignored.

Studies of steady two-phase systems will now be considered. Several works exist which consider the relatively low-speed, low-pressure deflagration of solid particles. Among these are the works of Kuo, et al. [37, 38], Ermolaev, et al. [35, 36], and Drew [31]. These works consider the particle phase to be incompressible and naturally have no discussion of shock waves. The work of Krier and Mozafarrian [34] considered a reactive

wave with a leading shock wave in the gas phase. Detonation structure was determined by numerically solving the steady two-phase ordinary differential equations. This work is of limited value because of the assumption of an incompressible solid phase. This assumption is unrealistic in the detonation regime. In addition they did not establish whether the model equations of their work are hyperbolic, leading one to question whether their model equations are well-posed for their initial value problem.

The most important studies of steady two-phase detonation are those of Sharon and Bankoff [33] and Condiff [32]. These works apply two-phase detonation theory to vapor explosions which can arise from the rapid mixing of a hot liquid and cold vaporizable liquid. Large differences in the features of the problem of vapor explosion and that of detonation of solid granular explosive prevent an extension of results of vapor explosion to detonations in granular explosives from being made. Among the differences are that in a vapor explosion both components come to an equilibrium where both components exist in finite quantities, while in a detonation of a solid propellant the solid is entirely consumed. There are also large differences in the functional form of the constitutive equations. Nevertheless, both these works discuss in detail many features of two-phase detonation theory which are held in common between vapor explosions and detonations in granular explosives. More importantly, these works outline a rational approach to the problem of two-phase detonation.

Both Sharon and Bankoff and Condiff describe a two-phase detonation in the context of one-phase steady detonation theory. That is they describe the detonation structure as a shock jump followed by a relaxation zone whose structure is determined by solving a set of ordinary differential equations. Both works describe the effective two-phase CJ state. Sharon and Bankoff argue that the CJ vapor explosion is the only steady solution which can exist. They also provide details of the detonation structure. Condiff argues that there is a larger range of solutions to choose from and that a phase plane analysis is necessary to choose which solutions can be accepted.

An issue which has long been troublesome for two-phase theory is that of whether the equations are well-posed. In two-phase detonation theory, only two models have been proposed which have been shown to be well-posed for initial value problems: the model of Baer and Nunziato [2] and Powers, Stewart, and Krier [41] . The feature of these models which guarantees that they are well-posed is an explicit time-dependent equation which models the change in volume fraction in a granular material. When models without such an equation are examined, it is found that there are regimes in which imaginary characteristics are present [8, 28, 48, 53]. Such models are not in general well-posed for initial value

problems; because of this any solution to an initial value problem for such a model can be shown to be unstable to disturbances of any frequency.

It should be said that for gas phase systems that the ZND assumption of one-dimensionality has been shown by experiments to be invalid in general. However the ZND predictions are able to roughly predict spatially averaged gas phase properties such as final pressure and wave speed. For solids, experimental results provide little evidence regarding the existence of multidimensional detonation structure. Regardless of whether or not detonations in solids are one or multidimensional, it is reasonable to consider the results of one-dimensional theory before proceeding to consider more complicated multidimensional theories.

Finally an issue relevant to models of particle burning must be considered, that of how an expression for the evolution of particle radius should be formulated. In two-phase models of granular materials the particle radius is a required variable for all interphase transfer terms (reaction, drag, and heat transfer are known empirically as functions of particle radius). In much of the two-phase granular explosive literature there is confusion as to how to determine the particle radius. The recent work of Baer and Nunziato [2] disregards the issue by not giving an expression for particle radius evolution. It would seem that this model is incomplete. The work of Krier and co-workers provides a relation for the particle radius evolution whose physical interpretation is unclear (see Appendix F). A rational way for determining particle radius is found by considering an evolution equation for the number density of particles. Several modelers do write explicit equations for number density evolution [10, 14, 26, 31, 39]. Generally these studies assume that the number density of particles is conserved. It can be shown that with such an equation it is possible to determine a clearly understood equation for the evolution of particle radius (see Appendix F).

III. THE UNSTEADY TWO-PHASE MODEL

A two-phase model is presented which is a slight modification of the model first presented in Ref. 41. It is similar to models used by Butler and Krier [1] and Baer and Nunziato [2]. Changes of two types have been made. First a simplified constitutive theory has been adopted in order to make the equations tractable. The trends predicted by the simpler constitutive equations are similar to the trends of Refs. 1 and 2. A second more substantial change is that an explicit expression for particle radius evolution has been adopted. No counterpart to this equation is found in either Ref. 1 or 2. For the proposed model it is assumed that each phase is a continuum; consequently, partial differential equations resembling one-phase equations are written to describe the evolution of mass, momentum, and energy in each constituent. In addition, each phase is described by a thermal state relation and a corresponding caloric state relation. Constituent one is assumed to be a gas, constituent two, a solid.

In order to close the system, a dynamic compaction equation similar to that of Ref. 2 is adopted. Choosing a dynamic compaction equation insures that the characteristics are real; thus, the initial value problem is well-posed. The unsteady two-phase model is posed in characteristic form in Appendix A. The dynamic compaction equation states that the solid volume fraction changes in response to 1) a difference between the solid pressure and the sum of the gas pressure and intragranular stress and 2) combustion. Most models use empirical data to model the intragranular stress. Here for simplicity it is assumed that the intragranular stress is a linear function of the solid volume fraction. This function is constructed such that no volume fraction change due to pressure differences is predicted in the initial state. It is emphasized that the choices made for the closure problem and for other constitutive relations place a premium on simplicity so that explicit analytic calculations can be made whenever possible. At the same time the model adopted here is representative of a wider class of two-phase detonation models currently in use.

The unsteady equations are

$$\frac{\partial}{\partial t}\left[\rho_1\phi_1\right]+\frac{\partial}{\partial x}\left[\rho_1\phi_1 u_1\right] = \left(\frac{3}{r}\right)\rho_2\phi_2 a P_1^m \tag{3.1}$$

$$\frac{\partial}{\partial t}\left[\rho_2\phi_2\right]+\frac{\partial}{\partial x}\left[\rho_2\phi_2 u_2\right] = -\left(\frac{3}{r}\right)\rho_2\phi_2 a P_1^m \tag{3.2}$$

$$\frac{\partial}{\partial t}\left[\rho_1\phi_1 u_1\right] + \frac{\partial}{\partial x}\left[P_1\phi_1 + \rho_1\phi_1 u_1^2\right] = u_2\left(\frac{3}{r}\right)\rho_2\phi_2 a P_1^m - \beta\frac{\phi_2\phi_1}{r}\left(u_1 - u_2\right) \quad (3.3)$$

$$\frac{\partial}{\partial t}\left[\rho_2\phi_2 u_2\right] + \frac{\partial}{\partial x}\left[P_2\phi_2 + \rho_2\phi_2 u_2^2\right] = -u_2\left(\frac{3}{r}\right)\rho_2\phi_2 a P_1^m + \beta\frac{\phi_2\phi_1}{r}\left(u_1 - u_2\right) \quad (3.4)$$

$$\frac{\partial}{\partial t}\left[\rho_1\phi_1\left(e_1 + u_1^2/2\right)\right] + \frac{\partial}{\partial x}\left[\rho_1\phi_1 u_1\left(e_1 + u_1^2/2 + P_1/\rho_1\right)\right] =$$

$$\left(e_2 + u_2^2/2\right)\left(\frac{3}{r}\right)\rho_2\phi_2 a P_1^m - \beta\frac{\phi_1\phi_2}{r}u_2\left(u_1 - u_2\right) - h\frac{\phi_1\phi_2}{r^{1/3}}\left(T_1 - T_2\right) \quad (3.5)$$

$$\frac{\partial}{\partial t}\left[\rho_2\phi_2\left(e_2 + u_2^2/2\right)\right] + \frac{\partial}{\partial x}\left[\rho_2\phi_2 u_2\left(e_2 + u_2^2/2 + P_2/\rho_2\right)\right] =$$

$$-\left(e_2 + u_2^2/2\right)\left(\frac{3}{r}\right)\rho_2\phi_2 a P_1^m + \beta\frac{\phi_1\phi_2}{r}u_2\left(u_1 - u_2\right) + h\frac{\phi_1\phi_2}{r^{1/3}}\left(T_1 - T_2\right) \quad (3.6)$$

$$\frac{\partial}{\partial t}\left[\phi_2/r^3\right] + \frac{\partial}{\partial x}\left[u_2\phi_2/r^3\right] = 0 \quad (3.7)$$

$$\frac{\partial\phi_2}{\partial t} + u_2\frac{\partial\phi_2}{\partial x} = \frac{\phi_1\phi_2}{\mu_c}\left[P_2 - P_1 - \frac{P_{20} - P_{10}}{\phi_{20}}\phi_2\right] - \left(\frac{3}{r}\right)\phi_2 a P_1^m \quad (3.8)$$

$$P_1 = \rho_1 R T_1\left(1 + b\rho_1\right) \quad (3.9)$$

$$e_1 = \frac{P_1}{\frac{R}{c_{v1}}\rho_1\left(1 + b\rho_1\right)} \quad (3.10)$$

$$c_1^2 = RT_1\left[1 + 2b\rho_1 + (R/c_{v1})(1 + b\rho_1)^2\right] \quad (3.11)$$

$$P_2 = \left(\gamma_2 - 1\right)c_{v2}\rho_2 T_2 - \frac{\rho_{20}^{\,s}}{\gamma_2} \quad (3.12)$$

$$e_2 = \frac{P_2 + \rho_{20}^{\,s}}{\left(\gamma_2 - 1\right)\rho_2} + q \quad (3.13)$$

$$c_2^2 = \gamma_2 (\gamma_2 - 1) c_{v2} T_2 \tag{3.14}$$

$$\phi_1 + \phi_2 = 1 \tag{3.15}$$

Here the subscript "0" denotes the undisturbed condition, "1" denotes the gas phase; "2," solid phase; ρ, density; ϕ, volume fraction; u, velocity; r, solid particle radius; P, pressure; m, burn index; a, burn constant; β, drag parameter; e, internal energy; h, heat transfer coefficient; R, gas constant; b, co-volume correction; c, sound speed; c_v, constant volume specific heat; s, non-ideal solid parameter; μ_c, compaction viscosity; γ_2, Tait parameter; and q, heat of reaction.

Numerical values for the parameters introduced above, representative of the solid high explosive HMX, are listed in Table I. When available, references are listed for each of the parameters. The unreferenced parameters have been estimated for this study. The initial gas density and temperature have arbitrarily been chosen to be 10 kg/m^3 and 300 K, respectively. Drag and heat transfer parameters have been chosen to roughly match empirical formulae given in Ref. 13. The gas constant R and virial coefficient b have been chosen such that predictions of CJ detonation states match the CJ detonation states predicted by the thermochemistry code TIGER [54] as reported in Ref. 1. The solid parameters s and γ_2 have been chosen such that solid shock and compaction wave predictions match experimental shock [55] and compaction wave data [43, 44]. As reported by Baer and Nunziato [2], there are no good estimates for the compaction viscosity μ_c. Ref. 2 chooses a value for compaction viscosity of 10^3 kg/m s. To demonstrate the existence of a two-phase detonation, it was necessary in this study to choose a higher value, 10^6 kg/m s, for the compaction viscosity.

Undisturbed conditions are specified as

$$\rho_1 = \rho_{10} \quad , \quad \rho_2 = \rho_{20} \quad , \quad \phi_1 = \phi_{10} \quad , \quad u_1 = 0,$$

$$u_2 = 0 \quad , \quad r = r_0 \quad , \quad T_1 = T_0 \quad , \quad T_2 = T_0$$

Undisturbed conditions for other variables can be determined by using the algebraic relations (3.9-15).

Equations (3.1,2) describe the evolution of each phase's mass; Equations (3.3,4), momentum evolution; and Equations (3.5,6), energy evolution. Homogeneous mixture

Table I

DIMENSIONAL INPUT PARAMETERS

a	[1]	[m / (s Pa)]	2.90×10^{-9}
ρ_{10}		[kg / m^3]	1.00×10^{1}
m	[1]		1.00×10^{0}
β		[kg / (s m^2)]	1.00×10^{4}
ρ_{20}	[1, 2]	[kg / m^3]	1.90×10^{3}
h		[J / (s K m$^{8/3}$)]	1.00×10^{7}
c_{v1}	[2]	[J / (kg K)]	2.40×10^{3}
c_{v2}	[1, 2]	[J / (kg K)]	1.50×10^{3}
R		[J / (kg K)]	8.50×10^{2}
s		[(m / s)^2]	8.98×10^{6}
q	[1]	[J / kg]	5.84×10^{6}
r_0	[1, 2]	[m]	1.00×10^{-4}
b		[m^3 / kg]	1.10×10^{-3}
γ_2			5.00×10^{0}
μ_c		[kg / (m s)]	1.00×10^{6}
T_0		[K]	3.00×10^{2}

equations are formed by adding Equations (3.1) and (3.2), (3.3) and (3.4), and (3.5) and (3.6). Thus for the mixture, conservation of mass, momentum, and energy is maintained.

The forcing functions, inhomogeneities in Equations (3.1-6), model inter-phase momentum, energy, and mass transfer. Functional forms of inter-phase transfer terms have been chosen to have a simple form. Figure 3.1 shows a comparison of the above drag model and the empirical model used by Baer [13], which is dependent on Reynolds number for particle radii from 0 to 300 μm. The Reynolds number has been found to lie in the range 0-1000 within the two-phase detonation reaction zones of this study. Figure 3.1 shows that the functional forms of the two relations are similar, though the magnitudes vary widely. A similar comparison is made in Figure 3.2 between the simplified inter-phase heat transfer modelled here and the empirical heat transfer model used by Baer. Again, the functional form of the two models is similar and wide variation exists in the magnitudes. For mass transfer a well-known empirical relation for the regression of particle radius is used. It is observed that the rate of change of particle radius is proportional to the surrounding pressure raised to some power. The right sides of the mass equations (3.1-2) are formulated to incorporate this feature.

By combining the solid mass evolution equation (3.2) with the number conservation equation (3.7), an explicit equation is obtained for particle radius evolution:

$$\frac{\partial r}{\partial t} + u_2 \frac{\partial r}{\partial x} = - aP_1^m - \frac{r}{3\rho_2}\left(\frac{\partial \rho_2}{\partial t} + u_2 \frac{\partial \rho_2}{\partial x}\right) \tag{3.16}$$

This equation demonstrates that following a particle, the particle radius may change in response to combustion, embodied in the empirically-based term $-aP_1^m$, and density changes, as described by the density derivative terms. Many two-phase particle-burning detonation models do not explicitly include an equation for the evolution of particle radius. In these models, which also do not explicitly enforce number conservation, it is unclear what physical principles are used to determine the particle radius. For a detailed derivation of the number conservation relation (3.7) and Equation (3.16) see Appendix F.

Other constitutive relations are given in Equations (3.8-15). The dynamic compaction equation is expressed in Equation (3.8). Constituent one is a gas described by a virial equation of state (3.9). Constituent two is a solid described by a Tait equation of state [69] (3.12). Assumption of a constant specific heat at constant volume for each phase allows caloric equations (3.10,13) and sound speed equations (3.11,14) consistent with the

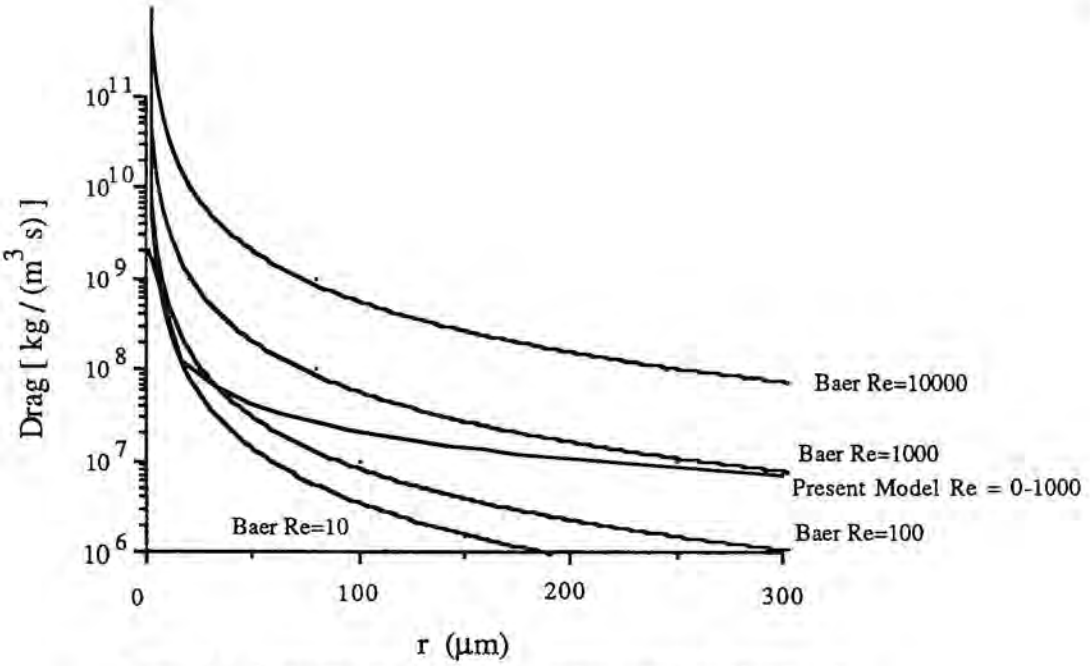

Figure 3.1 Comparison of Drag Model Used by Baer and Nunziato [13] to the Model of This Work

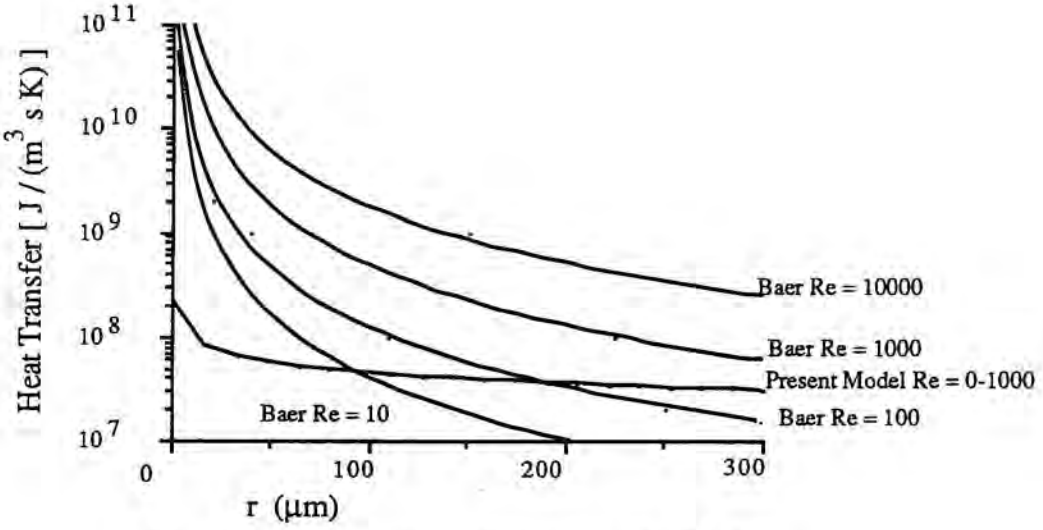

Figure 3.2 Comparison of Heat Transfer Model Used by Baer and Nunziato [13] to the Model of This Work

assumptions of classical thermodynamics to be written for each phase. Appendix B shows how thermodynamically consistent equations are derived and how relevant thermodynamic properties are determined for the state equations chosen here. The variable ϕ is defined as a volume fraction, $\phi \equiv$ constituent volume/total volume. Equation (3.15) states that all the volume is occupied by constituent one or two; no voids are permitted.

By writing Equations (3.1-15) in characteristic form, it is easy to show that the model is hyperbolic and the characteristic wave speeds are u_1, u_2, $u_1 \pm c_1$, and $u_2 \pm c_2$ (see Appendix A). Baer has reached a similar conclusion. The fact that the characteristic wave speeds are real is a consequence of the assumed form of the compaction equation. Other closure techniques will, in general, result in a model with imaginary characteristics which is not well-posed for initial value problems.

The momentum and energy equations of this model are slightly different from those of Baer and Nunziato's model. The momentum equations of this work, which are of the same general form of those of Ref. 1, differ with those of Ref. 2 by a term $P_1 \partial\phi_1/\partial x$. Also the energy equation of Ref. 2 includes a term called "compaction work," proportional to the volume fraction gradient which is not included in this model. Which form is correct is still controversial; a defense of the model presented here is described in detail in Appendix C. The methodology which is used here to determine detonation structure is unaffected by the particular choice of model form.

IV. STEADY STATE COMPACTION WAVE ANALYSIS

This chapter is concerned with steady compaction waves in granular materials. These waves are inert and thus fundamentally different from detonation waves. Before turning to the study of detonation waves in Chapter 5, there is a good reason to first consider compaction waves. That is, the simplicity of the two-phase equations allows a well-understood solution to be determined. The properties of this solution and the solution procedure itself are useful in the detonation analysis.

A compaction wave can arise from the impact of a piston on a granular material. It is shown here that the two-phase equations are able to describe such waves when no reaction is allowed and gas density is small relative to the solid. This chapter has a self-contained, complete discussion of compaction waves, essentially independent of the detonation analysis, except that the same model equations are used in different limits. A slightly different notation is introduced for this chapter which reflects the simpler nature of the compaction wave problem relative to the detonation wave problem.

It has been established by experiments with granular high energy solid propellants [23, 24] and by numerical solution of unsteady two-phase reactive flow models [1, 2] that deflagration to detonation transition (DDT) in a confined column of such granular energetic material involves material compaction and heat release. In many cases the origin of such a DDT can be traced to the influence of a compaction wave, defined as a propagating compressive disturbance of the solid volume fraction of the granular material. Steady compaction waves in porous HMX (cyclic nitramine) were observed by Sandusky and Liddiard [43] and Sandusky and Bernecker [44] arising from the impact of a constant velocity piston (piston velocity < 300 m/s). Compaction waves in these experiments travel at speeds less than 800 m/s, well below the ambient solid sound speed, which is near 3000 m/s. To understand compaction waves it is necessary to explain why this unusual result is obtained.

The first step in modeling compaction waves is to study steady compaction waves. With understanding gained from steady compaction waves, it is easier to understand the time-dependent development of these waves and how such a wave can evolve into a detonation wave. Although it is possible to numerically solve the coupled unsteady partial differential equations which model such dynamic compaction processes (including the formation of shock waves) [56], it is difficult to interpret from such models what physical properties dictate the speed, pressure changes, and porosity changes of compaction waves. It is the goal of this chapter to provide a simple method to predict these parameters as a

function of material properties with a representative model.

The experiments of Sandusky and Liddiard are simulated by studying steady solutions of two-phase flow model equations. Without considering wave structure, Kooker [57] has used an algebraic end state analysis to predict compaction wave speed as a function of piston velocity using full two-phase model equations. It is possible to extend this analysis in the limit where the effect of one of the phases is dominant. This approach was first used by Baer [45] in his study of steady compaction wave structure. Here a more detailed discussion is provided of steady structure and basic parameter dependencies. Throughout this chapter, the assumptions and results will be compared to those of Baer.

The results show a continuous dependence of compaction wave structure on the piston velocity supporting the wave; depending on the piston velocity, two broad classes of compaction zone structures exist. At low piston velocities the compaction wave travels at speeds less than the ambient sound speed of the solid. Such waves are called subsonic compaction waves. The structure is characterized by a smooth rise in pressure from the ambient to a higher pressure equal to the static pore collapse stress level. Subsonic compaction waves have been observed experimentally (though compaction zone widths have not been measured) and predicted by Baer. Above a critical piston velocity the compaction wave travels at speeds greater than the ambient sound speed in the solid. A discontinuous shock wave leads a relaxation zone where the pressure adjusts to its equilibrium static pore collapse value. Such waves are called supersonic compaction waves. Supersonic compaction waves with leading shocks have not as yet been observed nor predicted.

A shock wave in compaction wave structure is admitted because the model equations are hyperbolic. This model ignores the effects of diffusive momentum and energy transport. If included, these effects would define the width of the shock structure. Here it is assumed that the length scales on which these processes are important are much smaller than the relaxation scales which define compaction zone structure.

Compaction wave phenomena predicted here have analogies in gas dynamics. As described by Becker and Bohme [58], gas dynamic models which include thermodynamic relaxation effects predict a dispersed wave to result from the motion of a piston into a cylinder of gas. Steady solutions with and without discontinuous jumps are identified. These solutions have features which are similar to those predicted by the compaction wave model.

Here comments are made on the differences and similarities of the original Baer study and the present study. Baer's incompressibility assumption has been relaxed to allow a fully compressible solid. A complete characterization of compaction wave structure as a

function of piston wave speed including an analysis of the supersonic case is given here. With this analysis many new results are obtained. A unique equilibrium condition, determined algebraically, is obtained. As Baer does, it is demonstrated that the problem of determining compaction wave structure can be reduced to solving one ordinary differential equation for volume fraction. Other thermodynamic quantities (pressure, density, etc.) are algebraic functions of volume fraction. An analytic solution in the strong shock limit is given. A term used by Baer called "compaction work" is not included in this model. As shown in Appendix C, this term violates the principle of energy conservation.

Unsteady Model

The two-phase continuum mixture equations (3.1-15) are repeated in a condensed form in Equations (4.1-7). The model describes two-phase flow with inter-phase mass, momentum, and energy transport. A density, ρ_i; pressure, P_i; energy, e_i; temperature, T_i; velocity, u_i; and volume fraction, ϕ_i, is defined for each phase (for the gas i = 1, for the solid i = 2). A compaction equation similar to that of Baer and Nunziato is utilized. The compaction equation models the time-dependent pore collapse of a porous matrix and is based on the dynamic pore collapse theory of Carroll and Holt [59].

The unsteady two-phase equations are

$$\frac{\partial}{\partial t}\left(\rho_i\phi_i\right) + \frac{\partial}{\partial x}\left(\rho_i\phi_i u_i\right) = A_i \tag{4.1}$$

$$\frac{\partial}{\partial t}\left(\rho_i\phi_i u_i\right) + \frac{\partial}{\partial x}\left(P_i\phi_i + \rho_i\phi_i u_i^2\right) = B_i \tag{4.2}$$

$$\frac{\partial}{\partial t}\left(\rho_i\phi_i\left[e_i + u_i^2/2\right]\right) + \frac{\partial}{\partial x}\left(\rho_i\phi_i u_i\left[e_i + u_i^2/2 + P_i/\rho_i\right]\right) = C_i \tag{4.3}$$

$$\frac{\partial\phi_2}{\partial t} + u_2\frac{\partial\phi_2}{\partial x} = \frac{\phi_1\phi_2}{\mu_c}\left(P_2 - P_1 - f(\phi_2)\right) \tag{4.4}$$

$$P_i = P_i(\rho_i, T_i) \tag{4.5}$$

$$e_i = e_i(P_i, \rho_i) \tag{4.6}$$

$$\phi_1 + \phi_2 = 1 \tag{4.7}$$

Equations (4.1), (4.2), and (4.3) describe the evolution of mass, momentum, and energy, respectively, of each phase. Inter-phase transport is represented in these equations by the terms A_i, B_i, and C_i, which are assumed to be algebraic functions of P_i, u_i, ρ_i, etc. These terms are specified such that the following conditions hold:

$$\sum_{i=1}^{2} A_i = 0, \qquad \sum_{i=1}^{2} B_i = 0, \qquad \sum_{i=1}^{2} C_i = 0 \tag{4.8}$$

This insures that the mixture equations obtained by adding the constituent mass, momentum, and energy equations are conservative.

For each phase an initial temperature, density, velocity, and volume fraction is defined. The subscript 0 is taken to represent an initial condition.

$$T_i = T_{i0}\ , \quad \rho_i = \rho_{i0}\ , \quad u_{i0} = 0\ , \quad \phi_2 = \phi_{20} \tag{4.9}$$

Other variables are determined by the algebraic relations (4.5), (4.6), and (4.7).

Equation (4.4) is the compaction equation. A similar model equation has been used by Butcher, Carroll, and Holt [60] to describe time-dependent (dynamic) pore collapse in porous aluminum. The parameter μ_c is defined as compaction viscosity, not to be confused with the viscosity associated with momentum diffusion. The compaction viscosity defines the only length scale in this problem. The existence of such a parameter is still a modeling assumption and its value has not been determined. There is, however, a strong theoretical justification for the dynamic pore collapse model. It has been shown (Appendix A) that when dynamic compaction is incorporated into two-phase model equations, the equations are hyperbolic. The initial value problem is required to be hyperbolic in order to insure a stable solution.

In the compaction equation (4.4) f represents the intra-granular stress in the porous medium. It is assumed to be a function of the volume fraction. Baer has estimated f from Elban and Chiarito's [61] empirical quasi-static data obtained by measuring the static pressure necessary to compact a porous media to a given volume fraction. Carroll and Holt have suggested an analytical form for f for three regimes of pore collapse, an elastic phase, an elastic-plastic phase, and a plastic phase. In this chapter f will be modelled with an equation similar to Carroll and Holt's plastic phase equation. Here, two a priori assumptions about f are made. First, it is assumed that f is a monotonically increasing

function of volume fraction so that an increasing hydrostatic stress is necessary to balance the increased intra-granular stress which arises due to an increasing solid volume fraction. Second, it is assumed that at the initial state f must equal the difference of the solid and gas pressures so that the system is initially in equilibrium. The results show that with these assumptions, compaction wave phenomena are relatively insensitive to the particular functional form of f.

Equations (4.5) and (4.6) are state relations for each phase. Equation (4.7) arises from the definition of volume fraction. It states that all volume is occupied by either solid or gas.

Dimensionless Steady Model

To study compaction waves in the context of this model, the following assumptions are made: 1) a steady wave travelling at speed D exists, 2) gas phase equations may be neglected, 3) inter-phase transport terms may be neglected, and 4) the solid phase is described by a Tait equation of state. As a result of Assumption 1, Equations (4.1) through (4.4) may be transformed to ordinary differential equations under the Galilean transformation $\xi = x - Dt$, $v = u - D$. By examining the dimensionless form of Equations (4.1) through (4.7), it can be shown that in the limit as the ratio of initial gas density to initial solid density goes to zero, that there is justification in neglecting gas phase equations and inter-phase transport. To prove this contention, one can integrate the steady mixture mass, momentum, and energy equations formed by adding the component equations to form algebraic mixture equations. By making these equations dimensionless (as done in Chapter 5), it is seen that all gas phase quantities are multiplied by the density ratio ρ_{10}/ρ_{20}. As long as dimensionless gas phase properties are less than $O(\rho_{20}/\rho_{10})$, there is justification in neglecting the effect of the gas phase.

Because the gas phase is neglected, the subscripts 1 and 2 are discarded. All variables are understood to represent solid phase variables. The caloric Tait equation [69] for the solid is

$$e = \frac{P + \rho_0 s}{(\gamma - 1)\rho} \tag{4.10}$$

Here γ and s are parameters that define the Tait state equation. The value of γ is chosen to match shock Hugoniot data [55]. It is analogous to the specific heat ratio for an ideal

equation of state. The parameter s is defined as the non-ideal solid parameter. In this study s is viewed as an adjustable parameter which allows the equation of state to be varied in a simple way in order to show how the results are sensitive to non-ideal state effects. When $s = 0$, the state equation is an ideal state equation. For this study a value of s was chosen to match the compaction wave data of Sandusky and Liddiard [43].

To determine the ambient solid sound speed, an important term in this analysis, it is necessary to specify a thermal equation of state. By assuming a constant specific heat at constant volume c_v, a thermal equation of state consistent with Equation (4.10) can be derived.

$$P = (\gamma - 1)\, c_v\, \rho\, T - \rho_0 s / \gamma \tag{4.11}$$

Based on Equations (4.10) and (4.11) an equation for the solid sound speed c is easily derived by using the thermodynamic identity $T\, d\eta = de - P/\rho^2\, d\rho$, where η is the entropy.

$$c^2 = \frac{\partial P}{\partial \rho}\Big|_{\eta} = \gamma(\gamma - 1)\, c_v\, T \tag{4.12}$$

To simplify the analysis, dimensionless variables are denoted by a star subscript and are defined as follows

$$\rho_* = \rho / \rho_0 \,, \quad v_* = v / D \,, \quad e_* = e / D^2 \,, \quad T_* = c_v T / D^2 \,,$$

$$P_* = P / (\rho_0 D^2) \,, \quad \xi_* = \xi\, \rho_0\, D / \mu_c$$

With this choice of dimensionless variables four dimensionless parameters arise.

$$\gamma = \text{Tait Solid Parameter}, \quad \frac{s}{D^2 \gamma} = \sigma = \text{Non-Ideal Solid Parameter}$$

$$\frac{\gamma(\gamma - 1)\, c_v T_0 - s}{\gamma D^2} = \pi = \text{initial pressure} \,, \quad \phi_0 = \text{initial volume fraction}$$

For materials of interest ϕ_0 and γ are of order 1. Interesting limiting cases can be studied when $s \rightarrow 0$, corresponding to either the strong shock or weak non-ideal effect limit, or when $\pi \rightarrow 0$, corresponding to the strong shock limit.

With the assumptions made, steady dimensionless equations can be written to describe the compaction of an inert solid porous material as follows:

$$\frac{d}{d\xi_*}\left(\rho_* \phi v_*\right) = 0 \tag{4.13}$$

$$\frac{d}{d\xi_*}\left(P_* \phi + \rho_* \phi v_*^2\right) = 0 \tag{4.14}$$

$$\frac{d}{d\xi_*}\left(\rho_* \phi v_*\left[e_* + v_*^2/2 + P_*/\rho_*\right]\right) = 0 \tag{4.15}$$

$$\frac{d\phi}{d\xi_*} = \frac{\phi(1-\phi)}{v_*}\left(P_* - f_*(\phi)\right) \tag{4.16}$$

$$e_* = \frac{P_* + \gamma\sigma}{(\gamma - 1)\rho_*} \tag{4.17}$$

Initial conditions are specified as

$$\rho_* = 1\ , \quad \phi = \phi_0\ , \quad v_* = -1\ , \quad P_* = \pi \tag{4.18}$$

Equations (4.13-17) are equivalent to Baer's steady model except a term Baer calls "compaction work" is not included and a simpler state equation is used. Equations (4.13), (4.14), and (4.15) may be integrated subject to initial conditions (4.18) resulting in the following set of equations:

$$\frac{d\phi}{d\xi_*} = \frac{\phi(1-\phi)}{v_*}\left(P_* - f_*(\phi)\right) \tag{4.19}$$

$$\rho_* \phi v_* = -\phi_0 \tag{4.20}$$

$$P_* \phi + \rho_* \phi v_*^2 = \phi_0 (\pi + 1) \tag{4.21}$$

$$\rho_* \phi v_* \left(e_* + v_*^2 / 2 + P_* / \rho_* \right) = - \phi_0 \left(\frac{\pi + \gamma \sigma}{\gamma - 1} + 1 / 2 + \pi \right) \tag{4.22}$$

$$e_* = \frac{P_* + \gamma \sigma}{(\gamma - 1) \rho_*} \tag{4.23}$$

From Equations (4.20) through (4.23), equations for pressure and velocity as functions of volume fraction can be written. Equation (4.23) is used to eliminate energy from Equation (4.22). Velocity is eliminated from Equations (4.21) and (4.22) by using Equation (4.20). Then density is eliminated from Equation (4.22) by using Equation (4.21). What remains is a quadratic equation involving only pressure and volume fraction. It is possible to solve this equation for pressure explicitly in terms of volume fraction. The solution is

$$P_* = \frac{\phi_0}{\phi (\gamma + 1)} \left(\frac{\gamma \sigma \phi}{\phi_0} - 1 - \pi \right) \cdot \left[-1 \pm \sqrt{1 + \frac{(\gamma+1) \left[2\gamma\sigma \left(\frac{\phi}{\phi_0} (1+\pi) - 1 \right) - \pi \left(2 - \pi (\gamma - 1) \right) \right]}{\left(\frac{\gamma \sigma \phi}{\phi_0} - 1 - \pi \right)^2}} \right] \tag{4.24}$$

The solution corresponding to the positive branch is the physically relevant one. The negative branch is associated with negative pressure. Equations (4.20) and (4.21) may be simultaneously solved for velocity as a function of pressure and volume fraction. The velocity is given by

$$v_* = \frac{P_* \phi - \phi_0 (1 + \pi)}{\phi_0} \tag{4.25}$$

By using Equation (4.24) to substitute for pressure in Equation (4.25), velocity is available as a function of volume fraction alone. The mass equation (4.20) can be used to give density as a function of volume fraction and then the state equation (4.17) can be used to give energy as a function of volume fraction. Thus all variables in the compaction equation (4.19) can be expressed as functions of volume fraction; the compaction wave problem is reduced to solving one ordinary differential equation (4.19) for volume fraction subject to the condition $\phi = \phi_0$ at $\xi_* = 0$.

Next the technique is described for determining wave speed as a function of piston velocity. This calculation is algebraic and can be made without regards to structure. The solution is parameterized by the wave velocity through the definitions of π and σ. Instead of using a piston velocity as an input condition, it is easier to consider the wave speed to be known and from that wave speed calculate a piston velocity. By assuming a static pressure equilibrium end state in Equation (4.19) ($P_*(\phi) = f_*(\phi)$), it is possible to determine the equilibrium volume fraction and thus, from Equations (4.24) and (4.25), the final velocity v_*. The piston velocity (u_p) is found by transforming the final velocity to the lab frame by using the transformation $u_p = D(v_* + 1)$.

Pressure equilibrium end states are found when a volume fraction is found such that the pressure given by Equation (4.24) matches the intra-granular stress predicted by f. In the initial state, Equation (4.24) predicts a pressure of π, the dimensionless initial pressure. By assumption f also yields a value of π in the initial state so that the undisturbed material is stationary. In Figure 4.1, dimensional pressure in HMX is plotted as a function of volume fraction from Equation (4.24) for a series of wave speeds and an initial volume fraction of 0.73. Except for compaction viscosity μ_c parameters used to model HMX are those previously listed in Table I (c_v, μ_c, and ρ_0 of Baer is used, and the parameters γ and s are estimated by requiring predictions to match shock and compaction data. Unlike in detonation wave analysis, there is no special problem posed by using Baer's value of compaction viscosity, 1000 kg/(m s), in these calculations). All curves pass through the point of initial pressure and volume fraction.

The curve on Figure 4.1 for the ambient sonic wave speed (D = 3000 m/s) has a special property whose importance will be apparent in the following discussion. For this curve a volume fraction minimum exists at the initial volume value. It can be proven for a sonic wave speed, that the discriminant in Equation (4.24) is identically zero for $\phi = \phi_0$ and $D = \gamma(\gamma - 1)c_v T_0$ (the ambient solid sonic wave speed).

The positive pressure branch of Equation (4.24) is a double-valued function of volume fraction for wave velocities that exceed the ambient solid sound speed and single-valued for

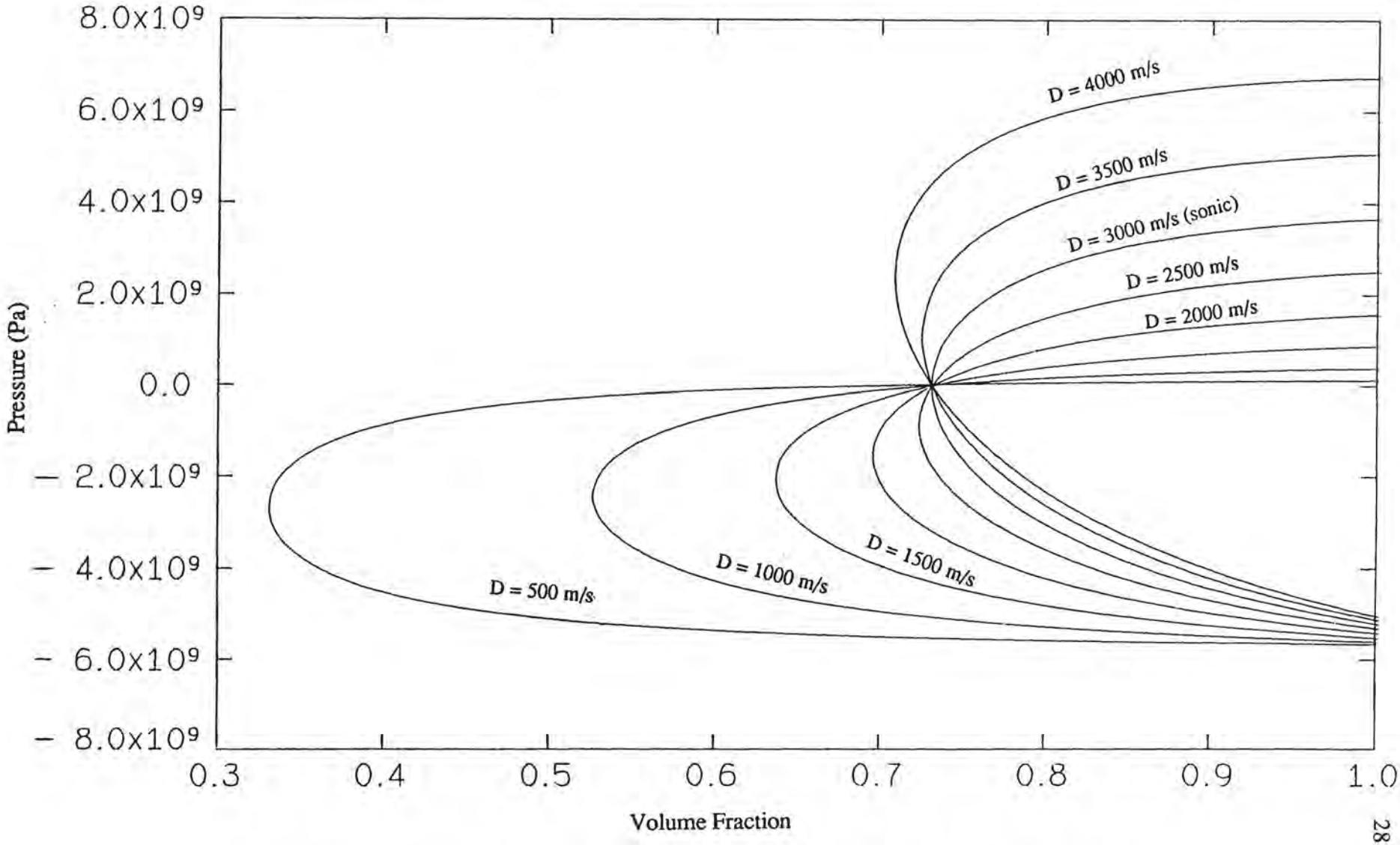

Figure 4.1 Pressure vs. Volume Fraction for Subsonic, Sonic, and Supersonic Wave Speeds

wave velocities less than or equal to the ambient solid sound speed. For subsonic wave speeds, small increases from the initial volume fraction cause small positive perturbations in pressure. For supersonic wave speeds a positive increase of the initial volume fraction is only acceptable if the pressure jumps discontinuously to a shocked value on the upper portion of the double-valued P_*-ϕ curve. Because the governing equations are hyperbolic, these shock jumps are admissible. From Equation (4.19) the shock jump condition for volume fraction is

$$\left[\phi \right]_0^s = 0 \tag{4.26}$$

where "0" denotes the initial state and "s" the shock state. Thus the shock volume fraction is always equal to the initial volume fraction.

From Equations (4.24) and (4.25) the shock pressure and particle velocity can be determined. The shocked values are independent of the initial solid volume fraction.

$$P_s = \frac{2 - (\pi + \sigma)(\gamma - 1)}{\gamma + 1} - \sigma \tag{4.27}$$

$$v_s = - \frac{(\gamma - 1) + 2\gamma(\pi + \sigma)}{\gamma + 1} \tag{4.28}$$

The combination of parameters $\pi + \sigma$ is independent of the non-ideal solid parameter s. So from Equations (4.27) and (4.28) it is deduced that non-ideal effects lower the shock pressure by a constant, σ, and do not affect the shock particle velocity.

Based on the implications of Equation (4.24), the structure analysis is thus conveniently split in two classes, subsonic and supersonic. As wave speed increases from subsonic values, the initial pressure at the wave front is the ambient pressure until the compaction wave speed is sonic. For wave speeds greater than the ambient solid sound speed the initial pressure jumps are dictated by Equation (4.27). A plot of the leading pressure versus compaction wave speed is shown in Figure 4.2.

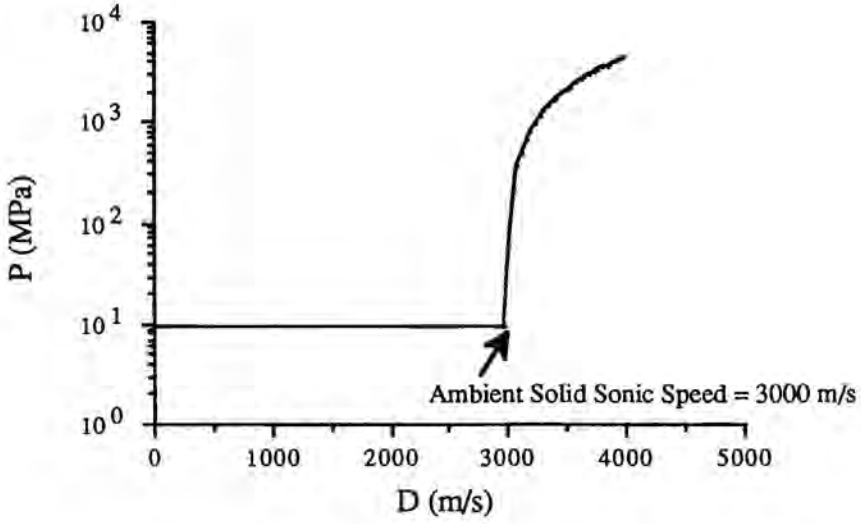

Figure 4.2 Pressure at Compaction Wave Head vs. Compaction Wave Speed

As an aside, it is noted that a criterion for a solid equation of state is that the candidate equation along with the Rankine-Hugoniot jump conditions be able to match experimental piston impact data. Typically parameters for solid equations of state are determined by choosing them such that shock data is matched. For voidless HMX ($\phi = 1$) observations of shock wave speed as a function of piston velocity are reported by Marsh [55]. By rewriting Equation (4.28) in dimensional form, the wave speed D is solved for as a function of piston velocity.

$$D = \frac{1+\gamma}{4} u_p + \sqrt{\left(\frac{1+\gamma}{4} u_p\right)^2 + \gamma(\gamma-1) c_v T_0} \qquad (4.29)$$

From Equation (4.12), the term $\gamma(\gamma\text{-}1) c_v T_0$ is the square of the ambient sound speed for the non-ideal solid. In a result familiar from gas dynamics, it can be deduced from Equation (4.29) that the minimum steady shock wave speed admitted in response to a piston boundary condition is the ambient sonic speed. For values of γ, c_v, and T_0 listed in Table I, the shock wave speed D is plotted as a function of piston velocity u_p and data from Marsh in Figure 4.3.

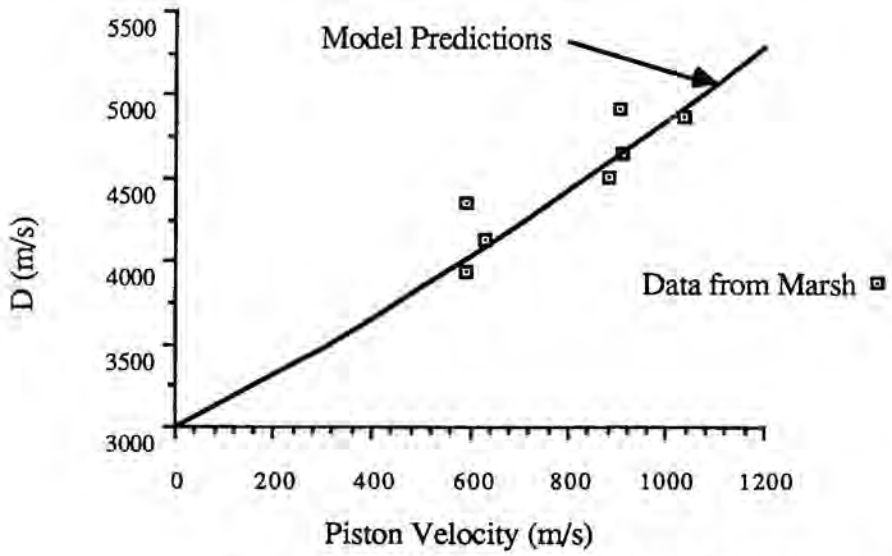

Figure 4.3 Piston Velocity vs. Solid Shock Speed

The parameter γ has been fixed such that there is agreement between the data and the model predictions. In the range of piston velocities shown, Equation (4.29) approximates a linear D vs. u_p relation used by other modelers to match this data.

Subsonic Compaction Waves

Subsonic End States

To study subsonic compaction waves admitted by Equation (4.19), a form for f_* is chosen:

$$f_*(\phi) = \pi \frac{\phi^2}{\phi_0^2} \frac{(2-\phi_0)^2}{(2-\phi)^2} \frac{\ln\left[\frac{1}{1-\phi}\right]}{\ln\left[\frac{1}{1-\phi_0}\right]} \tag{4.30}$$

This function satisfies the requirements described earlier, namely, it is a monotonically increasing function of volume fraction and is constructed such that the system is in equilibrium in the initial state. It has the same form as the plastic-phase static pore collapse relation given by Carroll and Holt [59]. It is not the Carroll and Holt relation, as the leading coefficient in the Carroll and Holt relation is the yield stress of the solid. In

Equation (4.30) the leading coefficient is a function of initial volume fraction. Predictions of Equation (4.30) approximately match the experimental results of Elban and Chiarito [61]. Figure 4.4 compares a curve fit of Elban and Chiarito's data for HMX with the approximation given by Equation (4.30).

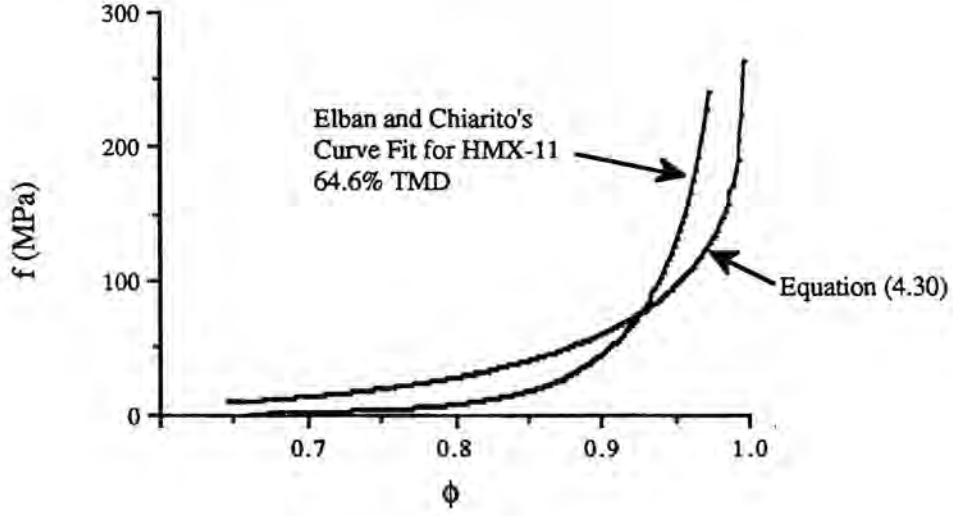

Figure 4.4 Comparison of Static Pore Collapse Data with Predictions of Equation (4.30)

To locate an end state, Equations (4.24) and (4.30) are solved simultaneously. For 73% theoretical maximum density (TMD) HMX (volume fraction = 0.73) and a variety of subsonic wave speeds, curves of pressure versus volume fraction from Equations (4.24) and (4.30) are plotted in Figure 4.5. As wave speed increases, the final volume fraction increases. For wave speeds above 600 m/s nearly complete compaction is predicted. For wave speeds of about 200 m/s or lower, no steady compaction wave is predicted. This is solely a consequence of the assumed form of f. The form of f chosen crosses through the initial point with a positive slope and fails to intersect the pressure-volume fraction curves for low wave speeds.

For 73% TMD HMX Figure 4.6 shows plots of compaction wave speed, final density, final volume fraction, final pressure, and final mixture pressure (mixture pressure = pressure * volume fraction) versus piston velocity. Also shown are the observations of Sandusky and Liddiard [43] and Sandusky and Bernecker [44] of wave speed and final volume fraction and their predictions of pressure. The relatively small density changes verify that Baer's incompressibility assumption is a good approximation. Figure 4.7 shows predictions of compaction wave speed, final volume fraction, and final mixture

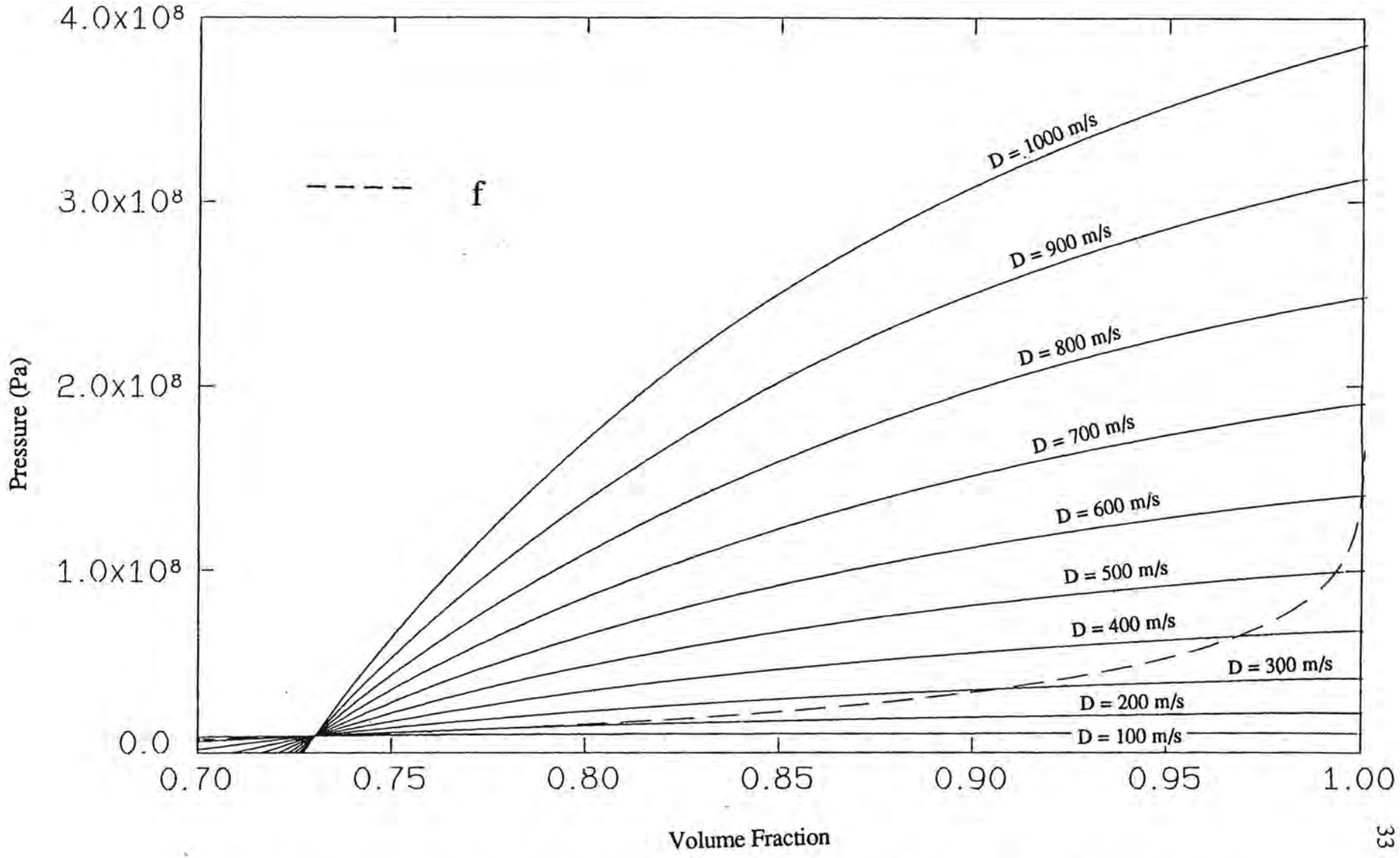

Figure 4.5 Pressure vs. Volume Fraction for Subsonic Wave Speeds and Pore Collapse Function, f

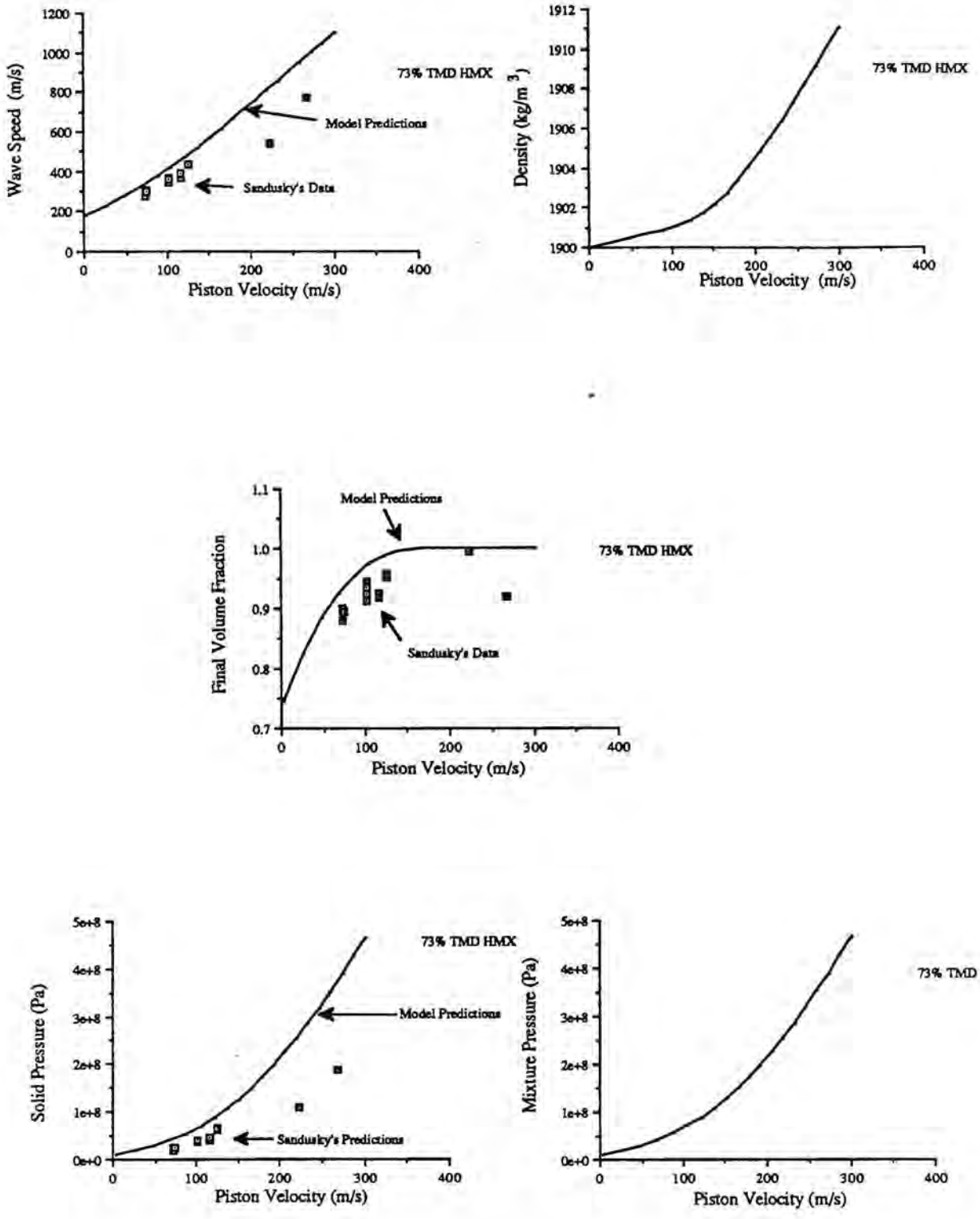

Figure 4.6 Compaction Wave End States vs. Piston Velocity

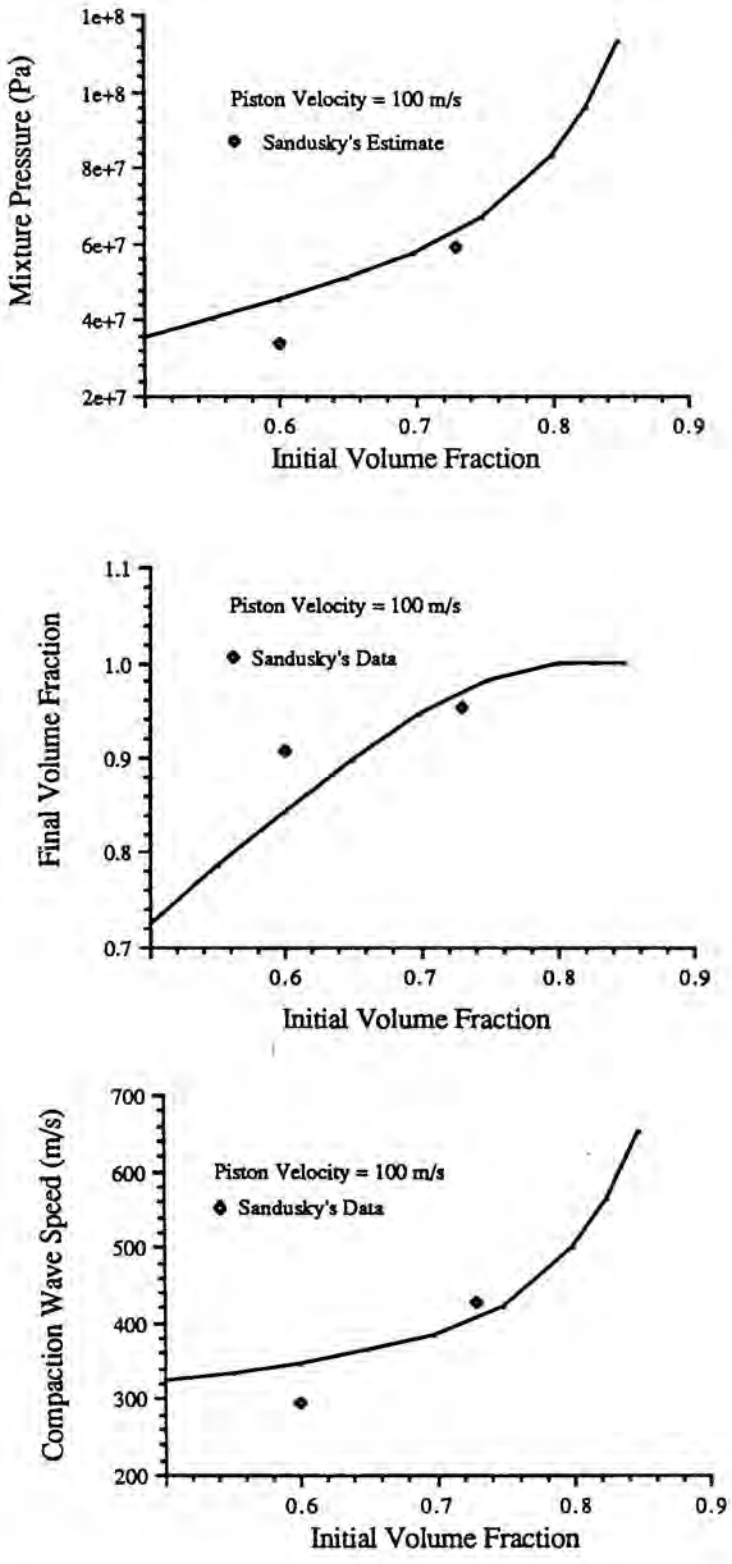

Figure 4.7 Compaction Wave End States vs. Initial Volume Fraction

pressure as a function of initial volume fraction for a constant piston velocity of 100 m/s along with Sandusky's predictions as reported by Kooker [62].

Subsonic Structure

Equation (4.19) has been numerically integrated to determine the structure of the subsonic compaction zone. The integration was performed using the IMSL routine DVERK, a fifth and sixth order Runge-Kutta routine. A step size was chosen such that the compaction zone structure was described by about 100 points. Using more points had little effect on the results. Run times to determine a structure were less than ten seconds on the UIUC Cyber 175 computer. In the numerical integrations pressure, velocity, and f are used as given by Equations (4.24), (4.25), and (4.30), respectively. The integration was performed starting at $\xi_* = 0$ and integrating towards $\xi_* \rightarrow -\infty$. To initiate the integration, a small positive perturbation of volume fraction was introduced which in this case causes a small positive perturbation in pressure.

Figure 4.8 shows the particle velocity, volume fraction, and pressure in the compaction zone for a subsonic compaction wave. Here the piston velocity is 100 m/s and the initial volume fraction is 0.73. The compaction wave speed is 404.63 m/s. For an assumed compaction viscosity of 1000 kg/(m s) a compaction wave thickness of 80 mm is predicted. Because compaction viscosity defines the only length scale in this problem, compaction viscosity only serves to define the compaction wave thickness. For the same value of compaction viscosity Baer reports a compaction wave thickness of 31.9 mm. The discrepancy could be due to many effects including the definition of compaction zone length. It is important to note that the length is of the same order of magnitude. Final pressure, wave speed, and final volume fraction are unaffected by the value chosen for compaction viscosity. By measuring a compaction wave thickness, an estimate could be made for the compaction viscosity.

Supersonic Compaction Waves

Supersonic End States

At 0.73 initial porosity for piston velocities greater than 884 m/s, supersonic compaction waves are also admitted. Figure 4.9 shows plots of compaction wave speed, final density, final volume fraction, final pressure, and final mixture pressure as a function of piston velocity. These curves encompass both the subsonic and supersonic compaction

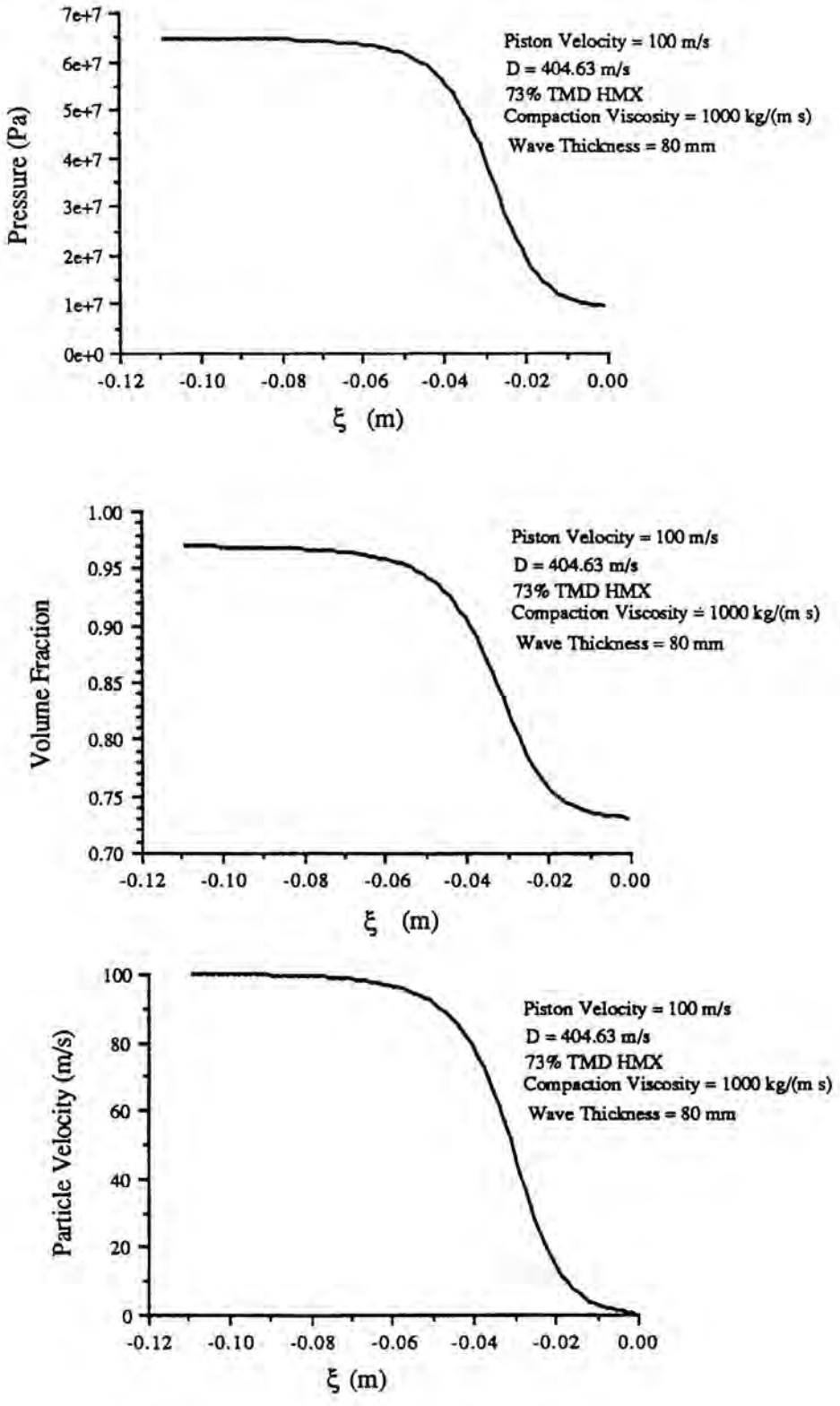

Figure 4.8 Subsonic Compaction Zone Structure

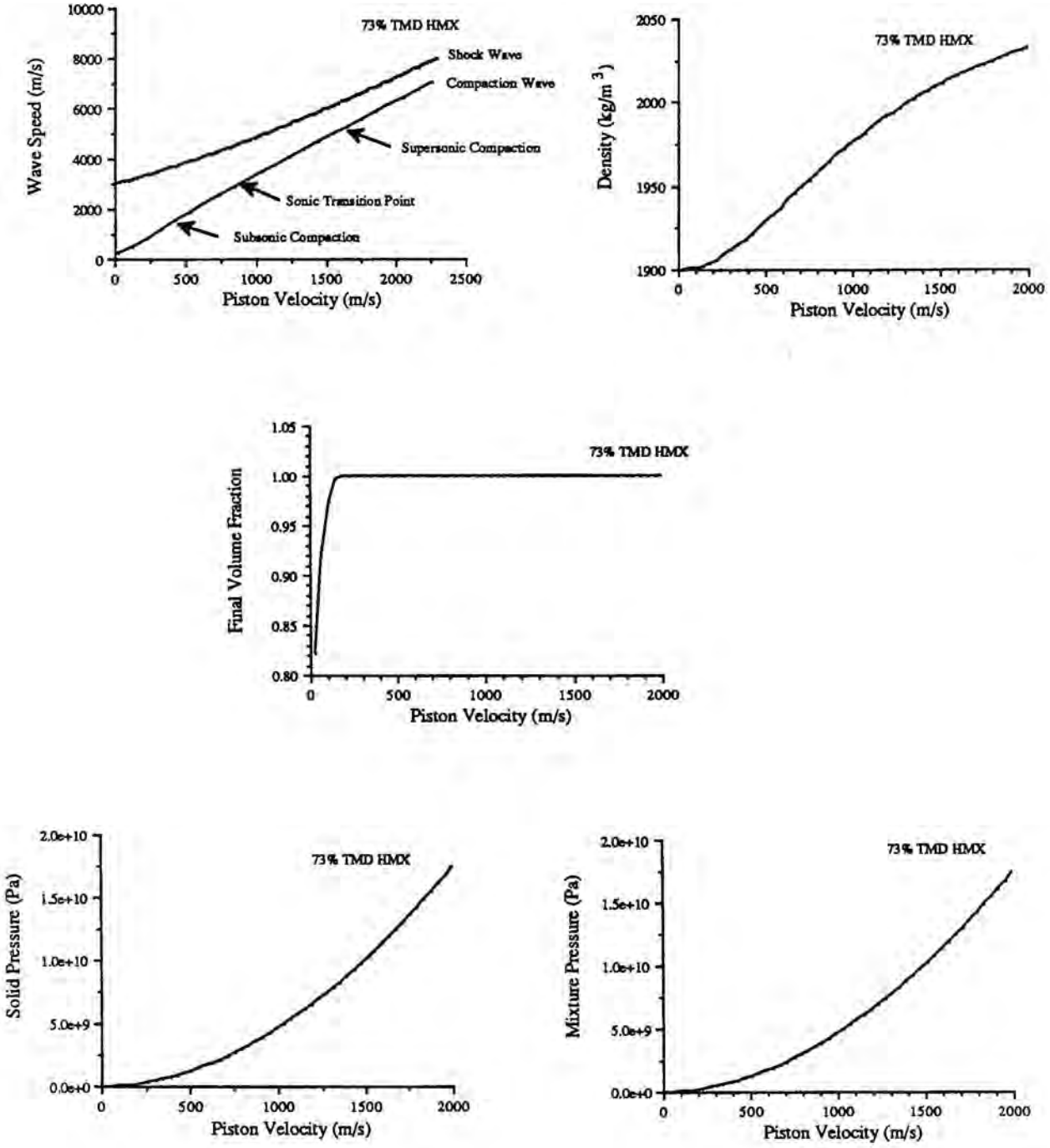

Figure 4.9 Subsonic and Supersonic Compaction End States vs. Piston Velocity

wave end states. It is seen that the end states are a continuous function of piston velocity. In Figure 4.9 the shock wave speed as a function of piston velocity is plotted alongside the compaction wave speed. For large wave speeds the predicted shock velocity converges with the compaction wave velocity. It is demonstrated next that this is a consequence of non-ideal effects having little importance at supersonic wave speeds. Furthermore it will be demonstrated that the existence of subsonic compaction waves can be attributed solely to non-ideal effects.

Supersonic Structure

Equations (4.24) and (4.25) can be simplified in the limit as $\sigma \rightarrow 0$. The limit of small σ corresponds either to negligible non-ideal effects or large wave speed. In the limit as $\sigma \rightarrow 0$ Equations (4.24), (4.25), and (4.19) can be written as

$$P_* = \frac{P_s \phi_0}{\phi} \tag{4.31}$$

$$v_* = v_s \tag{4.32}$$

$$\frac{d\phi}{d\xi_*} = \frac{1 - \phi}{v_s}\left(P_s \phi_0 - \phi f_* (\phi)\right) \tag{4.33}$$

Equation (4.32) holds that in this limit the velocity is constant in the relaxation zone and is equal to the shocked particle velocity. For $s \equiv 0$ (that is for an ideal state relation) Equation (4.32) is equivalent to Equation (4.29); thus, for an ideal state relation the minimum compaction wave speed is the ambient sonic speed. *Any subsonic compaction wave admitted by the model (Equations (4.19) - (4.23)) is a direct consequence of non-ideal state effects.*

In the strong shock limit $D \rightarrow \infty$, and both π and $\sigma \rightarrow 0$. Equation (4.33) has a simple solution in this limit, assuming f_* to be sufficiently bounded. (Note that because of the logarithmic singularity at $\phi = 1$, that Equation (4.30) does not meet this criterion. The general model is not, however, restricted to a function of this form) In this limit Equation (4.33) becomes

$$\frac{d\phi}{d\xi_*} = -\frac{2\phi_0}{\gamma - 1}\left(1 - \phi\right) \tag{4.34}$$

whose solution is

$$\phi = 1 - \left(1 - \phi_0\right)\exp\left(\frac{2\phi_0}{\gamma - 1}\xi_*\right) \tag{4.35}$$

In terms of dimensional parameters, the compaction zone thickness found by equating the exponent in Equation (4.35) to one and substituting the expression for piston velocity for wave speed is estimated as

$$L_{comp} = O\left(\frac{2(\gamma - 1)\mu_c}{(\gamma + 1)\rho_0\phi_0 u_p}\right) \tag{4.36}$$

The length is proportional to compaction viscosity and inversely proportional to piston velocity and the product of density and volume fraction.

An example of supersonic structure arising from the impact of a 1000 m/s piston is now given. Figure 4.10 shows the particle velocity, volume fraction, and pressure in the compaction zone for a supersonic compaction wave. Here the initial volume fraction is 0.73. The compaction wave speed is 3353.67 m/s and the wave thickness is 2.9 mm. It is seen that pressure and particle velocity undergo shock jumps. Volume fraction does not undergo a shock jump; however, its derivative does jump at the initial point.

Compaction Zone Thickness

It is possible to study the parametric dependence of compaction zone thickness. Given a constant compaction viscosity, the model can predict compaction zone thickness as a function of initial volume fraction and piston velocity. Should experiments be devised to measure the compaction zone thickness, the experiments could provide a means to verify the theory.

The thickness is defined as the distance at which the ratio of the difference of

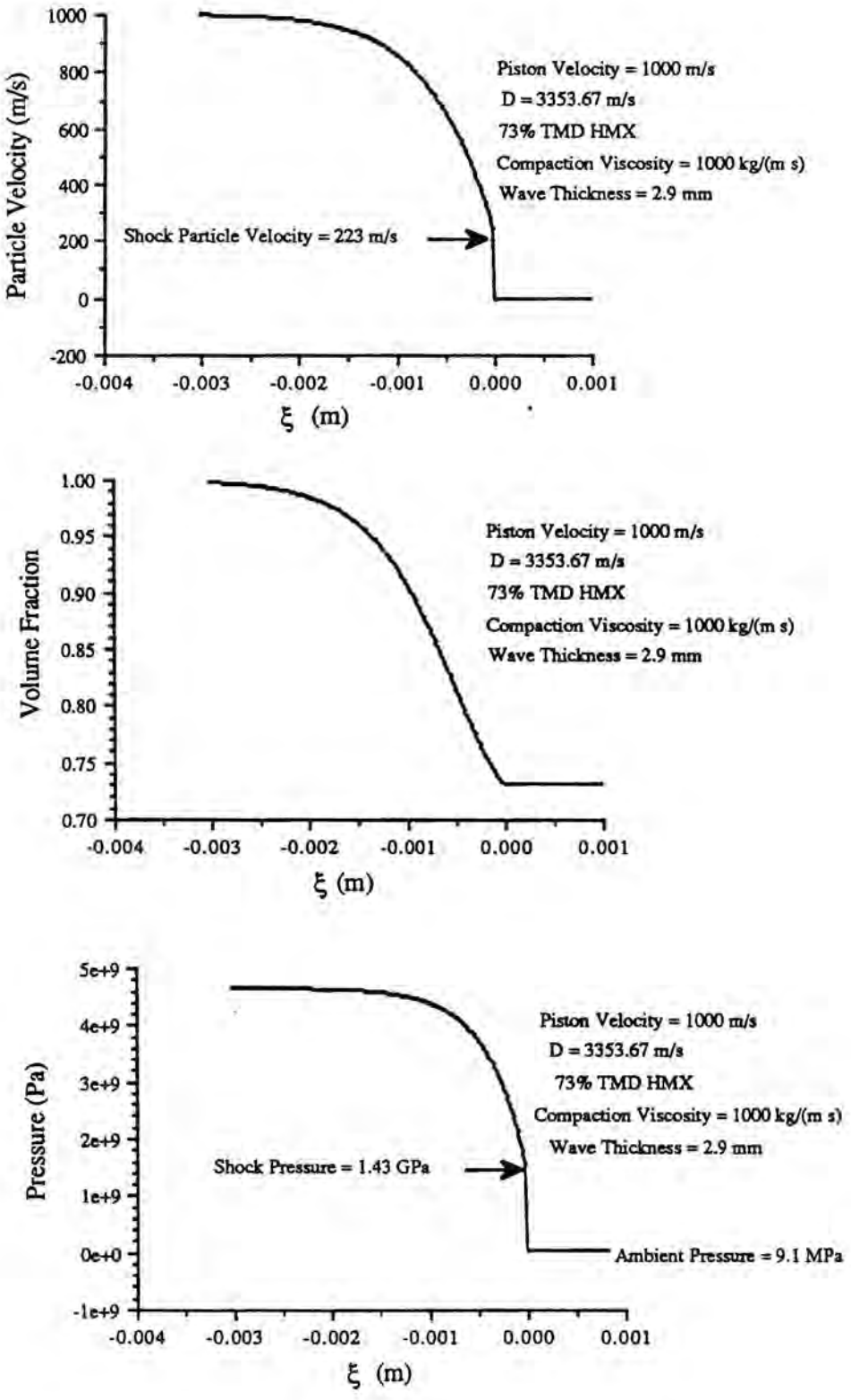

Figure 4.10 Supersonic Compaction Zone Structure

instantaneous volume fraction and initial volume fraction to the difference of final volume fraction and initial volume fraction is equal to 0.99. The final volume fraction is available from the algebraic end state calculation. Figure 4.11a shows the compaction zone length versus initial volume fraction for a piston velocity of 100 m/s and compaction viscosity of 1000 kg/(m s). It is not understood why the peak in this curve occurs. It is noted that for high initial volume fraction, the zone length decreases as initial volume fraction increases in accordance with the predictions of Equation (4.36) for supersonic compaction. It is speculated that for low porosity a different mechanism dictates the subsonic compaction zone length than supersonic length. Figure 4.11b shows compaction zone length versus piston velocity for 73% TMD HMX and compaction viscosity of 1000 kg/(m s). The compaction zone length decreases with increasing piston velocity in accordance with the predictions of Equation (4.36) for supersonic compaction. Figure 4.11c shows compaction zone length as a function of compaction viscosity for a 100 m/s piston velocity and 0.73 initial volume fraction. As no estimates are available for compaction viscosity, compaction zone lengths for a wide range of compaction viscosity have been plotted. Though plotted on a log scale, the relationship is truly linear with the compaction zone length equal to a constant multiplied by the compaction viscosity.

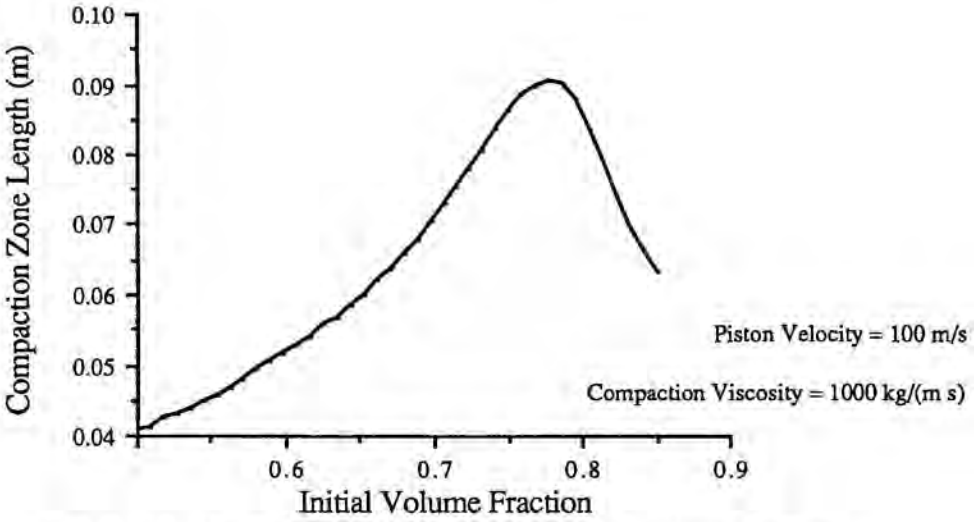

Fig. 4.11a Compaction zone length vs. initial volume fraction

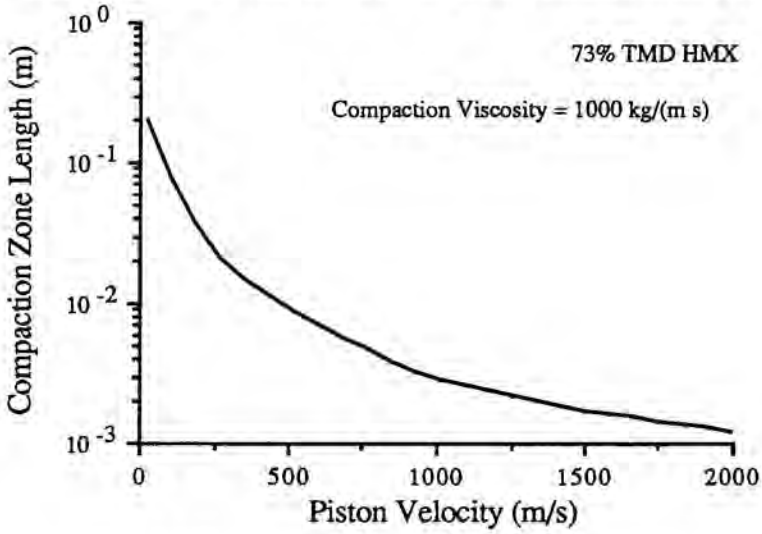

Fig. 4.11b Compaction zone length vs. piston velocity

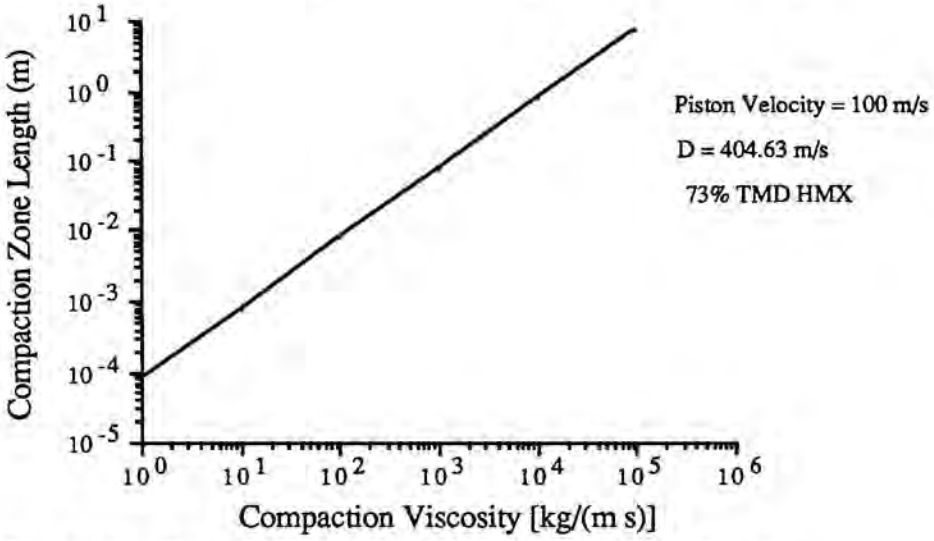

Fig. 4.11c Compaction zone length vs. compaction viscosity

V. STEADY STATE DETONATION WAVE ANALYSIS

Equations (3.1-15) can be re-cast in a more tractable form using the steady state assumption. First the equations are written in dimensionless form. For a right-running steady wave the Galilean transformation $\xi = x - Dt$, $v = u - D$ causes Equations (3.1-8) to become eight ordinary differential equations. Here D is a constant defined as the steady wave speed. Next, Equations (3.1), (3.3), and (3.5) may be eliminated in favor of homogeneous mixture equations formed by the addition of the steady form of Equations (3.1) and (3.2), (3.3) and (3.4), and (3.5) and (3.6), respectively. The resultant mixture equations and the steady form of Equation (3.7) may be integrated to form algebraic equations. Thus the steady two-phase model is described by four ordinary differential equations and eleven algebraic equations.

Dimensionless Steady Equations

To reduce the number of independent parameters, dimensionless equations are introduced. Define dimensionless variables where "$*$" indicates a dimensionless quantity:

$$\xi_* = \xi / L \qquad v_{*i} = v_i / D \qquad P_{*i} = P_i / (\rho_{i0} D^2)$$

$$\rho_{*i} = \rho_i / \rho_{i0} \qquad e_{*i} = e_i / D^2 \qquad T_{*i} = c_{vi} T_i / D^2 \qquad r_* = r / L$$

$$i = 1, 2$$

Here D is the wave speed; L, a length scale which can be associated with the reaction zone length; ρ_{i0}, the initial density of phase i; c_{vi}, the specific heat at constant volume of phase i. Define the following independent dimensionless parameters as

$$\pi_1 = 3a\rho_{10}^m D^{2m-1} \qquad \pi_2 = \beta / (\rho_{20} D) \qquad \pi_3 = h L^{2/3} / (\rho_{20} c_{v1} D)$$

$$\pi_4 = m \qquad \pi_5 = \rho_{10} / \rho_{20} \qquad \pi_6 = c_{v1} / c_{v2} \qquad \pi_7 = R / c_{v1} + 1$$

$$\pi_8 = s / (\gamma_2 D^2) \qquad \pi_9 = \rho_{20} D L / \mu_c \qquad \pi_{10} = q / D^2 \qquad \pi_{11} = \phi_{10}$$

$$\pi_{12} = r_0 / L \qquad \pi_{13} = b\rho_{10} \qquad \pi_{14} = c_{v2} T_0 / D^2$$

$$\pi_{17} = \gamma_2$$

and the following dependent dimensionless parameters as

$$\pi_{18} = \pi_{11} + \frac{1 - \pi_{11}}{\pi_5}$$

$$\pi_{19} = \left[\pi_7 - 1\right] \pi_6 \pi_{14} \left[1 + \pi_{13}\right]$$

$$\pi_{20} = 1 - \pi_{11}$$

$$\pi_{21} = \pi_{17} - 1 - \pi_8$$

$$\pi_{22} = \pi_{11}\left[\pi_6 \pi_{14} + \frac{1}{2} + \pi_{19}\right] + \frac{1 - \pi_{11}}{\pi_5}\left[\pi_{14} + \pi_{10} + \frac{1}{2} + \pi_{21}\right]$$

$$\pi_{23} = \pi_{11} \pi_{19} + \frac{1 - \pi_{11}}{\pi_5} \pi_{21}$$

$$\pi_{15} = \frac{\pi_{21} - \pi_5 \pi_{19}}{1 - \pi_{11}}$$

Then the dimensionless model differential equations (for compact notation the stars are dropped) can be written as

$$\frac{d}{d\xi}\left[\rho_2 \phi_2 v_2\right] = -\pi_1 \frac{\rho_2 \phi_2 P_1^{\pi_4}}{r} \tag{5.1}$$

$$\rho_2 \phi_2 v_2 \frac{dv_2}{d\xi} + \frac{d}{d\xi}\left[P_2 \phi_2\right] = -\pi_2\left[v_2 - v_1\right] \frac{\phi_1 \phi_2}{r} \tag{5.2}$$

$$\rho_2 v_2 \frac{de_2}{d\xi} + P_2 \frac{dv_2}{d\xi} = -\pi_3\left[\pi_6 T_2 - T_1\right] \frac{\phi_1}{r^{1/3}} \tag{5.3}$$

$$v_2 \frac{d\phi_2}{d\xi} = \pi_9 \phi_1 \phi_2\left[P_2 - \pi_5 P_1 - \pi_{15} \phi_2\right] - \pi_1 \frac{\phi_2 P_1^{\pi_4}}{r} \tag{5.4}$$

The supplemental algebraic mixture, number conservation, state, and volume fraction equations are

$$\rho_1 \phi_1 v_1 + \frac{1}{\pi_5} \rho_2 \phi_2 v_2 = -\pi_{18} \tag{5.5}$$

$$\rho_1 \phi_1 v_1^2 + P_1 \phi_1 + \frac{1}{\pi_5}\left[\rho_2 \phi_2 v_2^2 + P_2 \phi_2\right] = \pi_{18} + \pi_{23} \tag{5.6}$$

$$\rho_1 \phi_1 v_1 \left[e_1 + \frac{v_1^2}{2} + \frac{P_1}{\rho_1}\right] + \frac{1}{\pi_5} \rho_2 \phi_2 v_2 \left[e_2 + \frac{v_2^2}{2} + \frac{P_2}{\rho_2}\right] = -\pi_{22} \tag{5.7}$$

$$r = \pi_{12} \sqrt[3]{\frac{-v_2 \phi_2}{1 - \pi_{11}}} \tag{5.8}$$

$$P_1 = \left[\pi_7 - 1\right] \rho_1 T_1 \left[1 + \pi_{13} \rho_1\right] \tag{5.9}$$

$$e_1 = \frac{P_1}{(\pi_7 - 1)\, \rho_1 \,(1 + \pi_{13} \rho_1)} \tag{5.10}$$

$$c_1^2 = (\pi_7 - 1) T_1 \left[1 + 2\pi_{13} \rho_1 + (\pi_7 - 1)(1 + \pi_{13} \rho_1)^2\right] \tag{5.11}$$

$$P_2 = \left[\pi_{17} - 1\right] \rho_2 T_2 - \pi_8 \tag{5.12}$$

$$e_2 = \frac{P_2 + \pi_{17} \pi_8}{(\pi_{17} - 1) \rho_2} + \pi_{10} \tag{5.13}$$

$$c_2^2 = \pi_{17} (\pi_{17} - 1)\, T_2 \tag{5.14}$$

$$\phi_1 + \phi_2 = 1 \tag{5.15}$$

Undisturbed conditions for the ambient mixture are

$$\rho_2 = 1 \qquad v_2 = -1 \qquad \phi_2 = \pi_{20} \qquad T_2 = \pi_{14}$$

Equilibrium End State Analysis

To place a first restriction on the steady solutions admitted by Equations (5.1-15), equilibrium end states are considered. It is later shown that the complete reaction state is an equilibrium state for Equations (5.1-4). This result can be used at this point to completely describe the gas phase equilibrium state. In the complete reaction state the mixture equations (5.5-7) allow for the gas phase properties to be determined. For $\phi_2 = 0$ ($\phi_1 = 1$), Equations (5.5-7) can be combined to form an equivalent two-phase Rayleigh line (5.16) and two-phase Hugoniot (5.17)

$$P_1 - \pi_{23} = \pi_{18}^2 \left(1/\pi_{18} - 1/\rho_1 \right) \tag{5.16}$$

$$\left[e_1 - \frac{\pi_{11}\pi_6\pi_{14}}{\pi_{18}} \right] + \frac{1}{2}\left[P_1 + \pi_{23} \right]\left[1/\rho_1 - 1/\pi_{18} \right] = \frac{\left(1 - \pi_{11}\right)\left(\pi_{14} + \pi_{10}\right)}{\pi_5 \pi_{18}} \tag{5.17}$$

From the state relations (5.9,10) the energy e_1 can be written as $e_1(P_1,\rho_1)$ which is substituted into the Hugoniot equation (5.17). The Rayleigh line equation (5.16) allows ρ_1 to be eliminated in favor of P_1. Substituting this in the reduced Hugoniot equation results in a cubic equation for P_1. Depending on the wave speed three cases are possible: three distinct real solutions, two equal real solutions and a third real solution, and a real solution and a pair of complex conjugate solutions. When three distinct real solutions exist, two are analogous to the weak and strong solutions predicted by the simple one-phase theory. The third solution has no such counterpart and often is a nonphysical solution with $\rho_1 < 0$. A sketch of the two-phase Rayleigh lines and Hugoniots for wave speeds corresponding to the three classes of solutions is shown in Figure 5.1.

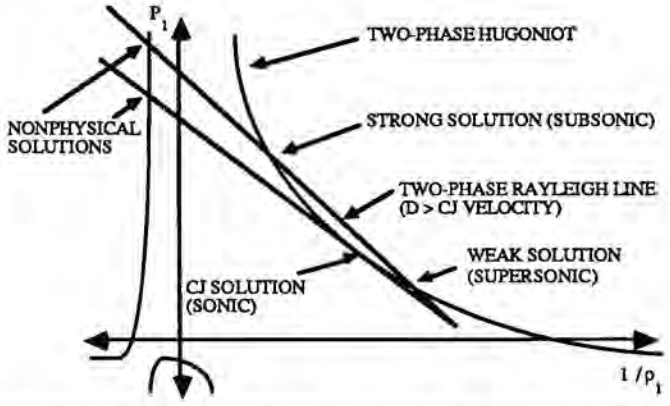

Figure 5.1 Sketch of Two-Phase Complete Reaction Rayleigh Line and Hugoniot

By imposing the condition that two real roots are degenerate (which forces the Rayleigh line and Hugoniot to be tangent) a minimum detonation velocity can be found. This will be called the CJ condition. Because the detonation velocity D is contained in the dimensionless parameters, it is convenient to return to dimensional variables to express CJ conditions. Define the bulk density, bulk pressure, and bulk internal energy ρ_a, P_a, and e_a:

$$\rho_a = \rho_{10}\phi_{10} + \rho_{20}\phi_{20} \quad , \quad P_a = P_{10}\phi_{10} + P_{20}\phi_{20} \qquad (5.18, 19)$$

$$e_a = \frac{\rho_{10}\phi_{10}e_{10} + \rho_{20}\phi_{20}e_{20}}{\rho_{10}\phi_{10} + \rho_{20}\phi_{20}} \qquad (5.20)$$

The dimensional equations which must be solved to determine the two-phase CJ end state are shown next.

$$P_1 = P_a + \rho_a^2 D^2 \left(1/\rho_a - 1/\rho_1\right) \qquad (5.21)$$

$$\frac{(P_a + P_1)(1/\rho_1 - 1/\rho_a)}{2} + \frac{c_{v1}P_1}{R\rho_1(b\rho_1 + 1)} - e_a = 0 \qquad (5.22)$$

$$\left.\frac{dP_1}{d\rho_1}\right|_{5.21} = \left.\frac{dP_1}{d\rho_1}\right|_{5.22} \qquad (5.23)$$

Equation (5.21) is the dimensional form of the Rayleigh line equation (5.16), Equation (5.22) is the dimensional form of the Hugoniot equation (5.17), and Equation (5.23) is the tangency condition. These three equations have been solved by iteration for the three unknowns, P_1, ρ_1, and D. The equations have an exact solution in terms of a quadratic equation in the ideal gas limit (b = 0). The ideal gas solution has been used as a first estimate for the iterative solution.

The effects of a non-ideal gas and small initial bulk pressure on CJ conditions can be seen by writing the CJ conditions as Taylor series expansions which are valid in the limit as the dimensionless groups $b\rho_a$ and $P_a/(\rho_a e_a)$ approach zero. These expressions were obtained with the aid of the computer algebra program MACSYMA and have been verified by comparing predictions to the solutions obtained by iteration. (The same technique can be used to obtain CJ deflagration conditions for a two-phase material; these conditions are

reported in Appendix D). The Taylor series expansions for the CJ detonation condition for a two-phase material are given below. The leading coefficients on the right hand sides of Equations (5.24-28) are the exact solutions in the limit of no non-ideal gas effects (b = 0) and zero initial bulk pressure ($P_a = 0$). The bracketed terms in these equations represent the first order corrections for finite non-ideal effects and finite initial bulk pressure. From the expressions, it is seen that non-ideal effects tend to raise the detonation wave speed and pressure, lower the density, and have no effect on the gas velocity or temperature. Finite initial bulk pressure tends to lower the detonation wave speed, pressure, density, and gas velocity, and has no effect on the temperature at this order of the expansion.

$$D_{CJ} \cong \frac{\sqrt{2e_a R\left(R + 2c_{v1}\right)}}{c_{v1}}\left(1 + b\rho_a - \frac{c_{v1}^2}{2R\left(R + 2c_{v1}\right)}\frac{P_a}{\rho_a e_a}\right) \tag{5.24}$$

$$P_{CJ} \cong \frac{2e_a R}{c_{v1}}\rho_a\left(1 + b\rho_a - \frac{c_{v1}^2}{2R\left(R + 2c_{v1}\right)}\frac{P_a}{\rho_a e_a}\right) \tag{5.25}$$

$$\rho_{CJ} \cong \frac{2c_{v1} + R}{c_{v1} + R}\rho_a\left(1 - \frac{c_{v1}}{c_{v1} + R}b\rho_a - \frac{c_{v1}^2}{2R\left(R + 2c_{v1}\right)}\frac{P_a}{\rho_a e_a}\right) \tag{5.26}$$

$$u_{CJ} \cong \sqrt{\frac{2e_a R}{R + 2c_{v1}}}\left[1 - \frac{c_{v1}}{2R}\frac{P_a}{\rho_a e_a}\right] \tag{5.27}$$

$$T_{CJ} \cong \frac{2(c_{v1} + R)}{2c_{v1} + R}\frac{e_a}{c_{v1}} \tag{5.28}$$

For $P_a = b = 0$ these formulae show that it is appropriate to treat the two-phase CJ condition as a one-phase CJ condition using ρ_a and e_a as effective one-phase properties. Fickett and Davis [40] give equations for one-phase CJ properties for an ideal gas in the limit of small initial pressure. In these equations, one can simply substitute the bulk density for the initial density and the bulk internal energy for the chemical energy to obtain the two-phase CJ equations. It is important to note that the two-phase CJ properties are predicted from the full model equations. The two-phase nature of the conditions is embodied in the definitions of bulk properties, which have no one-phase counterpart.

Figure 5.2 shows plots of the CJ properties predicted by Equations (5.24-28) along with the exact CJ properties predicted by iterative solution of Equations (5.21-23). Also

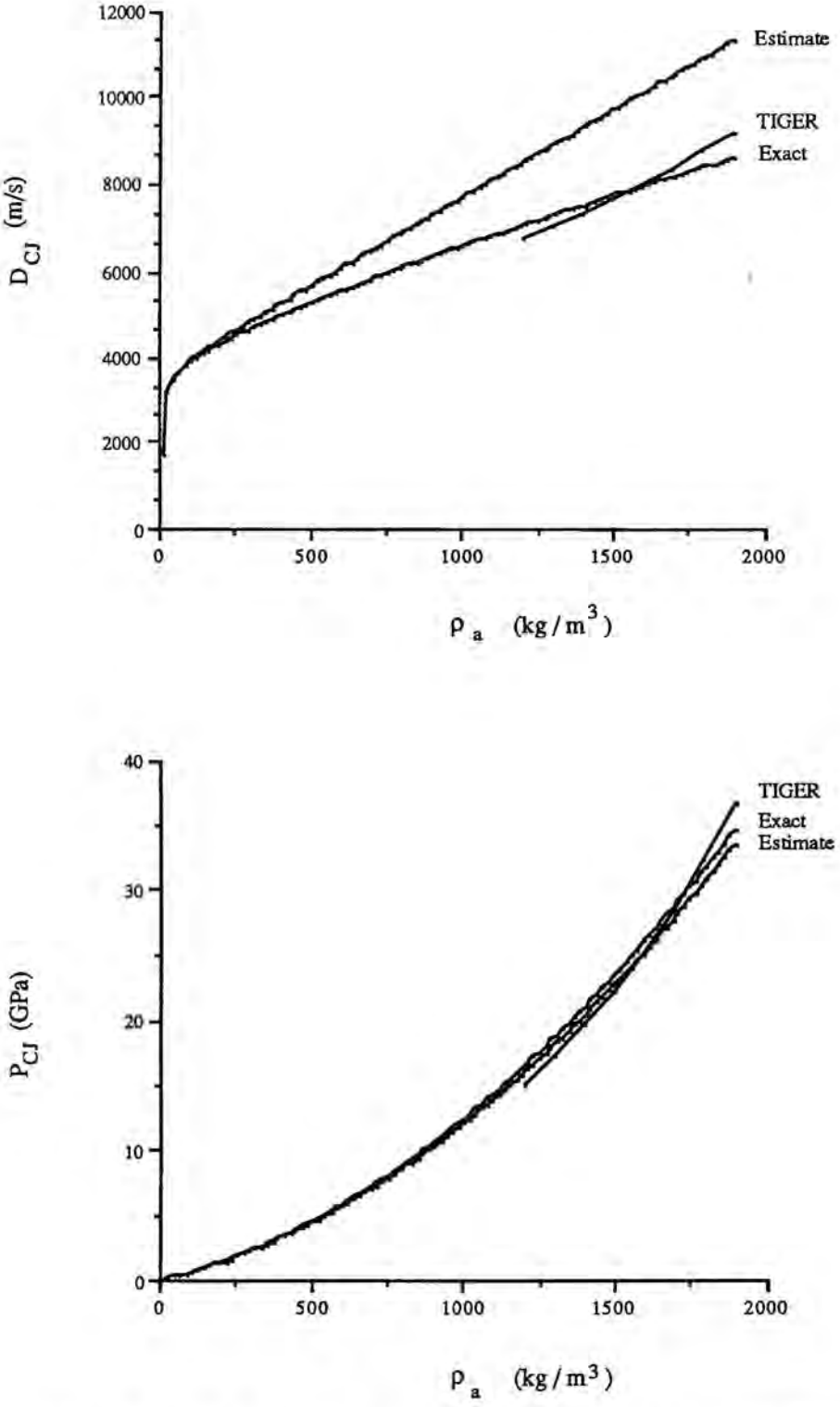

Figure 5.2a Exact CJ Properties, Approximate CJ Properties, and TIGER Estimates [1]

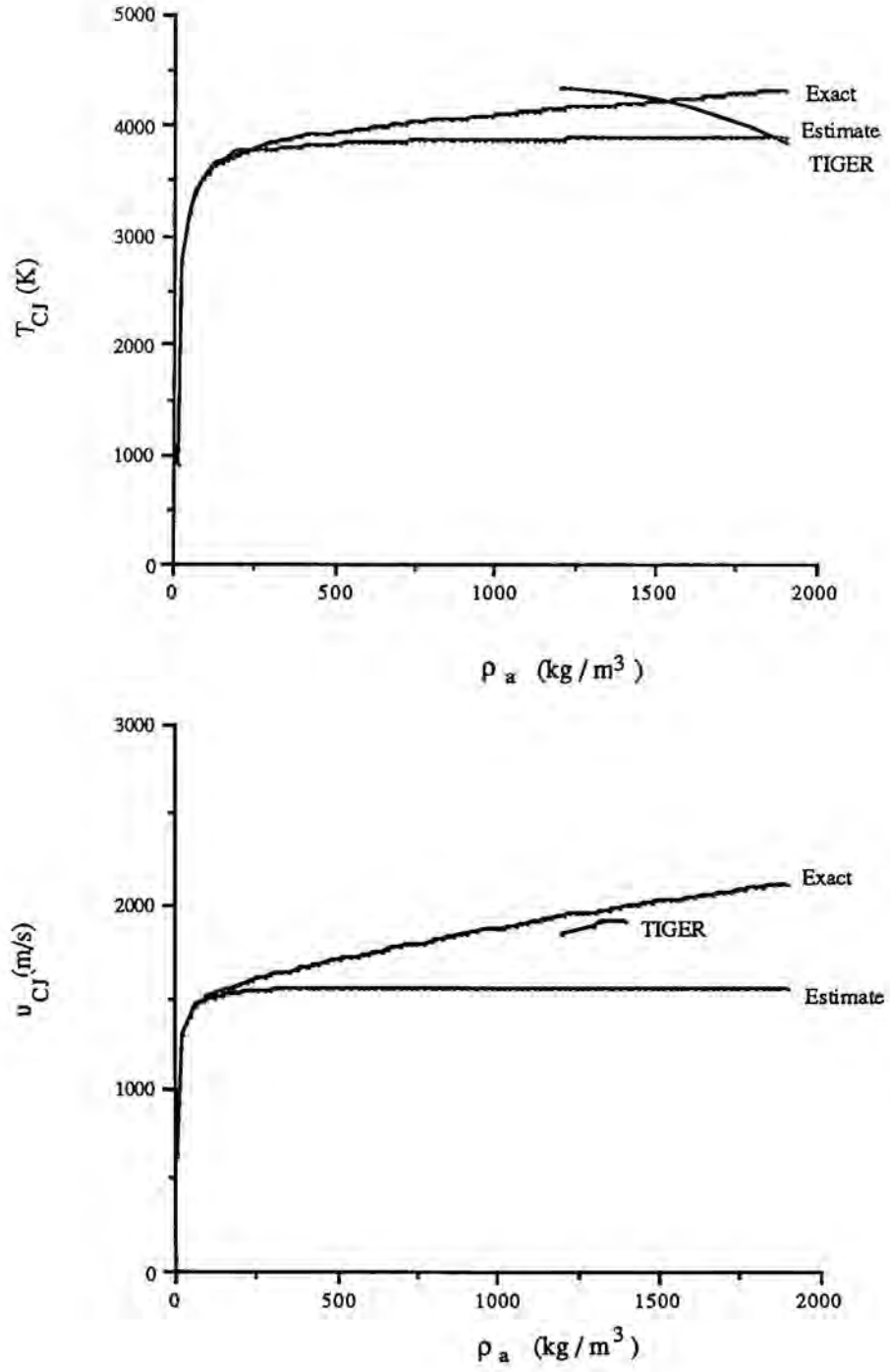

Figure 5.2b Exact CJ Properties, Approximate CJ Properties, and TIGER Estimates [1]

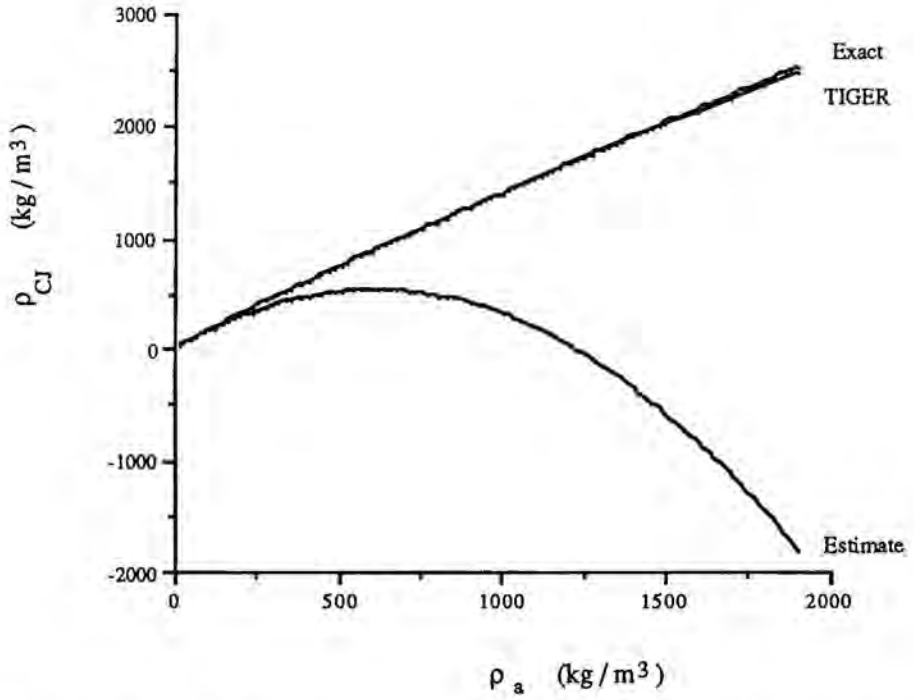

Figure 5.2c Exact CJ Properties, Approximate CJ Properties, and TIGER Estimates [1]

plotted on these curves are predictions of CJ properties from the thermochemistry code TIGER [54] as reported in Refs. 1 and 47. It is seen that the predictions of the approximate formulae more accurately predict the exact solutions for low initial bulk density. The improved accuracy for low initial bulk density can be attributed to the form of the Taylor series prediction, whose accuracy improves as the dimensionless parameter $b\rho_a$ approaches zero. Except for the CJ density, the approximate formulae estimate the general trends for a large range of initial bulk densities.

Equations (5.24, 25) indicate that the CJ state is quite sensitive to the non-ideal parameter b, a parameter allowed to vary in Ref. 47 to match CJ TIGER predictions. In particular, when the dimensionless group $b\rho_a$ is of order 1, non-ideal effects become quite important. This is demonstrated in Figure 5.3 which for constant bulk density plots CJ wave speed versus the non-ideal parameter b. This plot was obtained by solving the full non-linear equations (5.21-23).

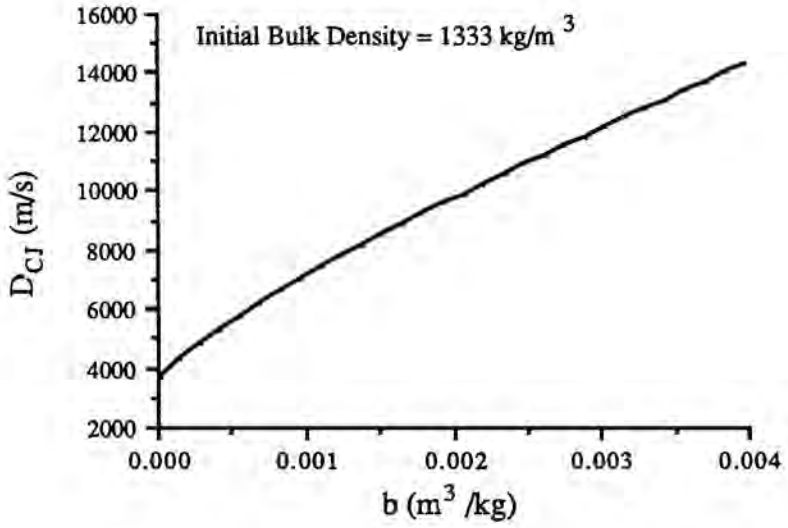

Figure 5.3 CJ Wave Speed vs. Non-Ideal Parameter b

By numerically studying exact two-phase CJ conditions, it can be inferred that the CJ point is a sonic point; that is, the gas velocity relative to the wave head is equal to the local gas phase sound speed. In addition, numerical studies indicate that for $D > D_{CJ}$ the gas velocity relative to the wave head is locally subsonic at the non-ideal strong point, while the gas velocity relative to the wave head is locally supersonic at the non-ideal weak point. This result agrees with the results of the simple one-phase theory.

Shock Discontinuity Conditions

A shock discontinuity is an integral part of a two-phase detonation. As in one-phase ZND theory the shock wave is a discontinuity that raises the pressure, temperature, and density of the material, initiating significant chemical reaction. In the context of the one-dimensional steady model, the shock wave is supported by the chemical energy which is released by the reaction; thus the process is self-sustaining.

The shock conditions are determined from an algebraic analysis and provide the initial conditions for integrating the steady equations (5.1-4). These conditions are defined by Equations (5.1-15) by assuming that within the shock wave, reaction, drag, heat transfer, and compaction have no effect. Thus through the shock discontinuity, differential equations (5.1-4) may be integrated to form algebraic relationships. These algebraic equations admit four physical solutions: 1) the ambient state, 2) shocked gas, unshocked solid, 3) unshocked gas, shocked solid, and 4) shocked gas, shocked solid.

This model ignores the effects of diffusive momentum and energy transport. If included, these effects would define a shock structure of finite width. Here it is assumed that the length scales on which these processes are important are much smaller than the relaxation scales which define two-phase detonation structure. To the author's knowledge, this assumption, common in the analysis of shocked systems, has not been examined either experimentally or theoretically for two-phase reactive systems.

The shock conditions are given below:

$$\left[\rho_2 \phi_2 v_2 \right]_0^s = 0 \tag{5.29}$$

$$\left[P_2 \phi_2 + \rho_2 \phi_2 v_2^2 \right]_0^s = 0 \tag{5.30}$$

$$\left[\rho_2 \phi_2 v_2 \left(e_2 + v_2^2/2 + P_2/\rho_2 \right) \right]_0^s = 0 \tag{5.31}$$

$$\left[\phi_2 \right]_0^s = 0 \tag{5.32}$$

Here "s" denotes the shocked state and "0" the undisturbed state. Equations (5.29-32) and state relations (5.12, 13) are sufficient to calculate the shock properties for phase two. The shock state for the solid phase is independent of the initial porosity. This is apparent from Equation (5.32), which says that the porosity does not change through the shock discontinuity ($\phi_{2s} = \phi_{20}$), and from Equations (5.29-31) where it is seen that a common factor ϕ_{20} cancels from each equation. For the solid phase there are two solutions to Equations (5.29-32): the inert solution and the shock solution. Exact expressions for the solid phase shock state are:

$$P_{2s} = \frac{2 - \pi_{14}\left(\pi_{17} - 1\right)^2}{\pi_{17} + 1} - \pi_8 \tag{5.33}$$

$$\rho_{2s} = \frac{\pi_{17} + 1}{(\pi_{17} - 1)\,(1 + 2\pi_{14}\pi_{17})} \tag{5.34}$$

$$T_{2s} = \frac{\left(2 - \pi_{14}(\pi_{17} - 1)^2\right)\left(1 + 2\pi_{14}\pi_{17}\right)}{(\pi_{17} + 1)^2} \tag{5.35}$$

$$e_{2s} = (1 + 2\pi_{14}\pi_{17})\frac{2 - (\pi_{14} - \pi_8)(\pi_{17} - 1)^2}{(\pi_{17} + 1)^2} + \pi_{10} \tag{5.36}$$

$$v_{2s} = \frac{1 - \pi_{17}(2\pi_{14}\pi_{17} - 2\pi_{14} + 1)}{\pi_{17} + 1} \tag{5.37}$$

$$\phi_{2s} = 1 - \pi_{11} \tag{5.38}$$

In Figure 5.4, the dimensional solid phase shock pressure is plotted versus the shock wave speed.

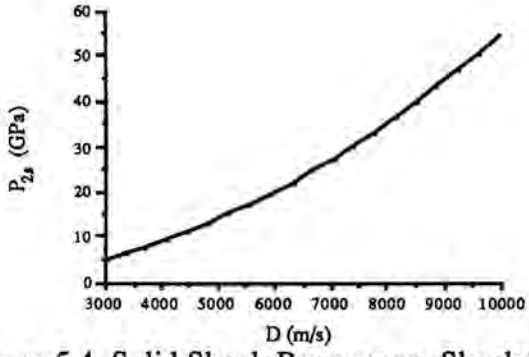

Figure 5.4 Solid Shock Pressure vs. Shock Wave Speed

The shock properties for phase one are implied by the mixture equations (5.5-7) and state relations (5.9-10). By subtracting the solid shock equations (5.29-31) from the respective mixture equations (5.5-7), one obtains gas shock jump equations which are dependent only on gas phase properties. As for the solid phase, in these equations a common factor of ϕ_{10} cancels from each equation. Three solutions to the gas shock jump relations exist: the inert solution, a nonphysical solution, and a shock solution. In the limit as π_{13} (or b) approaches zero, the nonphysical prediction of gas density approaches $-1/\pi_{13}$ and is therefore rejected. The full solution to the non-ideal shocked gas equations are lengthy, so here the shocked gas solution in the limit of an ideal gas will be presented. The full non-ideal shocked solution is determined by solving a cubic equation described in Appendix E. The shocked ideal gas state ($b = \pi_{13} = 0$) is described by the following equations, which can be easily rewritten as classical ideal gas shock relations by using the definitions of the dimensionless parameters to write these equations in dimensional form.

$$P_{1s} = \left[\frac{2 - \pi_{14}\pi_6\left(\pi_7 - 1\right)^2}{\pi_7 + 1} \right] \tag{5.39}$$

$$\rho_{1s} = \frac{\pi_7 + 1}{(\pi_7 - 1)(1 + 2\pi_{14}\pi_6\pi_7)} \tag{5.40}$$

$$e_{1s} = T_{1s} = \frac{(2\pi_{14}\pi_6\pi_7 + 1)\left(2 - \pi_{14}\pi_6(\pi_7 - 1)^2\right)}{(\pi_7 + 1)^2} \tag{5.41}$$

$$v_{1s} = \frac{-(\pi_7 - 1)(1 + 2\pi_{14}\pi_6\pi_7)}{\pi_7 + 1} \tag{5.42}$$

Figure 5.5 shows a plot of the dimensional gas phase shock pressure versus the shock wave speed for the non-ideal gas.

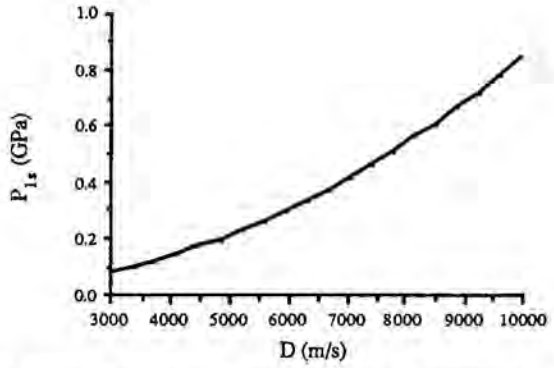

Figure 5.5 Non-Ideal Gas Phase Shock Pressure vs. Shock Wave Speed

Two-Phase Detonation Structure

Before studying solutions of the full equations (5.1-15), a simplified model, reduced to two differential equations is considered. These equations have a clear geometrical interpretation in the two-dimensional phase plane. Results from this model will be compared to those of the full model. In this section the steps necessary to reduce Equations (5.1-15) to two equations will be described. Next, a comparison of acceptable detonation structure predicted by the two-equation and full model equations is given. Finally, an example is given of an non-physical solution again comparing the results of the two-equation model with those of the full model, and an explanation is given for why this solution is non-physical.

The steady equations (5.1-15) are simplified significantly when heat transfer and compaction effects are ignored. This corresponds to the limit $\pi_3 \to 0$ and $\pi_9 \to 0$. From the definition of the dimensionless parameter π_3, it can be concluded that in this limit the heat transfer in the reaction zone, roughly h $L^{2/3}$ / D, is small compared to the thermal capacity $\rho_{20}c_{v1}$. By setting π_9 to zero, it is assumed that compaction effects are negligible; in this limit Equation (5.4) holds that all volume change is due to chemical reaction. This is achieved mathematically by allowing the compaction viscosity μ_c to approach infinity.

In these limits it is possible to integrate Equations (5.1) and (5.3) and write two autonomous ordinary differential equations in two unknowns, solid density and solid volume fraction, that determine the system completely. All other thermodynamic variables can be expressed as algebraic functions of solid density and volume fraction. With the two ordinary differential equations it is easy to study the geometry of the two-dimensional phase space in the ρ_2-ϕ_2 phase plane. The geometry of the phase plane determines whether a detonation structure can exist in theory.

To derive the two-equation model requires a lengthy algebraic analysis. Details can be found in Appendix E. To summarize the process, state relations (5.9, 10, 12, 13) are used to eliminate energy and temperature of both phases in all remaining equations. Number conservation (5.8) is used to eliminate particle radius r from all equations. Mixture equations (5.5-7) are used to write gas phase properties as algebraic functions of solid phase properties. In uncoupling the mixture equations, a complicated cubic equation must be solved. One root corresponds to a shocked gas, associated with what is known in one-phase ZND theory as the strong solution. Another root corresponds to an unshocked gas, associated with the weak solution in one-phase ZND theory. The third root is a non-physical consequence of the virial equation of state; negative gas density, temperature, and pressure are predicted with this root. Substitution of these results into Equations (5.1-4) yields four ordinary differential equations in four unknowns, ρ_2, ϕ_2, v_2, and P_2.

When the limit $\pi_3 \to 0$ and $\pi_9 \to 0$ is considered, combinations of two of these equations can be integrated. By eliminating the gradient of volume fraction by substituting Equation (5.4) into (5.1), a homogeneous equation is found for the product of solid density and velocity. When integrated this gives an algebraic relation between particle density and velocity. The solid energy equation (5.3) can then be written in terms of a homogeneous relation involving only solid pressure and density by using the integrated mass equation to eliminate velocity. Initial conditions are applied corresponding to either a shocked or unshocked solid state. These integrated equations allow both solid velocity and pressure to be written as functions of solid density. The integrated equations are given below.

$$v_2 = -\frac{1}{\rho_2} \tag{5.43}$$

$$P_2 = K \rho_2^{\pi_{17}} - \pi_8 \tag{5.44}$$

with
$$K = \begin{cases} \dfrac{2 - \pi_{14}\left(\pi_{17} - 1\right)^2}{\pi_{17} + 1}\left[\dfrac{(\pi_{17} - 1)\,(1 + 2\pi_{14}\pi_{17})}{(\pi_{17} + 1)}\right]^{\pi_{17}} & \text{shocked solid} \\ \pi_{21} + \pi_8 & \text{unshocked solid} \end{cases}$$

Here K is a constant which depends on whether the initial solid state is shocked or unshocked. With these results, the momentum equation (5.2) can be used to determine an explicit equation for the derivative of solid density. This equation along with the

compaction equation (5.4) form the two-equation model. The equations which govern the structure are written below as

$$\frac{d\rho_2}{d\xi} = \frac{f(\rho_2, \phi_2)}{g(\rho_2, \phi_2)} \tag{5.45}$$

$$\frac{d\phi_2}{d\xi} = \frac{h(\rho_2, \phi_2)}{g(\rho_2, \phi_2)} \tag{5.46}$$

with f, g, and h defined as follows

$$f(\rho_2, \phi_2) = \pi_2(v_1 - v_2)\rho_2^2\phi_1 - (K\rho_2^{\pi_{17}} - \pi_8)\pi_1\rho_2^3 P_1^{\pi_4} \tag{5.47}$$

$$g(\rho_2, \phi_2) = r\,(\pi_{17}K\rho_2^{\pi_{17}+1} - 1) \tag{5.48}$$

$$h(\rho_2, \phi_2) = \pi_1\rho_2\phi_2 P_1^{\pi_4}\,(\pi_{17}K\rho_2^{\pi_{17}+1} - 1) \tag{5.49}$$

These equations are expressed in terms of the functions f, g, and h, which are functions of ρ_2 and ϕ_2 only. It is seen from Equations (5.45, 47) that the solid density changes in response to drag effects, embodied in the terms multiplying the drag parameter π_2, and chemical reaction effects, embodied in terms multiplying the reaction parameter π_1. Drag terms are inherently present in the momentum equation, (5.2), from which Equation (5.45) is derived. Reaction effects arise since the momentum equation (5.2) predicts changes in momentum due to changes in volume fraction. By substituting the volume fraction equation (5.4) into the momentum equation, reaction effects are introduced. Effectively then the momentum equation predicts that solid density changes in response to drag and chemical reaction in the two-equation model. From Equations (5.46, 49) it is seen that volume fraction changes are predicted only in response to chemical reaction. Potential equilibrium states exist when f and h are simultaneously zero. From the functional form of f and h, it is seen that this corresponds to a state where density changes due to drag are balanced by density changes due to reaction and where volume fraction changes are zero due to complete reaction.

When $g(\rho_2,\phi_2) = 0$, and f, $h \neq 0$, infinite gradients are predicted. The condition $g = 0$ is either a complete reaction or solid phase sonic condition as described below. Appendix E shows in detail how for the two-equation model, the solid phase is sonic when Equation (5.51) holds.

$$r = 0 \tag{5.50}$$

$$\rho_2 = (\pi_{17} K)^{\frac{-1}{\pi_{17}+1}} \tag{5.51}$$

When either Equations (5.50) or (5.51) hold, forcing g to zero, it is seen from Equation (5.49) that h is simultaneously zero.

The condition $g(\rho_2,\phi_2) = 0$ leads to difficulties regarding the division by zero. The difficulties in the continuation of the solution through the $g = 0$ state are removed by introducing a new path variable z and considering ξ as an independent variable defined as follows

$$\frac{d\xi}{dz} = g(\rho_2, \phi_2) \qquad \xi(0) = 0 \tag{5.52}$$

In terms of the new independent variable z Equations (5.45, 46) are transformed to the following equations

$$\frac{d\rho_2}{dz} = f(\rho_2, \phi_2) \tag{5.53}$$

$$\frac{d\phi_2}{dz} = h(\rho_2, \phi_2) \tag{5.54}$$

Equations (5.53, 54) are autonomous in the ρ_2-ϕ_2 phase plane. Equation (5.52) may be thought of as an auxiliary relationship to determine ξ once the structure defined by the above equations is determined. Whether Equations (5.53, 54) should be integrated forward or backward in z is a relevant question. The equations should be integrated so that ξ goes from 0 to $-\infty$. From Equation (5.52) it is seen that the direction of change of ξ with respect to z depends on whether the solid phase is subsonic or supersonic. If the initial

state of the solid is unshocked, the solid is locally supersonic, $g > 0$, and a negative dz corresponds to a negative $d\xi$. If the initial state of the solid is shocked, the flow is locally subsonic, $g < 0$, and a positive dz must be chosen to recover a negative $d\xi$.

In the context of this reduced model there are several requirements for an admissible detonation structure. An admissible steady structure is defined by an integral curve which begins at the initial point in the ρ_2-ϕ_2 plane and travels in that plane to an equilibrium position where f and h are simultaneously zero. This point is defined by the intersection of the curves $f = 0$ and $h = 0$. In addition further restrictions are placed on the solution. It is required that the gas and solid thermodynamic variables density, pressure, and temperature, are always positive and real. Also it is required that all physical variables are single-valued functions of the position variable ξ. Based on these restrictions parametric conditions can be obtained for admissibility of a detonation solution.

The conditions under which thermodynamic variables become either negative or imaginary are checked numerically. By examining a few limited cases, it has been found that there are regions in the ρ_2-ϕ_2 plane where gas phase pressure, density, and temperature are negative. These regions are bounded by curves in the ρ_2-ϕ_2 plane where gas density, pressure, and temperature are zero. In solving the cubic equation for the gas phase properties, imaginary gas phase quantities are sometimes predicted. It has been found numerically that the border of the imaginary region corresponds to a sonic condition in the gas phase.

The geometry of the $f = 0$ and $h = 0$ curves is critical in determining the integral curve which defines the steady state solution. Depending on the relative orientation of these curves and the initial state, many classes of solutions, each with a distinct character, are available. Some solutions reach an equilibrium state, defined at the intersection of the $f = 0$ and $h = 0$ curves. The structure of the steady detonation solution is strongly influenced by the nature of the equilibrium point, which can be classified as a source, sink, saddle, or spiral. For example, if the equilibrium point to which the integral curve is drawn is a sink, then a continuum of wave speeds are found for which steady detonations are allowed. If the equilibrium point is a saddle, there is only one wave speed which will bring the integral curve to the equilibrium position. For some wave speeds the orientation of the $f = 0$ and $h = 0$ curves prevents solutions from reaching an equilibrium state; these solutions cannot be classified as steady solutions. Among these types of solutions are those that pass through a solid sonic point and become physically unacceptable, multivalued functions of distance. Figure 5.6 shows sketches of phase planes for two classes of solutions, one an acceptable detonation structure, the other a nonphysical solution.

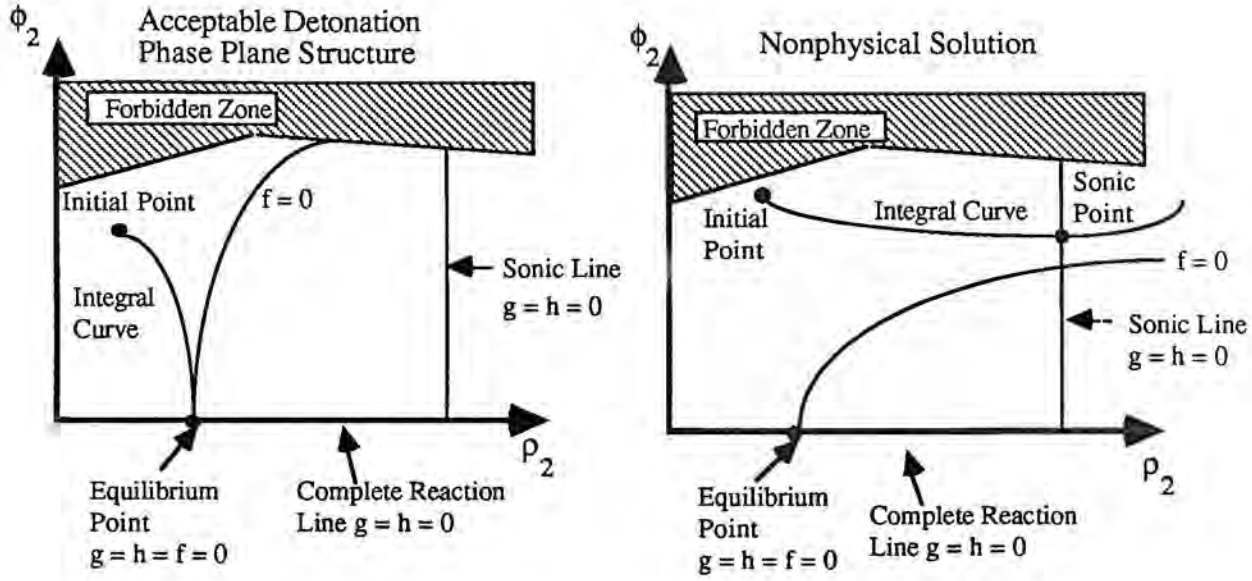

Figure 5.6 Phase Plane Sketches of Physical and Nonphysical Solutions

Each sketch shows the separatrix lines f = 0 and g = h = 0. The equilibrium position is at the intersection of these curves. Each curve shows a solid phase sonic line, g = h = 0, forbidden regions in which gas phase properties are not physical, and integral curves which originate from the initial condition. For the acceptable structure the integral curve travels from the initial state to the equilibrium position. By changing the flow conditions, the topology of this phase plane is altered, shown in the adjacent sketch. In this sketch, the integral curve is driven through the solid sonic line and is incapable of reaching the equilibrium point. As explained below, past the solid sonic line, the solution is double-valued and therefore not physical.

Thermodynamic variables become double-valued functions of distance when a solid sonic condition (g = 0) is reached at a non-equilibrium point in the phase plane ($f \neq 0$). From Equation (5.52), it is seen that the direction of change of ξ with respect to z changes when the solution passes through a solid sonic point. Thus ξ, which starts at zero and moves towards $-\infty$ as reaction progresses, changes direction and moves towards $+\infty$ at a critical point ξ_{min} when a solid sonic condition is reached. Through this point Equations (5.53, 54) predict a continuous variation of density and volume fraction. At the solid sonic point the derivatives of ρ_2 and ϕ_2 with respect to z are finite, and the derivatives with respect to ξ are infinite. At any given location ξ, $\xi > \xi_{min}$, two values of each thermodynamic variable will be predicted. This is physically unacceptable.

Results analogous to one-phase ZND theory can be obtained with the two-equation model. For the input conditions of Table I, with the heat transfer coefficient h = 0 and compaction viscosity $\mu_c \rightarrow \infty$, an initial porosity greater than 0.19, and an initially shocked gas and unshocked solid, a CJ structure can be defined. In these limits there is no heat transfer or volume change due to pore collapse. The CJ wave speed is determined from solving the earlier-described equation set (5.21-23). Wave speeds less than the CJ speed are rejected because imaginary gas phase quantities are predicted near the complete reaction end state. Wave speeds greater than CJ are admitted by this model and correspond to the strong ZND solution. Such a wave leaves the gas at a velocity which is subsonic relative to the wave front. As in ZND theory, piston support is required to prevent rarefaction waves from damping the reaction zone structure. For the CJ wave, the final velocity is sonic and no piston support is necessary to support the wave.

The solution is driven to a sink in the ρ_2-ϕ_2 plane. To show this point is a sink, one first finds the equilibrium point by solving the algebraic problem $f(\rho_2, \phi_2) = 0$, $h(\rho_2, \phi_2) = 0$. The differential equations (4.53, 54) are then linearized about this equilibrium point. These linear differential equations can be solved exactly to determine the behavior of any integral curve which approaches the equilibrium point. In this study, for an shocked solid and shocked or unshocked gas, it was found that all integral curves in the neighborhood of the equilibrium point were attracted to the equilbrium point; in the terminology of ordinary differential equation theory, that point is classified as a sink.

The ordinary differential equations of the two-equation model and full, four-equation model were solved numerically. Integration was performed using the IMSL subroutine DVERK, a fifth and sixth order Runge-Kutta routine, on the UIUC Cyber 175. Step sizes were chosen such that none of the fundamental variables, ρ_2, ϕ_2, v_2, and P_2, changed by more than 5% in value in any given integration step. Typically about two hundred integration steps were sufficient to describe the reaction zone. A typical integration took twenty seconds to complete.

For an initial solid volume fraction of 0.70, Figure 5.7 shows a plot of the phase plane for a CJ wave speed of 7369 m/s. This curve shows the sonic line (g = h = 0) on ρ_2 = 1.35, the complete reaction line (g = h = 0) on $\phi_2 = 0$ and the f = 0 line. It is seen from this curve that the only equilibrium point is at (ρ_2,ϕ_2) = (1.04, 0). The vector field superimposed on this figure, defined by Equations (5.53, 54), shows this point is a sink which is confirmed by a local linear analysis near the equilibrium point. The integral curve connecting the initial state to the equilibrium point is also plotted on this figure. This curve is obtained by numerical integration of Equations (5.53, 54). This integral curve moves in a direction defined by the vector field of the phase plane. Curves of zero gas phase

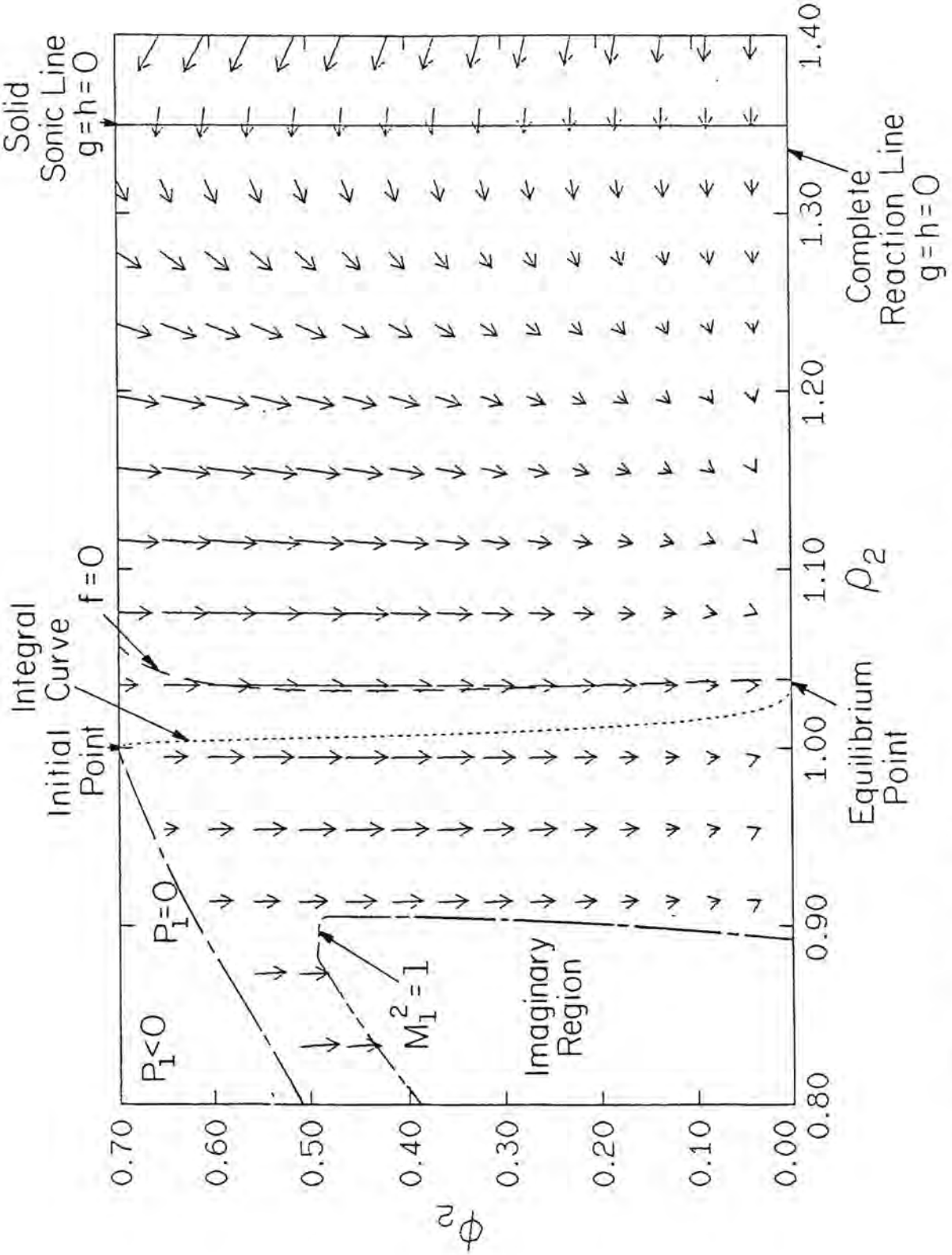

Figure 5.7 Phase Plane for CJ Detonation with Leading Gas Phase Shock.

pressure are plotted in this figure along with the curve defining the boundary between pure real and imaginary gas phase quantities. The gas velocity is locally sonic ($M_1^2 = 1$) on the boundary of the region where imaginary gas phase properties exist. This indicates that the solution is non-physical if the gas passes through a sonic condition at a point of incomplete reaction.

When the full model equations are considered, general results from the two-equation model are retained. It is more difficult to interpret these results as the phase space is four-dimensional. With a given set of initial conditions, the gas phase CJ end state is the same whether the two-equation or four-equation model is used. The solid phase end state and details of the reaction zone structure do depend on which model equations are used. Plots of predicted detonation structure are shown in Figure 5.8, which plots solid and gas density, lab velocity u, pressure, temperature, Mach number, particle radius, and solid volume fraction versus distance ξ. Also plotted on this figure are results from the two-equation model. It is seen that both models predict results of the same order of magnitude. Gas phase quantities are nearly identical for both models. While there are small differences in solid phase predictions, these results are remarkable as there is no real basis to assume the the limits taken are appropriate for this class of models. These results show that material compaction and heat transfer are not important mechanisms in determining two-phase detonation structure and that there is justification in using the two-equation model as a tool for understanding the full model equations. A comparison of some results of the two models is given in Table II.

In Figure 5.8 it is seen that the gas phase is shocked while the solid phase is unshocked. It is noted from Figure 5.8c that the gas pressure continues to rise past the initial shock gas pressure, in contrast to the results of the simple one-phase ZND theory, which predicts the pressure to be a maximum at the shock state. From this maximum, known as the "Von Neumann spike," the pressure decreases to the equilibrium CJ pressure. It should also be noted that the high gas phase temperature (~ 10,000 K) indicates that ionization, dissociation, and radiative heat transfer could be important mechanisms in the reaction zone. These effects have not been considered but could be incorporated into future work.

Non-physical solutions are now considered. Such solutions exist below a critical value of initial solid volume fraction. The critical point is shown in Figure 5.9, which plots CJ wave speed versus initial bulk density ρ_a ($\rho_a = \rho_{10}\phi_{10} + \rho_{20}\phi_{20}$). This figure also compares predictions of this model with those of the unsteady model of Butler and Krier [1] and those of the equilibrium thermochemistry code TIGER given in Ref. 1. The feature of a critical initial bulk density has not been identified by other models.

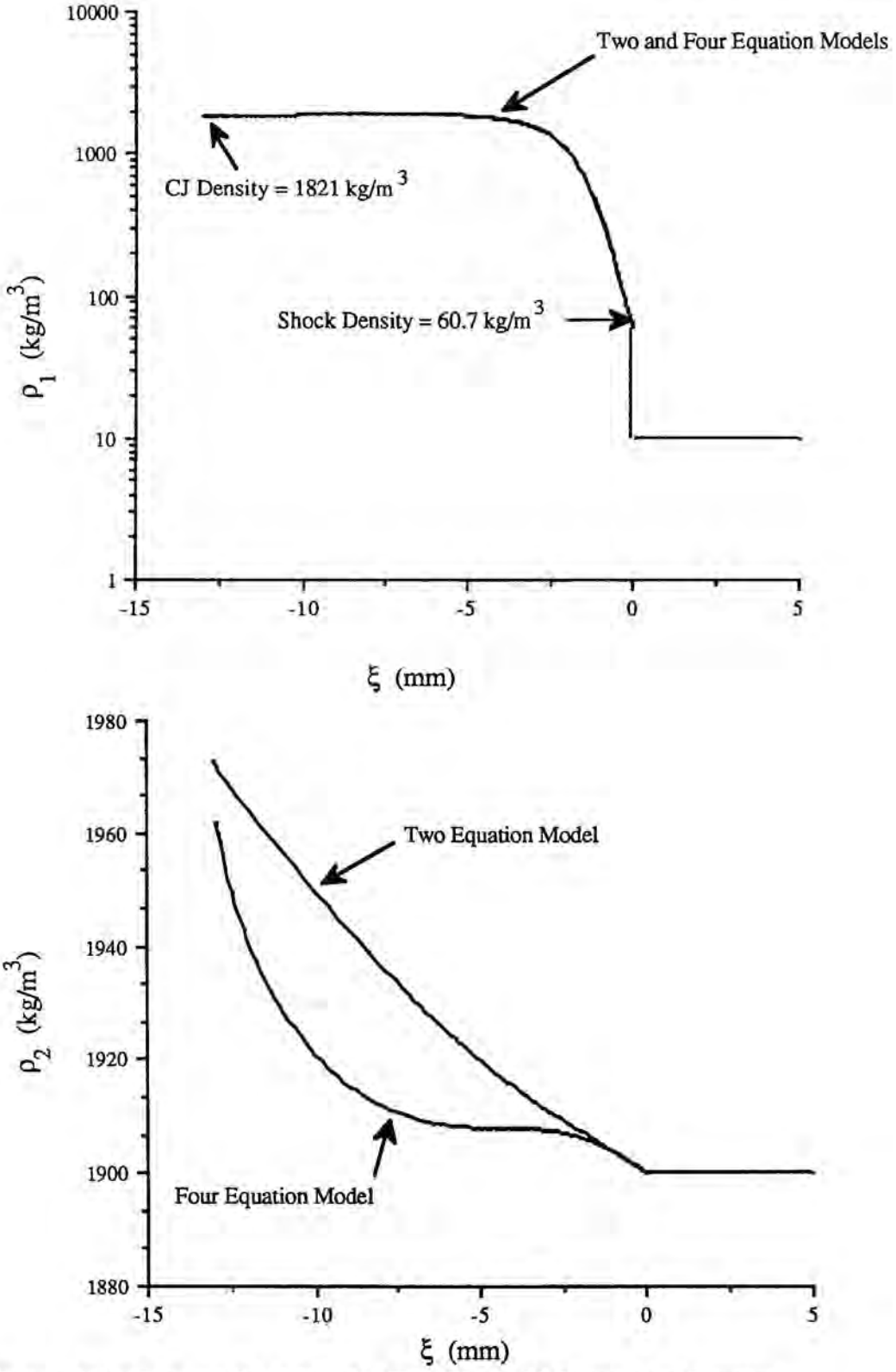

Figure 5.8a Gas and Solid Density Two-Phase CJ Detonation Structure

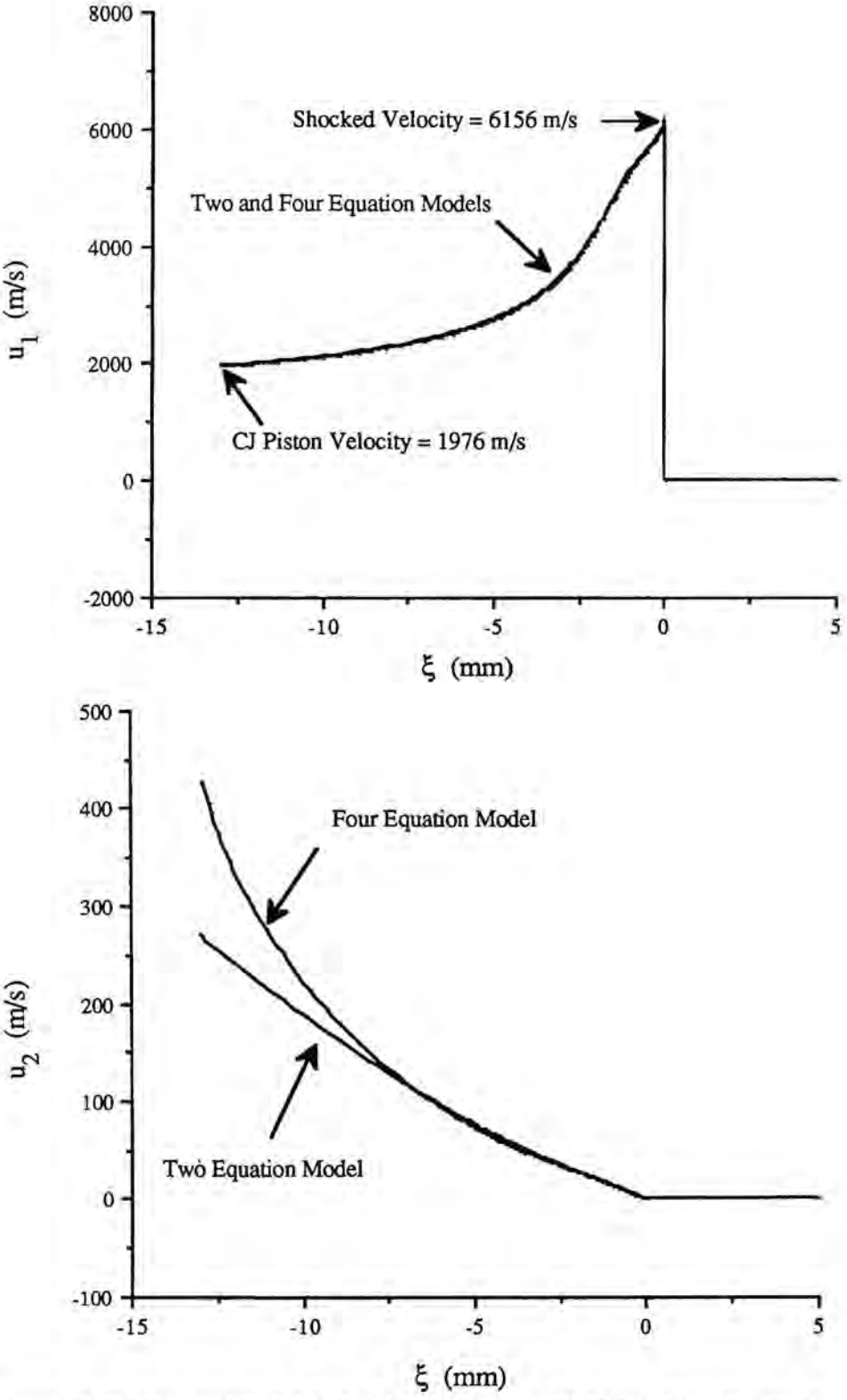

Figure 5.8b Gas and Solid Velocity Two-Phase CJ Detonation Structure

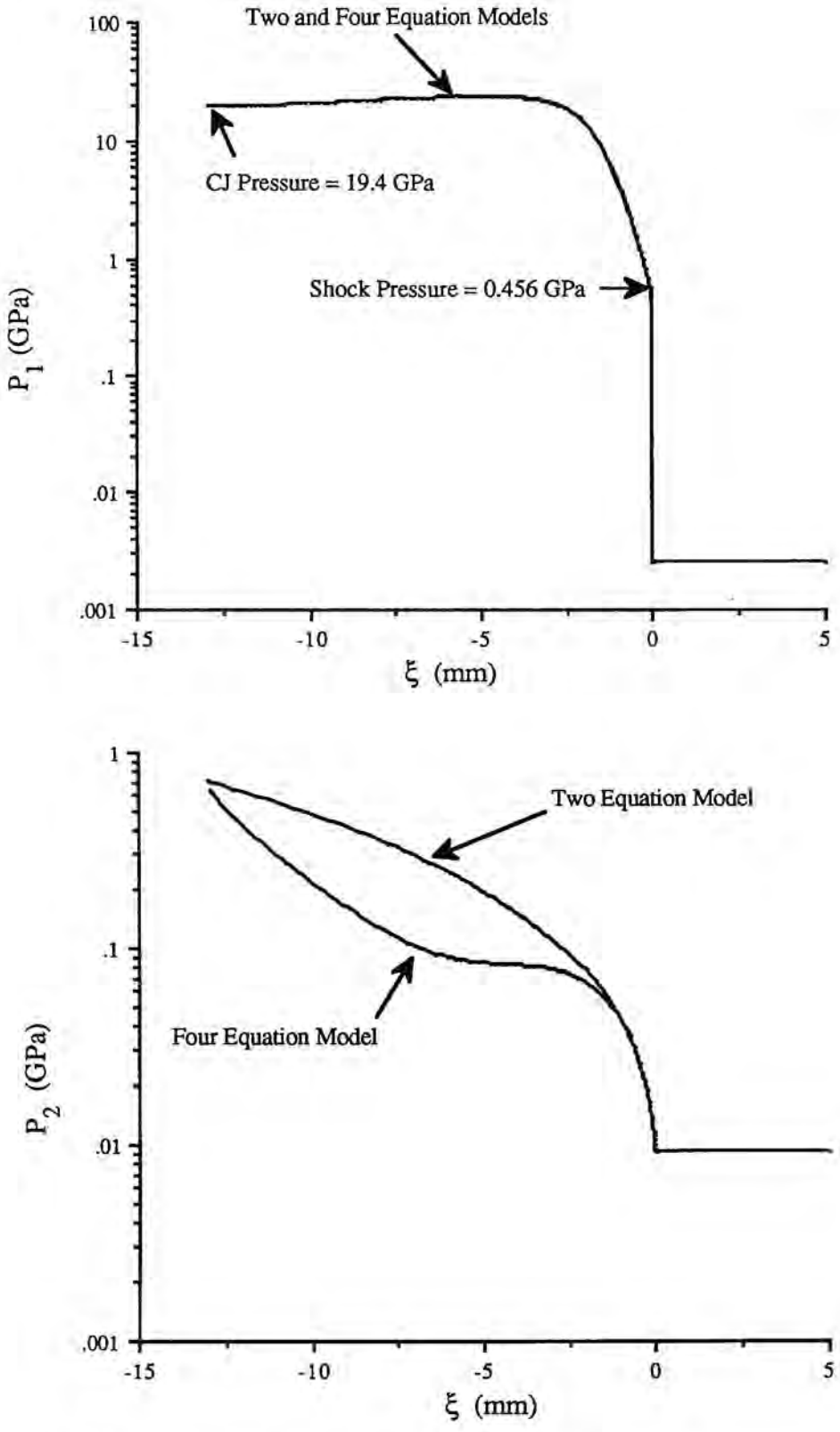

Figure 5.8c Gas and Solid Pressure Two-Phase CJ Detonation Structure

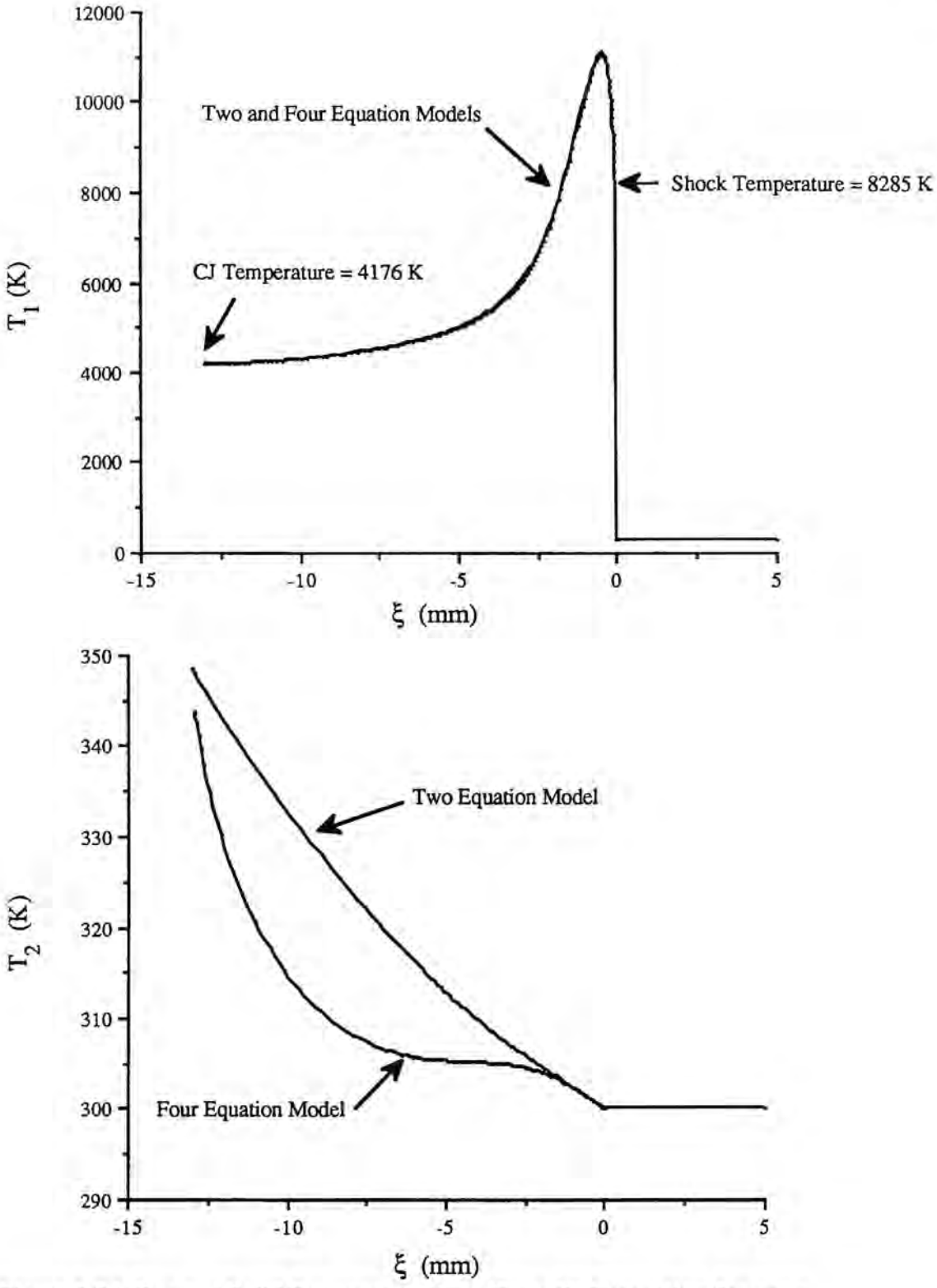

Figure 5.8d Gas and Solid Temperature Two-Phase CJ Detonation Structure

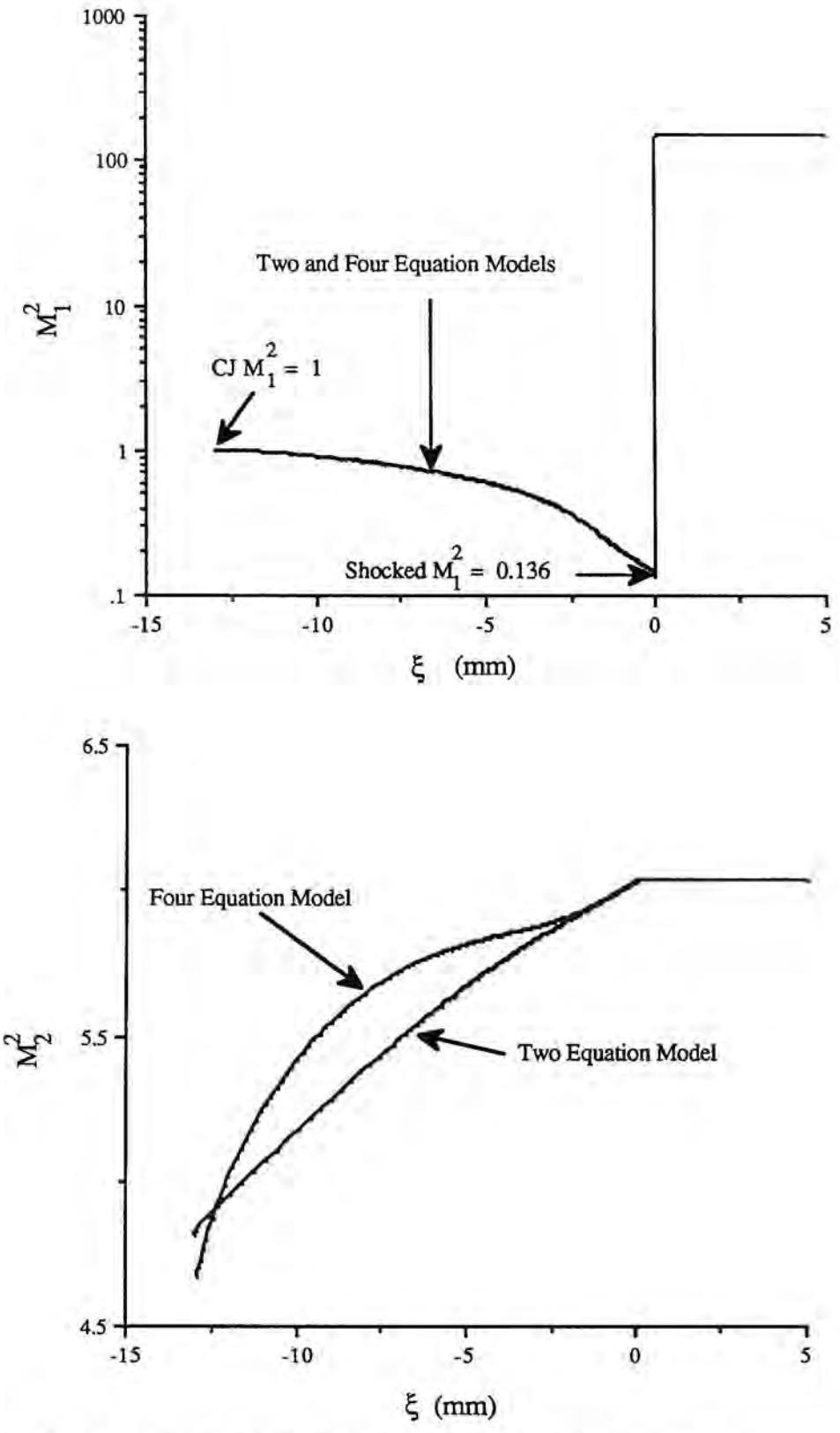

Figure 5.8e Gas and Solid Mach Number Two-Phase CJ Detonation Structure

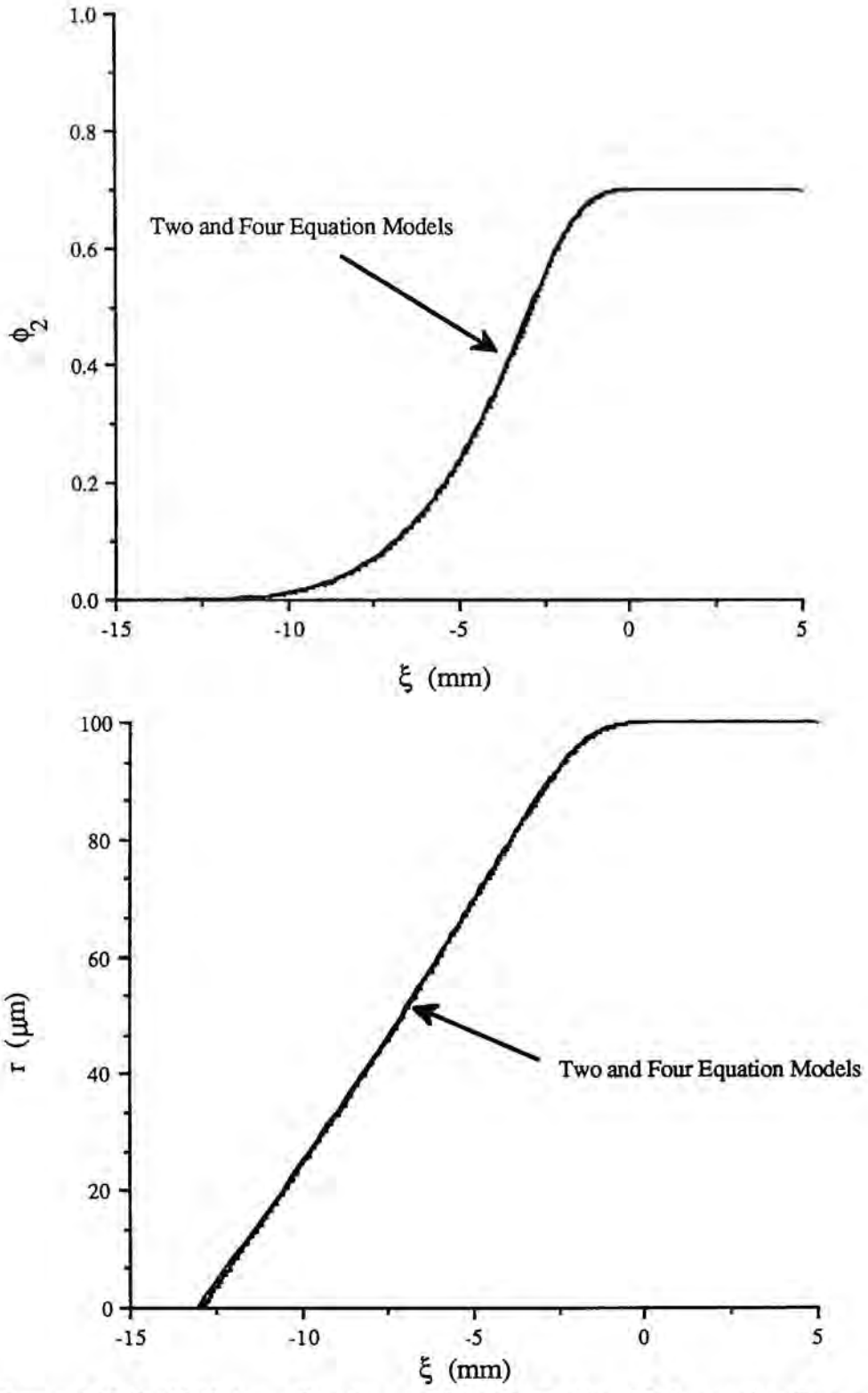

Figure 5.8f Solid Volume Fraction and Particle Radius CJ Detonation Structure

Table II

COMPARISON OF TWO AND FOUR EQUATION MODEL PREDICTIONS FOR CJ WAVES WITH AND WITHOUT LEADING GAS PHASE SHOCK

	Leading Gas Shock		No Leading Gas Shock	
	Two-Equation	Full	Two-Equation	Full
Initial Bulk Density	1,333 kg/m^3	1,333 kg/m^3	1,333 kg/m^3	1,333 kg/m^3
Reaction Zone Length	13.00 mm	12.89 mm	62.1 mm	61.7 mm
CJ Wave Speed	7,369 m/s	7,369 m/s	7,369 m/s	7,369 m/s
CJ Pressure	19.4 GPa	19.4 GPa	19.4 GPa	19.4 GPa
CJ Density	1,821 kg/m^3	1,821 kg/m^3	1,821 kg/m^3	1,821 kg/m^3
CJ Temperature	4,176 K	4,176 K	4,174 K	4,174 K
CJ Gas Velocity	1,976 m/s	1,976 m/s	1,974 m/s	1,974 m/s
(CJ Gas Mach Number)^2	1	1	1	1
Maximum Gas Temperature	11,119 K	11,108 K	4,174 K	4,174 K
Final Solid Pressure	0.716 GPa	0.636 GPa	0.716 GPa	0.636 GPa
Final Solid Density	1,973 kg/m^3	1,962 kg/m^3	1,973 kg/m^3	1,962 kg/m^3
Final Solid Temperature	349 K	344 K	349 K	344 K
Final Solid Velocity	272 m/s	429 m/s	272 m/s	428 m/s
(Final Solid Mach Number)^2	4.82	4.67	4.82	4.67

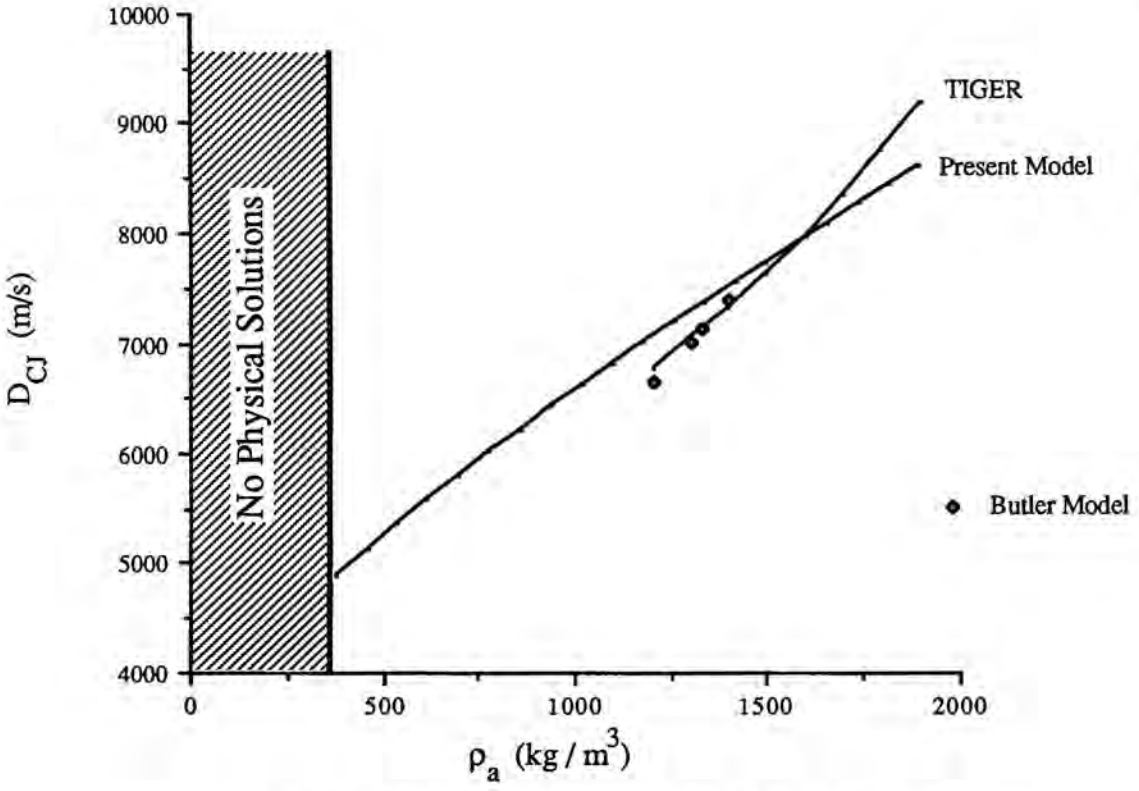

Figure 5.9 CJ Wave Speed vs. Initial Bulk Density

For a value of initial solid volume fraction of 0.20, very near the critical bulk density, an acceptable detonation structure is obtained. A phase portrait, vector map, and integral curve is shown in Figure 5.10. The figure resembles Figure 5.6, but the curves have all been skewed. Note that the integral curve nearly reaches the sonic state before turning around and travelling to the complete reaction end state.

For an initial solid volume fraction of 0.15, a non-physical solution is obtained for a CJ wave speed. The two-equation model's phase plane is shown in Figure 5.11. The integral curve in this plane passes through the solid sonic line at a non-equilibrium point causing the solution to become double-valued. A plot of the solid phase Mach number is shown in Figure 5.12 for both the two and four equation models. Again both models predict nearly identical results. It is seen from Figure 5.12 that infinite gradients with respect to ξ are predicted precisely at the point where the solid phase reaches a sonic velocity ($M_2^2 = 1$).

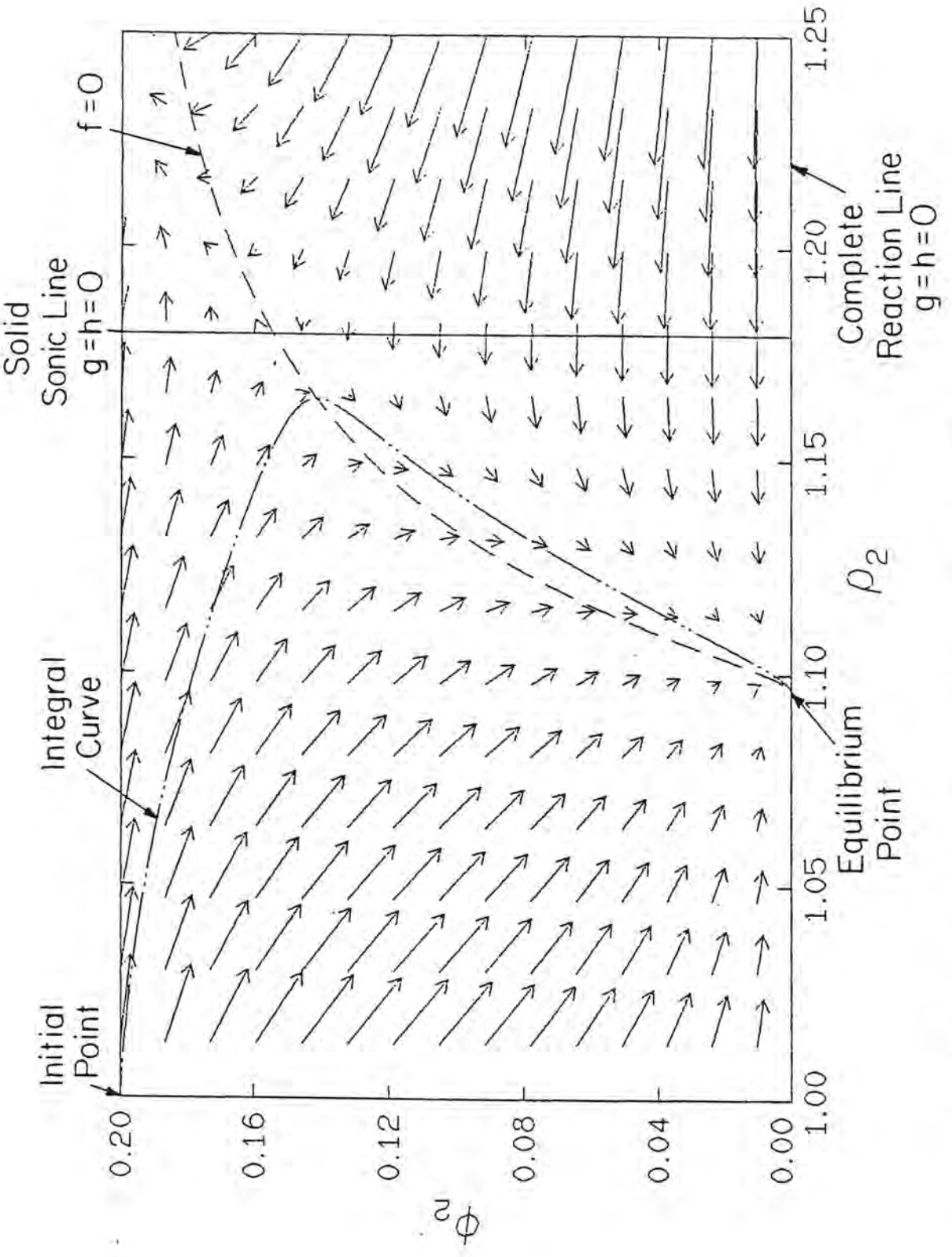

Figure 5.10 Phase Plane for CJ Detonation Near Critical Initial Bulk Density

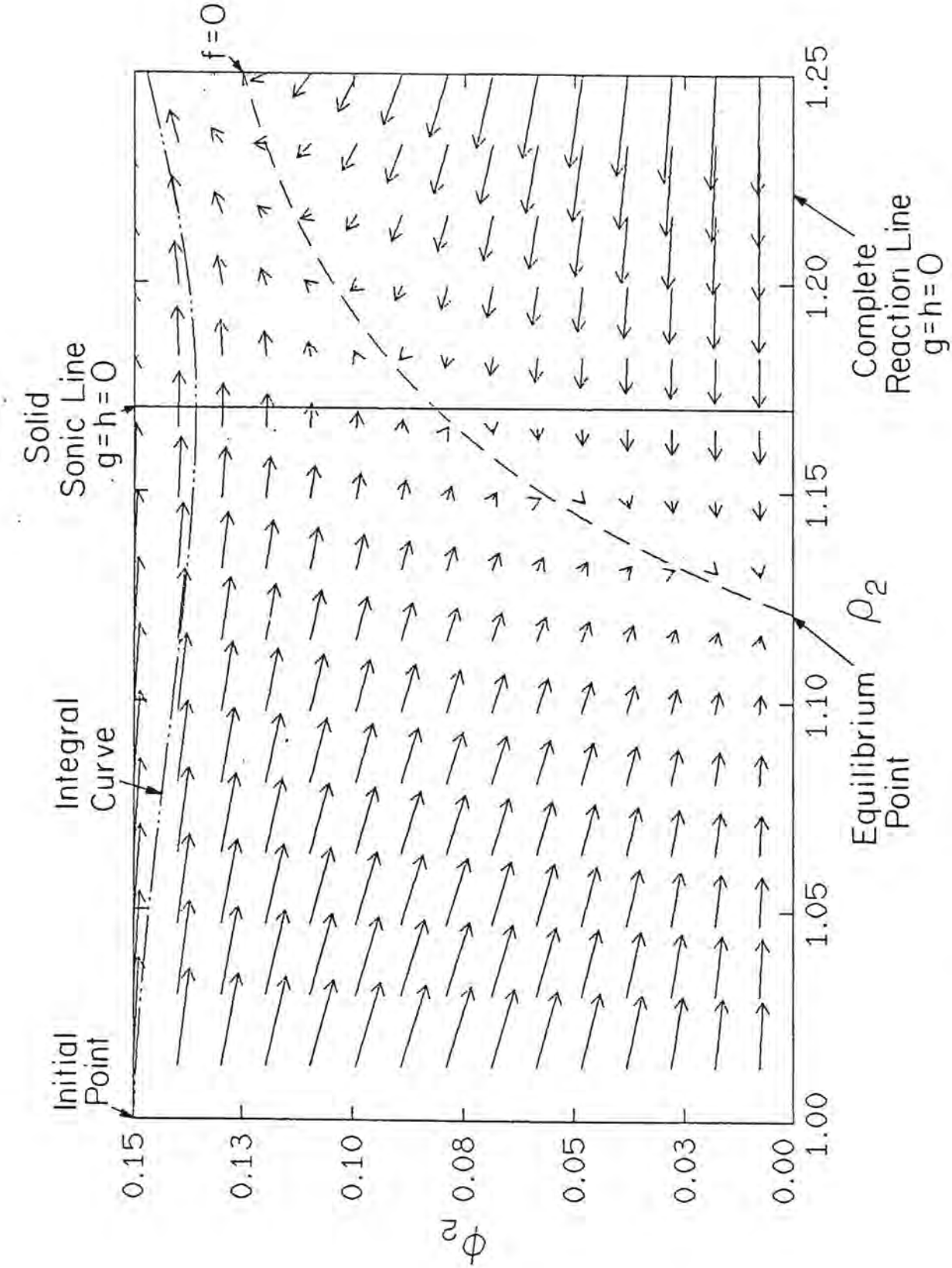

Figure 5.11 Phase Plane for Non-Physical Solution

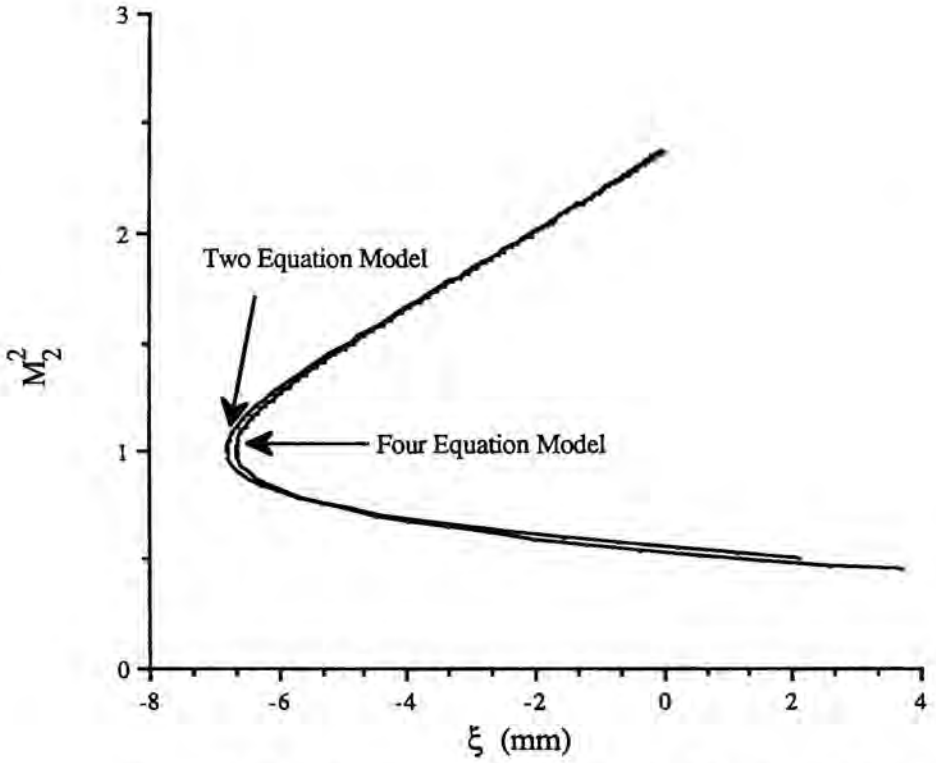

Figure 5.12 Solid Phase Mach Number for Nonphysical Solution

Solutions with no leading shock in either the gas or solid phase are also admitted by this model. Figure 5.13 shows the phase portrait, vector map and integral curve for a CJ wave with no leading gas or solid shock propagating through a mixture with an initial solid volume fraction of 0.70. Again, the equilibrium point is a sink. As summarized in Table II, the main difference between this case and the case with the leading gas phase shock is that the reaction zone is much longer (62 mm vs. 13 mm) for no leading shock in the gas phase. Again both two and four equation models predict similar results. The CJ gas phase end state is identical regardless of whether the initial gas state is shocked or unshocked, or whether the two or four equation model is used. This is because the complete reaction CJ state is independent of the structure of the detonation. Small differences in the CJ temperatures and gas velocities can be attributed to numerical roundoff errors as the CJ state is extremely sensitive to the CJ wave speed. In general the solid end state can vary for each state presented in Table II. It is noted that the solid phase end state predicted by the two-equation model is nearly the same for both the unshocked and shocked gas as is the solid phase end state for the full equation model.

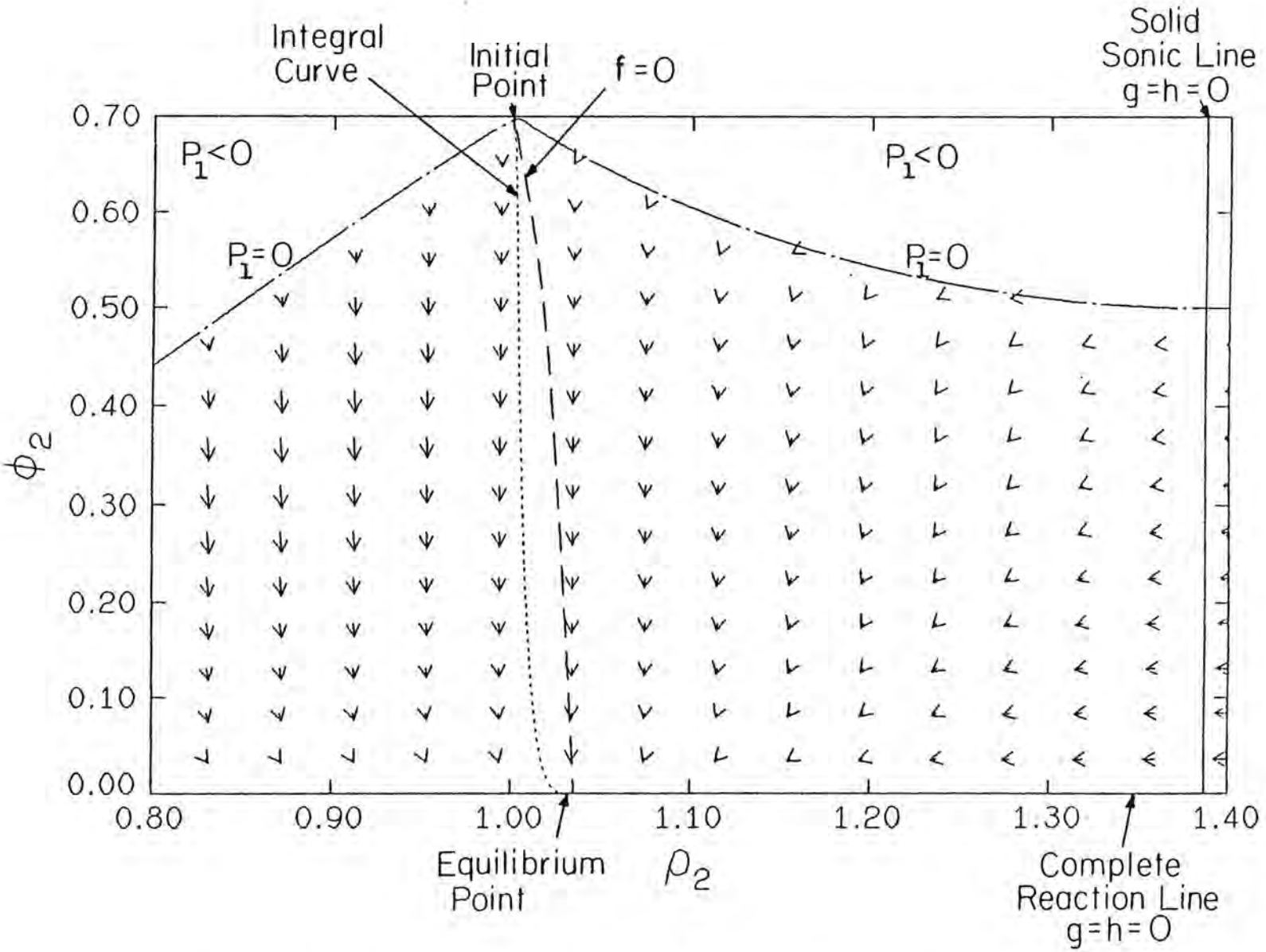

Figure 5.13 Phase Plane for CJ Detonation with no Leading Gas Phase Shock

For wave speeds greater than CJ, strong and weak waves can be predicted. For an initial solid volume fraction of 0.70 and a wave speed of 8,000 m/s (which is greater than the CJ wave speed of 7369 m/s) Figures 5.14 and 5.15 show plots of the two-equation model's phase portraits for the strong (initially shocked gas) and weak (initially unshocked gas) case. In each case the solid is initially unshocked. The equilibrium points are sinks in both cases. The results of these calculations for both two and four equation models are summarized in Table III. For the strong case the reaction zone is shorter than for the corresponding CJ wave with a leading gas phase shock. For the weak case the reaction zone is longer than for the corresponding CJ wave without a leading gas phase shock. Again two and four equation models predict similar results.

This study predicts a continuum of two-phase detonation wave speeds as a function of piston velocity. CJ wave speed is plotted as a function of piston velocity in Figure 5.16. For wave speeds greater than CJ, piston support is required to support the wave. The CJ wave can propagate with or without piston support as the complete reaction point is a gas phase sonic point.

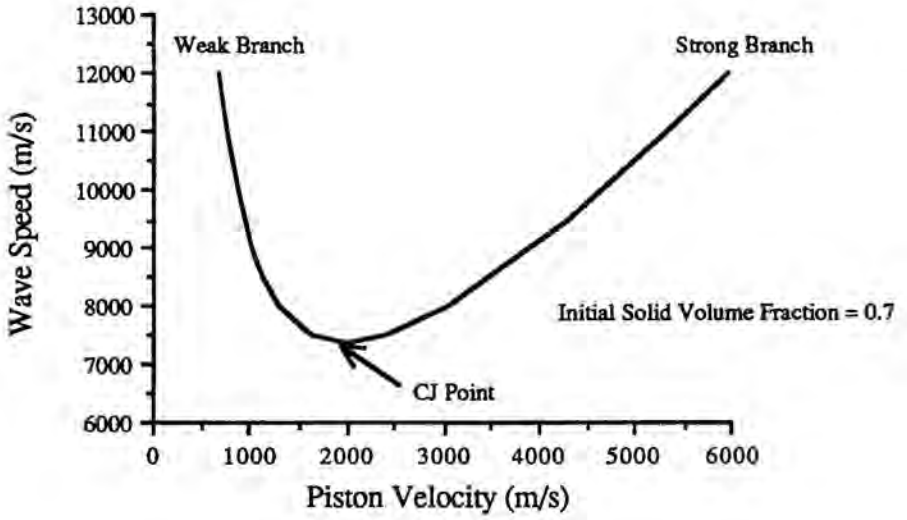

Figure 5.16 Two-Phase Detonation Wave Speed vs. Piston Velocity

For piston velocities below CJ, a continuum of weak waves are predicted. The implications of this are unclear. As the complete reaction point is supersonic, the piston support is not necessary. This suggests that the solution may not be unique. Simple one-phase ZND theory also predicts a continuum of weak waves. Fickett and Davis [40]

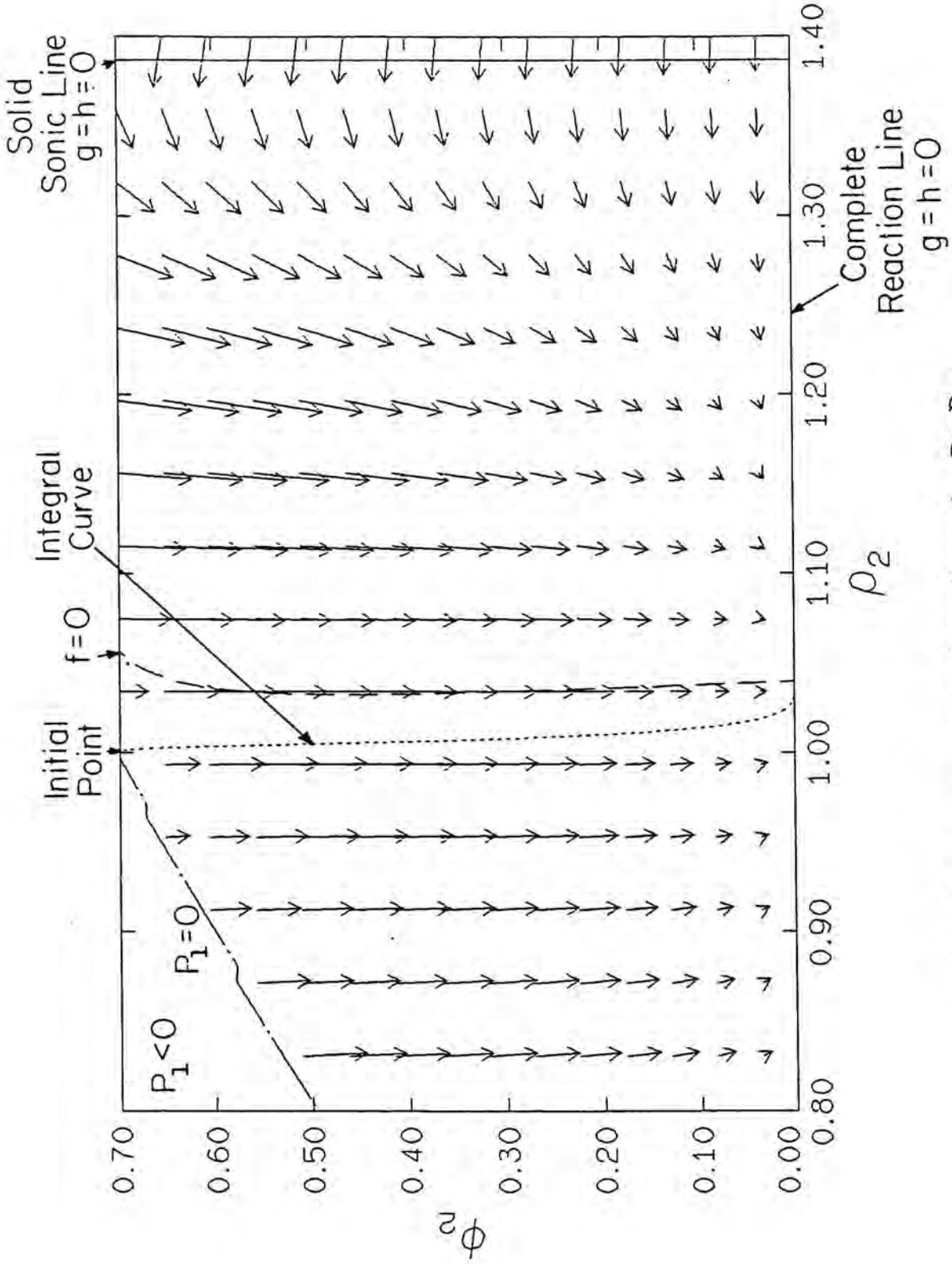

Figure 5.14 Phase Plane for Strong Detonation, $D > D_{CJ}$

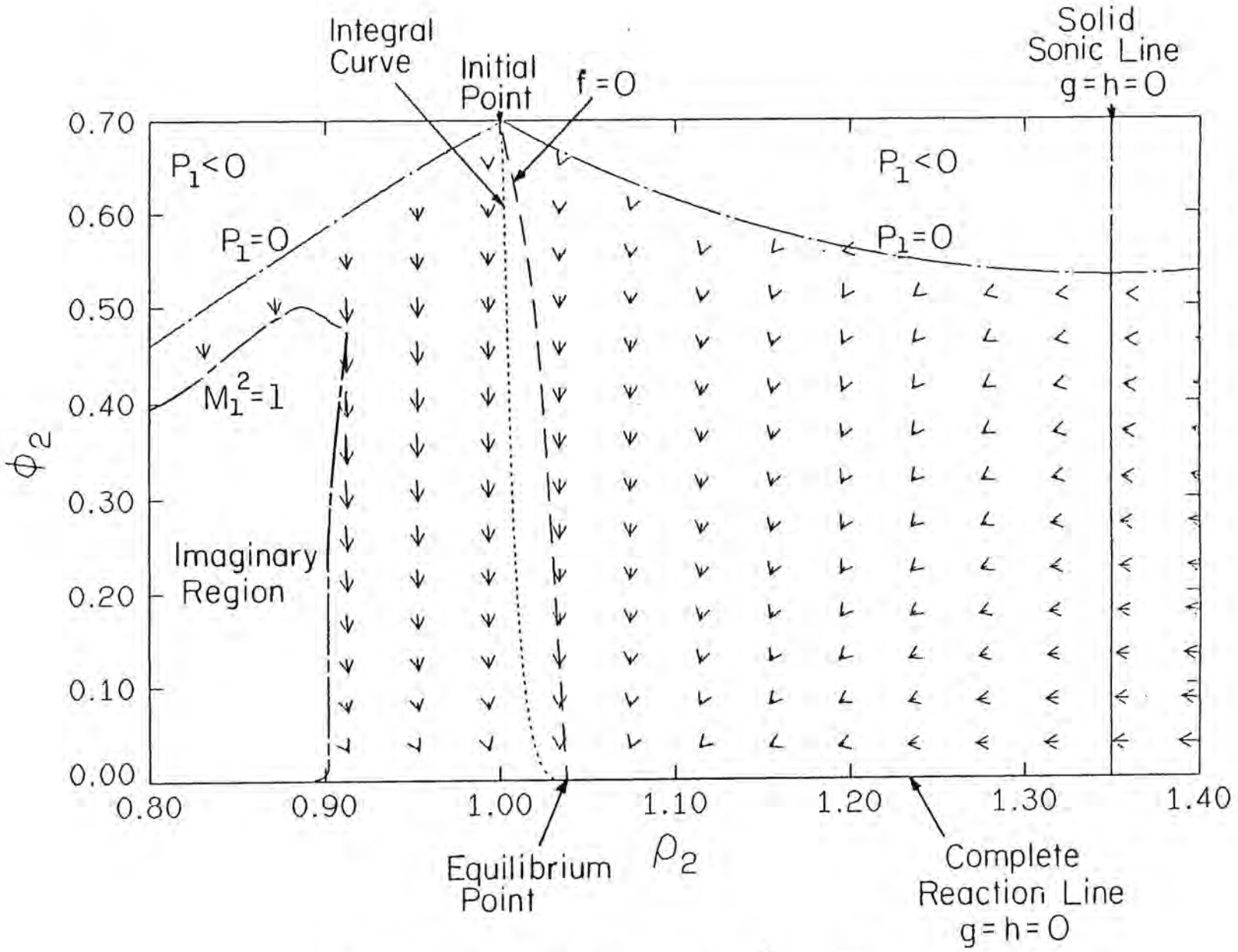

Figure 5.15 Phase Plane for Weak Detonation, $D > D_{CJ}$

Table III

COMPARISON OF TWO AND FOUR EQUATION MODEL PREDICTIONS FOR STRONG AND WEAK DETONATIONS, D = 8,000 M/S

	Leading Gas Shock (Strong)		No Leading Gas Shock (Weak)	
	Two-Equation	Full	Two-Equation	Full
Initial Bulk Density	1,333 kg/m^3	1,333 kg/m^3	1,333 kg/m^3	1,333 kg/m^3
Reaction Zone Length	10.2 mm	10.1 mm	71.4 mm	70.9 mm
Wave Speed	8,000 m/s	8,000 m/s	8,000 m/s	8,000 m/s
Final Gas Pressure	32.3 GPa	32.3 GPa	13.8 GPa	13.8 GPa
Final Gas Density	2,145 kg/m^3	2,145 kg/m^3	1,590 kg/m^3	1,590 kg/m^3
Final Gas Temperature	5,274 K	5,274 K	3,710 K	3,710 K
Final Gas Velocity	3,029 m/s	3,029 m/s	1,291 m/s	1,291 m/s
(CJ Gas Mach Number)^2	0.567	0.567	1.99	1.99
Maximum Gas Temperature	12,526 K	12,514 K	3,710 K	3,710 K
Final Solid Pressure	0.744 GPa	0.676 GPa	.657 GPa	.542 GPa
Final Solid Density	1,975 kg/m^3	1,966 kg/m^3	1,967 kg/m^3	1,953 kg/m^3
Final Solid Temperature	351 K	346 K	345 K	337 K
Final Solid Velocity	306 m/s	484 m/s	273 m/s	432 m/s
(Final Solid Mach Number)^2	5.63	5.44	5.78	5.66

discuss this issue for one-phase theory. Though this issue is still not settled for the one-phase model, some have suggested that the weak waves may be ruled out as unphysical because of a lack of an initiation mechanism. Fickett and Davis show results of more complicated one-phase models which indicate that a unique weak wave speed exists when such mechanisms as diffusive heat and momentum transfer are taken into account. A similar result may hold for two-phase detonations.

VI. CONCLUSIONS AND RECOMMENDATIONS

Compaction Waves

The piston-impact problem for a compressible porous solid has been solved in the context of a steady two-phase model neglecting gas phase effects. With this model, it is possible to obtain an exact solution for the compaction wave speed, final porosity, and final pressure. The degree of accuracy of the predictions can be attributed to the ad hoc estimates for the non-ideal solid parameter and the assumed form of the static pore collapse function, f. Within the framework of this model it is possible to understand the general features of a compaction wave. Two classes of compaction waves have been identified, subsonic waves with no leading shock, and supersonic waves with a leading shock. It is predicted that the magnitude of the supporting piston velocity determines which class of wave exists, with low piston velocities resulting in a subsonic structure and high piston velocities resulting in a supersonic structure.

A compaction wave with structure has been predicted because a dynamic pore collapse equation has been used. As summarized by Kooker [62], many compaction wave models do not consider dynamic pore collapse; rather they enforce static pore collapse (P =f) throughout the flow field. In zero gas density limit, such an assumption results in a compaction wave without structure. The pressure discontinuously adjusts to a static equilibrium value. However, it is not established whether two-phase models with static pore collapse are hyperbolic, a necessary condition if discontinuities are to be admitted and for a well-posed initial value problem. For two-phase models assuming pressure equilibrium between phases but not incorporating quasi-static compaction data, Lyczkowski, et. al. [53] have identified regimes in which unsteady two-phase equations are not hyperbolic.

There are many ways to extend the compaction wave study. By including the effects of the gas phase, it should be possible to determine how the gas phase's presence modifies the compaction wave structure. By including the effect of particle size in f, it should be possible to model the experiments of Elban, et al. [63] which show that the static pore collapse stress level is a function of both volume fraction and particle size. By considering the solid to be composed of particles, it may be possible to model the effect of particle breakup on the results when f is assumed to be a function of particle size.

It is thought that the most important contribution of this study is that existence conditions have been predicted for a steady, one-dimensional, two-phase detonation in a granular material. The available detonation solutions are restricted by both algebraic equilibrium end state analysis and by an analysis of the structure of the steady wave.

Though gas phase end state analysis has been performed by many others, it is believed that the work here clarifies this analysis by finding simple analogies between one-phase CJ conditions and two-phase CJ conditions along with simple corrections for non-ideal gas phase effects. These simple two-phase conditions are analogous to, but not identical to, the one-phase CJ condition and cannot be obtained a priori from the one-phase model. The similarity in results is due to the similarities which exist between the one-phase conservation equations and two-phase conservation equations. The common notion that one-phase CJ results can be directly applied to two-phase systems is disproved by this work.

The variation of CJ properties with initial bulk density reported here accurately matches the TIGER predictions for a single set of gas phase state parameters. Thus it is not necessary to vary the gas phase state equation parameters as initial bulk density changes to match the TIGER predictions as done by other researchers. In Ref. 47 a virial equation of state identical in form to the gas state equation of this study was used. In that study as the initial bulk density varied, the value of b was varied within the range from 0.00361 m^3/kg to 0.00486 m^3/kg in order to match the TIGER predictions. As shown in Figure 5.3 of the present study the CJ properties are very sensitive to changes in b on the order of those studied in Ref. 47. In Ref. 2 a JWL gas state equation is used, and it is reported that CJ data is adequately reproduced when the constants are allowed to vary with the initial bulk density. It is believed that the approach of the present study in determining CJ properties has the advantage over the approach taken in Refs. 47 and 2. Though all the studies fix gas state equation parameters so that CJ predictions or data is matched, a single set of parameters is used only in the present study.

An analysis of the structure of a two-phase detonation wave has further restricted the class of available steady solutions. The structure analysis has shown that below a critical initial bulk density no steady solution can exist when the solid particles reach a sonic state. The mathematical consequence of this is that the solution is becomes a double-valued function of distance, a physically unacceptable result. This particular result and the general technique of using structure analysis to limit the available solutions is new to two-phase detonation theory.

As a result of this study it is possible to predict the features of a steady two-phase detonation structure. It has been shown that when a leading shock wave exists in the gas phase and the solid is unshocked, that two-phase equivalents to the one-phase ZND strong and CJ solutions are predicted. As in ZND theory, the two-phase theory predicts that piston support is required for the strong solution to exist, and that a two-phase CJ detonation can propagate with or without piston support. It has also been shown that when both the gas and solid phases are unshocked, that the model equations yield two-phase equivalents of weak and CJ solutions. These types of solutions are also found using the simple one-phase ZND theory but are commonly dismissed because it is thought there is no mechanism to initiate reaction. The model yields such solutions because the functional form of the combustion model allows a small amount of reaction to occur even at ambient conditions. The model allows the small heat released by the reaction to accumulate and cause a thermal explosion after an induction time.

This work has clarified the role of shock jumps in two-phase detonation theory. No previous work on two-phase detonation theory has considered the four possible states admitted by the shock jump conditions. This study has shown that two-phase detonation structure is possible when the gas phase is shocked or unshocked and the solid is unshocked. The possibility of a two-phase detonation with a shocked solid has not been ruled out; an example of such a detonation has not been found yet. This study does not consider how the structure of an unshocked solid and shocked gas can arise. To show how this could occur would require an unsteady analysis which is beyond the scope of this study.

To speculate on how such a scenario could develop, on could imagine a slow, unconfined burning of reactive particles. If the system were suddenly confined, a local region of high gas pressure could develop which could give rise to a propagating shock wave in the gas but not the solid. It should also be said that the idea of shocked gas and unshocked solid is common in the literature of shock waves in dusty gases. A standard assumption is that there is a shock wave in the gas but that the solid particles are incompressible, thus unshocked. Rudinger [64] provides an example of such a model.

This study has for the first time unambiguously identified a finite-valued gas and solid complete reaction end state. Though others have discussed the gas phase complete reaction end state, the solid end state has never been considered. In each of the physical detonation solutions presented here the final values of both the solid and gas can be precisely stated. In all cases, the complete reaction end state analysis allows the final gas phase properties to be determined. For the two-equation model, the final solid properties can be determined by an algebraic analysis without regard to the detonation structure.

The complete reaction singularity which exists due to the 1/r terms in the governing equations leads one to question whether unbounded properties are predicted at complete reaction. Previous studies have neglected this question. Here it has been shown that a two-phase detonation can be predicted when proper account is taken for the complete reaction singularity.

This study has also identified for the first time the importance of sonic singularities in two-phase detonation systems. It has been shown that in general if a sonic condition is reached in the solid phase, that double-valued properties are predicted, and that if a sonic condition is reached in the gas phase at a point of incomplete reaction, that imaginary gas phase properties are predicted. The sonic conditions are particular for each phase and have no relation to the mixture sound speed.

Techniques which are new in the two-phase detonation modeling field have been used to simplify the governing equations. An algebraic method for uncoupling the mixture mass, momentum, and energy equations to solve for gas phase variables in terms of solid phase variables has been developed. It has been shown that the equations can be reduced to a set of four uncoupled ordinary differential equations in four unknowns and how in the limit of zero heat transfer and compaction these equations reduce to two ordinary differential equations. The two-equation model makes it possible to exploit the simple two-dimensional phase plane to gain understanding of the complete model. Similarity of the results of the two and four equation models suggests that heat transfer and compaction are not important mechanisms in determining two-phase detonation structure.

Much work remains to be done in two-phase detonation theory. It is highly likely that other classes of steady detonations can be predicted which have not been studied here. The complexity of the model equations makes this search a trial and error process. However, one can envision several different detonation scenarios by making minor adjustments in the relative positions of the separatrices in the two-dimensional phase plane.

Two-phase steady detonation results can be effectively used in the unsteady two-phase DDT problem. Predictions of any unsteady model would be strengthened by comparing them to the predictions of a steady model. Unsteady model results can be used to verify that the unsupported two-phase detonation wave is a CJ wave. This would simply require an examination of the two-phase end state conditions.

Reaction zone lengths predicted by the steady model must match those predicted by the unsteady model. This however raises an important question regarding numerical resolution. This study predicts reaction zone lengths of the order of 10 mm. Unsteady two-phase models now use a cell size on the order of 1 mm. It is highly unlikely that with the ratio of cell size to reaction zone length so high that one could use unsteady results to

distinguish features of the reaction zone identified by steady analysis, in particular, shock waves. The results are smeared by artificial viscosity and lack of an adequate number of cells. Thus the results of this study suggest that a cell size on the order of 0.01-0.1 mm be employed in unsteady calculations. Cell sizes of this magnitude present a dilemma. Typical particle sizes for detonation applications range from 0.1-1 mm. One assumption of continuum modeling of granular materials is a large number of particles exist in any averaging volume. If cell sizes of the order of 0.01-0.1 mm are employed, as the results suggest is necessary, then the continuum assumptions may not be valid.

The results of two-phase steady theory can be used as the basis for further studies. At this time, the stability of two-phase detonations has yet to be investigated. Also multidimensional two-phase theory is undeveloped. It may be possible to obtain a relationship to determine the critical diameter of a cylinder containing a two-phase explosive much in the same way these relations have been developed for one-phase materials [65]. Finally, it should be possible to use the method of characteristics to study the unsteady two-phase problem in a new way which has the potential to provide more understanding of what processes actually cause a two-phase detonation.

VII. REFERENCES

[1] Butler, P. B., and Krier, H., "Analysis of Deflagration to Detonation Transition in High-Energy Solid Propellants," *Combust. Flame* **63**, 31-48, 1986.

[2] Baer, M. R., and Nunziato, J. W., "A Two-Phase Mixture Theory for the Deflagration-to-Detonation Transition (DDT) in Reactive Granular Materials," *Int. J. Multiphase Flow* **12**, 861-889, 1986.

[3] Baer, M. R., Benner, R. E., Gross, R. J., and Nunziato, J. W., "Modeling and Computation of Deflagration-to-Detonation Transition in Reactive Granular Materials," *Lectures in Applied Mathematics* **24**, 1-30, 1986.

[4] Baer, M. R., Gross, R. J., Nunziato, J. W., and Igel, E. A., "An Experimental and Theoretical Study of Deflagration-to-Detonation Transition (DDT) in the Granular Explosive, CP, *Combust. Flame* **65**, 15-30, 1986.

[5] Gavrilenko, T. P., Grigoriev, V. V., Zhdan, S. A., Nikolaev, YU. A., Boiko, V. M., and Papyrin, A. N., "Acceleration of Solid Particles by Gaseous Detonation Products," *Combust. Flame* **66**, 121-128, 1986.

[6] Markatos, N. C., "Modelling of Two-Phase Transient Flow and Combustion of Granular Propellants," *Int. J. Multiphase Flow* **12**, 913-933, 1986.

[7] Krier, H., Cudak, C. A., Stewart, J. R., and Butler, P. B., "A Model for Shock Initiation of Porous Propellants by Ramp-Induced Compression Processes," *Proceedings-Eighth Symposium (International) on Detonation*, NSWC MP 86-194, Naval Surface Weapons Center, White Oak, MD, 962-971, 1985.

[8] Ermolaev, B. S., Novozhilov, B. V., Posvyanskii, V. S., and Sulimov, A. A., "Results of Numerical Modeling of the Convective Burning of Particulate Explosive Systems in the Presence of Increasing Pressure," *Combustion, Explosion, and Shock Waves* **21**, 505-514, 1985.

[9] Price, C. F., and Boggs, T. L., "Modeling the Deflagration to Detonation Transition in Porous Beds of Propellant," *Proceedings-Eighth Symposium (International) on Detonation*, NSWC MP 86-194, Naval Surface Weapons Center, White Oak, MD, 934-942, 1985.

[10] Akhatov, I. Sh., and Vainshtein, P. B., "Transition of Porous Explosive Combustion into Detonation," *Combustion, Explosion, and Shock Waves* **20**, 63-69, 1984.

[11] Nunziato, J. W., "Initiation and Growth-to-Detonation in Reactive Mixtures," in *Shock Waves in Condensed Matter-1983*, J. R. Asay, R. A. Graham, and G. K. Straub, eds., Elsevier, New York, 1984.

[12] Kim, K., "Numerical Simulation of Convective Combustion of Ball Powders in Strong Confinement," *AIAA J.* **22**, 793-796, 1984.

[13] Baer, M. R., and Nunziato, J. W., "A Theory for Deflagration-to Detonation Transition (DDT) in Granular Explosives," Sandia National Laboratories SAND 82-0293, 1983.

[14] Akhatov, I. Sh., and Vainshtein, P. B., "Nonstationary Combustion Regimes in Porous Powders," *Combustion, Explosion, and Shock Waves* **19**, 297-304, 1983.

[15] Markatos, N. C., and Kirkcaldy, D., "Analysis and Computation of Three-Dimensional Transient Flow and Combustion Through Granulated Propellants," *Int. J. Heat Mass Transfer* **26**, 1037-1053, 1983.

[16] Butler, P. B., Lembeck, M. F., and H. Krier, H., "Modeling of Shock Development and Transition to Detonation Initiated by Burning in Porous Propellant Beds," *Combust. Flame* **46**, 75-93, 1982.

[17] Gokhale, S. S., and Krier, H., "Modeling of Unsteady Two-Phase Reactive Flow in Porous Beds of Propellant," *Prog. Energy Combust. Sci.* **8**, 1-39, 1982.

[18] Hoffman, S. J., and Krier, H., "Fluid Mechanics of Deflagration-to-Detonation Transition in Porous Explosives and Propellants," *AIAA J.* **19**, 1571-1579, 1981.

[19] Kooker, D. E., and Anderson, R. D., "A Mechanism for the Burning Rate of High Density, Porous, Energetic Materials," *Proceedings-Seventh Symposium (International) on Detonation*, NSWC MP 82-334, Naval Surface Weapons Center, Dahlgren, VA, 198-215, 1981.

[20] Krier, H., and Gokhale, S. S., "Modeling of Convective Mode Combustion through Granulated Propellant to Predict Detonation Transition," *AIAA J.* **16**, 177-183, 1978.

[21] Krier, H., and Kezerle, J. A., "A Separated Two-Phase Flow Analysis to Study Deflagration-to-Detonation Transition (DDT) in Granulated Propellant," *Seventeenth Symposium (International) on Combustion*, The Combustion Institute, Pittsburgh, PA, 23-34, 1977.

[22] Bernecker, R. R., and Price, D., "Studies in the Transition from Deflagration to Detonation in Granular Explosives--I. Experimental Arrangement and Behavior of Explosives Which Fail to Exhibit Detonation," *Combust. Flame* **22**, 111-118, 1974.

[23] Bernecker, R. R., and Price, D., "Studies in the Transition from Deflagration to Detonation in Granular Explosives--II. Transitional Characteristics and Mechanisms Observed in 91/9 RDX/wax," *Combust. Flame* **22**, 119-129, 1974.

[24] Price, D., and Bernecker, R. R., "Sensitivity of Porous Explosives to Transition from Deflagration to Detonation," *Combust. Flame* **25**, 91-100, 1975.

[25] Eidelman, S., and Burcat, A., "Numerical Solution of a Nonsteady Blast Wave Propagation in Two-Phase ('Separated Flow') Reactive Medium," *J. Computational Physics* **39**, 456-472, 1981.

[26] Eidelman, S., and Burcat, A., "Evolution of a Detonation Wave in a Cloud of Fuel Droplets: Part I. Influence of Igniting Explosion," *AIAA J.* **18**, 1103-1109, 1980.

[27] Burcat, A., and Eidelman, S., "Evolution of a Detonation Wave in a Cloud of Fuel Droplets: Part II. Influence of Fuel Droplets," *AIAA J.* **18**, 1233-1236, 1980.

[28] Gough, P. S., and Zwarts, F. J., "Modeling Heterogeneous Two-Phase Reacting Flow," *AIAA J.* **17**, 17-25, 1979.

[29] Kuo, K. K., Koo, J. H., Davis, T. R., and Coates, G. R., "Transient Combustion in Mobile Gas Permeable Propellants," *Acta Astronautica* **3**, 573-591, 1976.

[30] Kuo, K. K., Vichnevetsky, R., and Summerfield, M., "Theory of Flame Front Propagation in Porous Propellant Charges under Confinement," *AIAA J.* **11**, 444-451, 1973.

[31] Drew, D. A., "One-Dimensional Burning Wave in a Bed of Monopropellant Particles," *Combust. Sci. Tech.* **11**, 1986.

[32] Condiff, D. W., "Contributions Concerning Quasi-Steady Propagation of Thermal Detonations Through Dispersions of Hot Liquid Fuel in Cooler Volatile Liquid Coolants," *Int. J. Heat Mass Transfer* **25**, 87-98, 1982.

[33] Sharon, A., and Bankoff, A., "On the Existence of Steady Supercritical Plane Thermal Detonations," *Int. J. Heat Mass Transfer* **24**, 1561-1572, 1981.

[34] Krier, H., and Mozaffarian, A., "Two-Phase Reactive Particle Flow Through Normal Shock Waves," *Int. J. Multiphase Flow* **4**, 65-79, 1978.

[35] Ermolaev, B. S., Khasainov, B. A., Borisov, A. A., and Korotkov, A. I., "Theory of Steady-State Convective Combustion," *Combustion, Explosion, and Shock Waves* **13**, 140-146, 1977.

[36] Ermolaev, B. S., Khasainov, B. A., Borisov, A. A., and Korotkov, A. I., "Convective-Combustion Propagation in Porous Low and High Explosives," *Combustion, Explosion, and Shock Waves* **11**, 614-621, 1975.

[37] Kuo, K. K., and Summerfield, M., "High Speed Combustion of Mobile Granular Solid Propellants: Wave Structure and the Equivalent Rankine-Hugoniot Relation," *Fifteenth Symposium (International) on Combustion*, The Combustion Institute, Pittsburgh, PA, 515-527, 1975.

[38] Kuo, K. K., and Summerfield, M., "Theory of Steady-State Burning of Gas-Permeable Propellants," *AIAA J.* **12**, 49-56, 1974.

[39] Borisov, A. A., Gel'fand, B. E., Gubin, S. A., Kogarko, S. M., and Podgrebenkov, A. L., "Detonation Reaction Zone in Two-Phase Mixtures," *Combustion, Explosion, and Shock Waves* **6**, 327-336, 1970.

[40] Fickett, W., and Davis, W. C., *Detonation*, University of California Press, Berkeley, 1979.

[41] Powers, J. M., Stewart, D. S., and Krier, H., "Two-Phase Steady Detonation Analysis,", presented at the 11th International Colloquium on Dynamics of Explosions and Reactive Systems, 1987, to appear in AIAA Progress Series.

[42] Bilicki, Z., Dafermos, C., Kestin, J., Majda, G., and Leng, D. L., "Trajectories and Singular Points in Steady-State Models of Two-Phase Flows," *Int. J. Multiphase Flow* **13**, 511-533, 1987.

[43] Sandusky, H. W., and Liddiard, T. P., "Dynamic Compaction of Porous Beds," NSWC TR 83-256, Naval Surface Weapons Center, 1985.

[44] Sandusky, H. W., and Bernecker, R. R., "Compressive Reaction in Porous Beds of Energetic Materials," *Proceedings-Eighth Symposium (International) on Detonation*, NSWC MP 86-194, Naval Surface Weapons Center, White Oak, MD, 881-891, 1985.

[45] Baer, M. R., "Numerical Studies of Dynamic Compaction of Inert and Energetic Granular Materials," to appear in *J. Appl. Mech.*, 1988.

[46] Powers, J. M., Stewart, D. S., and Krier, H., "Analysis of Steady Compaction Waves in Porous Materials," to appear in *J. Appl. Mech.*, 1988.

[47] Butler, P. B., "Analysis of Deflagration to Detonation Transition in High-Energy Solid Propellants," PhD Dissertation, University of Illinois at Urbana-Champaign, 1984.

[48] Drew, D. A., "Mathematical Modeling of Two-Phase Flow," *Annual Review of Fluid Mechanics* **15**, 261-291, 1983.

[49] Truesdell, C., *Rational Thermodynamics*, McGraw-Hill, New York, 1984.

[50] Nigmatulin, R. I., *Fundamentals of the Mechanics of Continuous Media* [in Russian], Nauka, Moscow, 1978.

[51] Arnold, V. I., *Ordinary Differential Equations*, MIT Press, Cambridge, MA, 1973.

[52] Guckenheimer, J., and Holmes, P., *Dynamical Systems and Bifurcations of Vector Fields*, Springer, New York, 1983.

[53] Lyczkowski, R. W., Gidaspow, D., Solbrig, C., and Hughes, E. D., "Characteristics and Stability Analyses of Transient One-Dimensional Two-Phase Flow Equations and Their Finite Difference Approximations," *Nuclear Science and Engineering* **66**, 378-396, 1978.

[54] Coperthwaite, M., and Zwisler, W. H., " 'TIGER' Computer Code Documentation," Report PYV-1281, Stanford Research Institute, 1974.

[55] Marsh, S., P., ed., *LASL Shock Hugoniot Data*, University of California Press, Berkeley, CA, 1980.

[56] Krier, H., and Stewart, J. R., "Prediction of Detonation Transition in Porous Explosives from Rapid Compression Loadings," UILU-ENG-85-4007, Department of Mechanical and Industrial Engineering, University of Illinois at Urbana-Champaign, 1985.

[57] Kooker, D. E., "A Numerical Study of Compaction Waves in Class D HMX, 1986 JANNAF Propulsion Systems Hazards Meeting, CPIA Publication 446, Vol 1, 213-238, 1986.

[58] Becker, E., and Bohme, G., "Steady One-Dimensional Flow; Structure of Compression Waves," in *Nonequilibrium Flows*, ed. P. P. Wegener, Marcel Dekker, New York, 1969.

[59] Carroll, M. M., and Holt, A. C., "Static and Dynamic Pore-Collapse Relations for Ductile Porous Materials," *J. Appl. Phys.* **43**, 1626-1635, 1972.

[60] Butcher, B. M., Carroll, M. M., and Holt, A. C., "Shock-Wave Compaction of Porous Aluminum," *J. Appl. Phys.* **45**, 3864-3875, 1974.

[61] Elban, W. L., and Chiarito, M. A., "Quasi-Static Compaction Study of Coarse HMX Explosive," *Powder Tech.* **46**, 181-193, 1986.

[62] Kooker, D. E., "A Workshop Summary of Compaction Waves in Granular Material: Numerical Predictions," 1987 JANNAF Propulsion Systems Hazards Meeting, CPIA Publication 464, Vol. 1, 127-138, 1987.

[63] Elban, W. L., Coyne, P. J., and Chiarito, M. A., "The Effect of Particle Size on the Quasi-Static Compaction Behavior of Granular HMX Beds," 1987 JANNAF Propulsion Systems Hazards Meeting, CPIA Publication 464, Vol. 1, 61-75, 1987.

[64] Rudinger, G., "Some Properties of Shock Relaxation in Gas Flows Containing Small Particles," *Phys. Fluids* **7**, 658-663, 1964.

[65] Bdzil, J. B., and D. S. Stewart, "Time-Dependent Two-Dimensional Detonation: The Interaction of Edge Rarefactions with Finite Length Reaction Zones," *J. Fluid Mech.* **171**, 1-26, 1986.

[66] Whitham, G. B., *Linear and Nonlinear Waves*, Wiley, New York, 1974.

[67] Courant, R., and K. O. Friedrichs, *Supersonic Flow and Shock Waves*, Springer, New York, 1948.

[68] Nunziato, J. W., Private Communication, 1988

[69] Bdzil, J. B., Engelke, R., and Christenson, D. A., "Kinetics Study of a Condensed Detonating Explosive," *J. Chem. Phys.* **74**, 5694-5699, 1981.

APPENDIX A. CHARACTERISTIC FORM OF GOVERNING EQUATIONS

This appendix will identify the characteristic directions and characteristic form of Equations (3.1-15). First a simplified, compact form of Equations (3.1-15) is presented. This form is useful when deriving the characteristic form of the equations. Because Equations (3.1-15) are hyperbolic, it is guaranteed that these equations are well-posed for initial value problems. If these equations were not well-posed, any solution to the initial value problem would be unstable. This analysis is very similar to the analysis performed by Baer and Nunziato [2] for their two-phase model equations. Here the same characteristic eigenvalues are obtained.

Though the characteristic form is not immediately relevant to the work presented in this thesis, it could be important for future work in the unsteady DDT problem. The characteristic form is in some sense the natural frame in which to study the unsteady equations. The unsteady equations are transformed from a set of partial differential equations to a set of ordinary differential equations. Previous studies of the unsteady problem have used the method of lines to solve the equations (see Ref. 47). With this method both time and space derivatives are discretized. Also to describe shock waves, it is necessary to use a special technique, such as artificial viscosity or flux-corrected-transport (FCT) to spread the shock jump over a few finite difference cells. When the characteristic form of the equations is studied, no shock-smearing method is required to describe shock jumps.

This analysis will follow the technique described by Whittam [66] for determining the characteristic eigenvalues and eigenvectors. Consider a system of partial differential equations of the form

$$A_{ij}\frac{\partial u_j}{\partial t} + B_{ij}\frac{\partial u_j}{\partial x} = C_i \tag{A.1}$$

Multiply both sides of Equation (A.1) by a vector l_i.

$$l_i A_{ij}\frac{\partial u_j}{\partial t} + l_i B_{ij}\frac{\partial u_j}{\partial x} = l_i C_i \tag{A.2}$$

The vector l_i is chosen such that Equation (A.2) can be transformed into a system of ordinary differential equations. To insure that Equation (A.2) can be transformed to such a system, it is sufficient to require that the following condition hold.

$$l_i B_{ij} = \lambda l_i A_{ij} \tag{A.3}$$

where λ is a variable scalar quantity. If Equation (A.3) holds, then Equation (A.2) can be written as

$$l_i A_{ij}\left(\frac{\partial u_j}{\partial t} + \lambda \frac{\partial u_j}{\partial x}\right) = l_i C_i \tag{A.4}$$

Equation (A.4) can be transformed to an ordinary differential equation on special curves in the x-t plane. On curves specified by

$$\frac{dx}{dt} = \lambda \tag{A.5}$$

Equation (A.4) becomes

$$l_i A_{ij} \frac{du_j}{dt} = l_i C_i \tag{A.6}$$

To get the form of Equation (A.6) it is required that the eigenvalue problem specified by Equation (A.3) holds, that is

$$l_i\left(\lambda A_{ij} - B_{ij}\right) = 0 \tag{A.7}$$

For a non-trivial solution to this equation to exist it is necessary that

$$\det\left(\lambda A_{ij} - B_{ij}\right) = 0 \tag{A.8}$$

Solution of Equation (A.8) will provide a set of eigenvalues λ. For each eigenvalue, it is then possible to use Equation (A.7) to determine the vector l_i. This vector will have an arbitrary magnitude. Using this vector for the particular eigenvalue, equation (A.6) can be used to determine the characteristic ordinary differential equation for the characteristic direction of interest. When substituted into Equation (A.6) the arbitrary magnitude appears as a factor on both sides of the equation and cancels.

To study the characteristic form of Equations (3.1-15), it is first important to write these equations in the reduced form required by Equation (A.1). To achieve this form, several steps are necessary. First, the gas and solid mass equations are used to eliminate density derivatives in gas and solid momentum and energy equations. Next, the reduced gas and solid momentum equations are used to eliminate velocity derivatives in the gas and solid energy equations. Then the gas and solid Gibbs equations are used in the gas and solid energy equations to rewrite derivatives of gas and solid energy in terms of derivatives of gas and solid entropy and density. Finally, thermodynamic relations developed in Appendix B are used in the gas and solid momentum equations to rewrite derivatives of gas and solid pressure in terms of derivatives of gas and solid entropy and density.

With these steps and adopting Equation (3.16) in favor of the number conservation equation (3.7), the unsteady two-phase equations can be written compactly as follows

$$\rho_i \frac{\partial \phi_i}{\partial t} + \phi_i \frac{\partial \rho_i}{\partial t} + \rho_i \phi_i \frac{\partial u_i}{\partial x} + \rho_i u_i \frac{\partial \phi_i}{\partial x} + u_i \phi_i \frac{\partial \rho_i}{\partial x} = \delta \frac{\phi_2}{r} \left[\pi_1 \rho_2 P_1^{\pi_4} \right] \tag{A.9}$$

$$\rho_i \phi_i \frac{\partial u_i}{\partial t} + \rho_i \phi_i u_i \frac{\partial u_i}{\partial x} + P_i \frac{\partial \phi_i}{\partial x} + \phi_i c_i^2 \frac{\partial \rho_i}{\partial x} + \phi_i \left(P_i - \frac{\delta - 1}{2} \pi_8 \right) \frac{\partial s_i}{\partial x} =$$

$$\delta \frac{\phi_2}{r} \left[\pi_1 \rho_2 P_1^{\pi_4} (u_2 - u_i) + \pi_2 \phi_1 (u_2 - u_1) \right] \tag{A.10}$$

$$\rho_i \phi_i T_i \frac{\partial s_i}{\partial t} + \rho_i \phi_i T_i u_i \frac{\partial s_i}{\partial x} - P_i \frac{\partial \phi_i}{\partial t} - P_i u_i \frac{\partial \phi_i}{\partial x} =$$

$$\delta \frac{\phi_2}{r} \left\{ \pi_1 \rho_2 P_1^{\pi_4} \left[e_2 - e_i + \frac{1}{2}(u_2 - u_i)^2 - P_i/\rho_i \right] + \pi_2 \phi_1 (u_2 - u_1)(u_2 - u_i) + \pi_3 \phi_1 (\pi_6 T_2 - T_1) r^{2/3} \right\} \tag{A.11}$$

$$\frac{\partial \phi_2}{\partial t} + u_2 \frac{\partial \phi_2}{\partial x} = \frac{\phi_2}{r}\left[\pi_9 r \phi_1 \left(P_2 - \pi_5 P_1 - f(\phi_2)\right) - \pi_1 P_1^{\pi_4}\right] \tag{A.12}$$

$$\frac{3}{r}\frac{\partial r}{\partial t} + \frac{3}{r} u_2 \frac{\partial r}{\partial x} + \frac{1}{\rho_2}\frac{\partial \rho_2}{\partial t} + \frac{1}{\rho_2} u_2 \frac{\partial \rho_2}{\partial x} = -\pi_1 P_1^{\pi_4} \tag{A.13}$$

$$\text{with} \begin{cases} \text{gas phase} & i = 1 \quad \delta = 1 \\ \text{solid phase} & i = 2 \quad \delta = -1 \end{cases}$$

Equation (A.9) represents the gas and solid mass equations; Equation (A.10) represents the gas and solid momentum equations; Equation (A.11) represents the gas and solid energy equations; Equation (A.12) is the compaction equation; and Equation (A.13) represents a combination of the number conservation equation and solid mass equation.

The algebraic details required to derive the characteristic equations are very lengthy and not immediately relevant to this work. For this reason, only the results will be presented here. Six characteristic eigenvalues λ are found

$$\lambda = \begin{cases} u_1 \pm c_1 \\ u_2 \pm c_2 \\ u_1 \\ u_2 \end{cases} \tag{A.14}$$

The characteristics are real and analogous to the characteristics found for one-phase equations.

The characteristic equations have been determined in the limit when the gas phase is ideal. There is nothing in principle preventing the characteristic equations from being determined for a non-ideal gas; however, the algebraic details are much more complicated. The characteristic directions given by Equation (A.14) apply to both ideal and non-ideal gas phase state equations, and the non-ideal solid assumption has not been relaxed in any calculations. Let $\gamma_1 = \pi_7$ and $\gamma_2 = \pi_{17}$. The equations in characteristic form in the ideal gas limit are

$$\frac{1}{\rho_i \phi_i c_i^2} \frac{d(P_i \phi_i)}{dt_{i\pm}} \pm \frac{1}{c_i} \frac{du_i}{dt_{i\pm}} =$$

$$\delta \frac{\phi_2}{\rho_i \phi_i r} \left\{ \pi_1 \rho_2 P_1^{\pi_4} \pm \frac{\pi_1 \rho_2 P_1^{\pi_4} (u_2 - u_i) + \pi_2 \phi_1 (u_2 - u_1)}{c_i} \right\}$$

$$+ \delta \frac{\phi_2}{\gamma_i \rho_i \phi_i T_i r} \left\{ \pi_1 \rho_2 P_1^{\pi_4} \left(e_2 - e_i + \frac{1}{2}(u_2 - u_i)^2 - P_i/\rho_i \right) + \pi_2 \phi_1 (u_2 - u_1)(u_2 - u_i) + \pi_3 \phi_1 (\pi_6 T_2 - T_1) r^{2/3} \right\}$$

$$+ \frac{\delta - 1}{2} \frac{\gamma_2 \pi_8}{\rho_2 c_2^2} \left\{ \pi_9 \phi_1 \left(P_2 - \pi_5 P_1 - \pi_{15} \phi_2 \right) - \pi_1 \frac{P_1^{\pi_4}}{r} \right\} \qquad \text{(A.15)}$$

$$\frac{1}{\gamma_i} \frac{ds_i}{dt_{i0}} - (\gamma_i - 1) \frac{P_i}{\rho_i c_i^2} \frac{1}{\phi_i} \frac{d\phi_i}{dt_{i0}} =$$

$$+ \delta \frac{\phi_2}{\gamma_i \rho_i \phi_i T_i r} \left\{ \pi_1 \rho_2 P_1^{\pi_4} \left(e_2 - e_i + \frac{1}{2}(u_2 - u_i)^2 - P_i/\rho_i \right) + \pi_2 \phi_1 (u_2 - u_1)(u_2 - u_i) + \pi_3 \phi_1 (\pi_6 T_2 - T_1) r^{2/3} \right\}$$

(A.16)

$$\frac{1}{\phi_2} \frac{d\phi_2}{dt_{20}} = \pi_9 \phi_1 \left[P_2 - \pi_5 P_1 - \pi_{15} \phi_2 \right] - \pi_1 \frac{P_1^{\pi_4}}{r} \qquad \text{(A.17)}$$

$$\frac{3}{r} \frac{dr}{dt_{20}} + \frac{1}{\rho_2} \frac{d\rho_2}{dt_{20}} = - \pi_1 P_1^{\pi_4} \qquad \text{(A.18)}$$

where the derivatives are defined as follows

$$\frac{d}{dt_{i\pm}} = \frac{\partial}{\partial t} + (u_i \pm c_i) \frac{\partial}{\partial x} \qquad \frac{d}{dt_{i0}} = \frac{\partial}{\partial t} + u_i \frac{\partial}{\partial x}$$

These definitions lead to the following differential equations defining the characteristic directions

$$\frac{dx}{dt} = u_i \pm c_i \quad \text{on i}\pm \text{ characteristics}$$

$$\frac{dx}{dt} = u_i \quad \text{on i0 characteristics}$$

It should be noted that Equations (A.15-16) reduce to familiar one-phase formulae given by Courant and Fredrichs [67] in the one-phase inert limit.

APPENDIX B. THERMODYNAMIC RELATIONS

In this appendix, it will be shown how, given a thermal equation of state for pressure as a function of density and temperature, one can derive a thermodynamically consistent caloric equation for internal energy as a function of density and temperature. This technique will be applied to the virial gas state equation and solid Tait equation. Equations for sound speed and partial derivative of pressure with respect to entropy at constant density are derived for each phase. The analysis that will follow is well-known in classical thermodynamics and can be found in most thermodynamics textbooks.

General Analysis

For this analysis let the specific volume v be defined as $v = 1/\rho$. The task is to derive a caloric state equation [$e = e(T,v)$] given a thermal state equation [$P = P(T,v)$]. If energy is to be a function of temperature and volume, then the differential of energy can be written as follows:

$$de = \left.\frac{\partial e}{\partial T}\right|_v dT + \left.\frac{\partial e}{\partial v}\right|_T dv \tag{B.1}$$

The Gibbs equation, $Tds = de + Pdv$, can be used to write an expression for the partial derivative of energy with respect to volume:

$$\left.\frac{\partial e}{\partial v}\right|_T = T\left.\frac{\partial s}{\partial v}\right|_T - P \tag{B.2}$$

The specific heat at constant volume is defined as

$$c_v = \left.\frac{\partial e}{\partial T}\right|_v \tag{B.3}$$

Equations (B.2) and (B.3) are then substituted into Equation (B.1) to yield the following:

$$de = c_v dT + \left(T \frac{\partial s}{\partial v}\Big|_T - P \right) dv \tag{B.4}$$

Using the Maxwell relation

$$\frac{\partial P}{\partial T}\Big|_v = \frac{\partial s}{\partial v}\Big|_T \tag{B.5}$$

in Equation (B.4) the following equation is obtained for the differential of energy:

$$de = c_v dT + \left(T \frac{\partial P}{\partial T}\Big|_v - P \right) dv \tag{B.6}$$

which is a convenient formula for determining a caloric equation given a thermal equation of state.

Gas Phase Analysis

It is assumed that the gas thermal equation of state is given by

$$P_1 = \frac{RT_1}{v_1}\left(1 + b/v_1\right) \tag{B.7}$$

By substituting Equation (B.7) into Equation (B.6), the following equation is obtained for the differential of gas internal energy

$$de_1 = c_{v1} dT_1 \tag{B.8}$$

By making the assumption of a constant specific heat at constant volume, integrating Equation (B.8), and setting the arbitrary integration constant to zero, the following formula is obtained for the gas internal energy:

$$e_1 = c_{v1} T_1 \tag{B.9}$$

Internal energy can be written in terms of pressure and density by substituting Equation (B.7) into Equation (B.9) and using the definition of specific volume.

$$e_1 = \frac{c_{v1}}{R} \frac{P_1}{\rho_1(1 + b\rho_1)} \tag{B.10}$$

The Gibbs equation, $T_1 ds_1 = de_1 - P_1/\rho_1^2 \, d\rho_1$, can be used with Equation (B.10) to determine an expression for sound speed c_1, defined below:

$$c_1^2 = \left.\frac{\partial P_1}{\partial \rho_1}\right|_s \tag{B.11}$$

By using Equation (B.10) to determine the differential of energy in terms of pressure and density and substituting this result into the Gibbs equation, the following expression is obtained:

$$T_1 ds_1 = \frac{c_{v1}}{R} \frac{1}{\rho_1(1 + b\rho_1)} dP_1 - \frac{c_{v1}}{R} \frac{P_1}{\rho_1^2} \frac{(1 + 2b\rho_1)}{(1 + b\rho_1)^2} d\rho_1 - \frac{P_1}{\rho_1^2} d\rho_1 \tag{B.12}$$

By holding entropy constant ($ds_1 = 0$), and using Equation (B.7) to reintroduce temperature, Equation (B.12) can be used to determine an expression for gas phase sound speed:

$$c_1^2 = RT_1 \left[1 + 2b\rho_1 + (R/c_{v1})(1 + b\rho_1)^2 \right] \tag{B.13}$$

It is easily verified by setting $b = 0$ that Equation (B.12) reduces to the well-known ideal gas sound speed.

Solid Phase Analysis

For the solid phase the assumed thermal state equation is

$$P_2 = \frac{(\gamma_2 - 1)c_{v2}T_2}{v_2} - \frac{\rho_{20}{}^s}{\gamma_2} \tag{B.14}$$

By substituting Equation (B.14) into Equation (B.6), the following expression is obtained for the differential of solid energy:

$$de_2 = c_{v2}dT_2 + \frac{\rho_{20}{}^s}{\gamma_2} dv_2 \tag{B.15}$$

By assuming a constant specific heat at constant volume, integrating Equation (B.15) and assuming the arbitrary integration constant is the chemical energy q, the following equation is obtained:

$$e_2 = c_{v2}T_2 + \frac{\rho_{20}{}^s}{\gamma_2} v_2 + q \tag{B.16}$$

Using the thermal state equation (B.14) and the definition of specific volume, Equation (B.16) can be rewritten to give internal energy as a function of density and pressure.

$$e_2 = \frac{P_2 + \rho_{20}{}^s}{(\gamma_2 - 1)\rho_2} + q \tag{B.17}$$

As for the gas phase, the sound speed for the Tait solid may be determined by considering the Gibbs equation. The Gibbs equation for the Tait solid in terms of differential pressure and density, obtained from differentiating Equation (B.17), is

$$T_2 ds_2 = \frac{1}{(\gamma_2 - 1)\rho_2} dP_2 - \frac{P_2 + \rho_{20}{}^s}{(\gamma_2 - 1)\rho_2^2} d\rho_2 - \frac{P_2}{\rho_2^2} d\rho_2 \tag{B.18}$$

By setting the entropy change to 0 in Equation (B.18), solving for the derivative representing sound speed, and using the thermal state equation (B.14) to reintroduce temperature, the following formula for the sound speed of a Tait solid is obtained:

$$c_2^2 = \gamma_2(\gamma_2 - 1)\, c_{v2} T_2 \qquad \text{(B.19)}$$

Equation (B.19) is identical to the formula one finds for the sound speed of an ideal gas; when the sound speed is expressed as a function of pressure and density, there is a non-ideal term present.

APPENDIX C. MODEL COMPARISONS: MOMENTUM AND ENERGY EQUATIONS

In this appendix, the momentum and energy equations of this work are compared to those of Baer and Nunziato [2]. The differences lie in the particular form of the pressure gradient term in the momentum equations and in a term known as compaction work in the energy equations.

Momentum Equations

The formulation of the momentum equations used in this work, adopted from the work of Butler and Krier [1], has been criticized because it fails to describe the equilibrium configuration of solid particles at rest in a less dense fluid in the presence of a gravity field. This is not in dispute. It has been argued that the two-phase equations as formulated by Baer and Nunziato are able to describe such a situation and thus are to be preferred to the Butler-Krier equations. Here, it is shown that both formulations are in general unable to predict the equilibrium situation described above.

The problem is sketched below in Figure C.1.

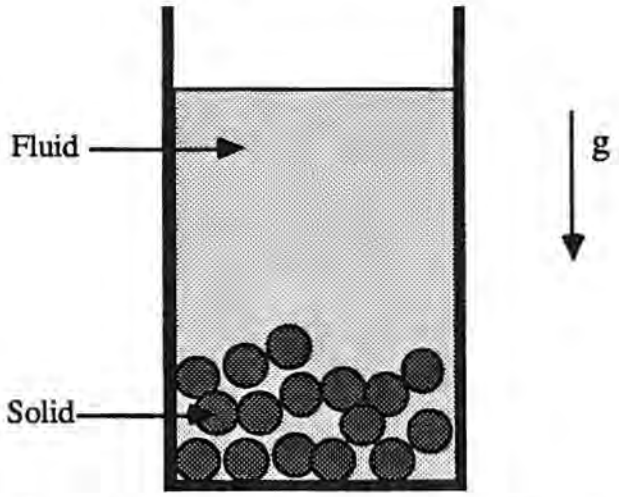

Figure C.1. Sketch of vertical settling problem

This sketch shows a mixture of a fluid and solid particles at rest in a tube. Here a gravitational acceleration, g, has caused the heavier solid particles to settle to the bottom of the tube.

Consider the following two-phase model equations, which are inclusive of both the Nunziato-Baer and Butler-Krier formulations.

$$\rho_1\phi_1\frac{\partial u_1}{\partial t} + \rho_1\phi_1 u_1\frac{\partial u_1}{\partial x} + \phi_1\frac{\partial P_1}{\partial x} + \kappa P_1\frac{\partial \phi_1}{\partial x} = -\delta(u_1-u_2) - \rho_1\phi_1 g \qquad (C.1)$$

$$\rho_2\phi_2\frac{\partial u_2}{\partial t}+\rho_2\phi_2 u_2\frac{\partial u_2}{\partial x}+\phi_2\frac{\partial P_2}{\partial x}+P_2\frac{\partial \phi_2}{\partial x}+(1-\kappa)P_1\frac{\partial \phi_1}{\partial x} = -\delta(u_2-u_1)-\rho_2\phi_2 g \qquad (C.2)$$

$$\frac{\partial \phi_2}{\partial t} + u_2\frac{\partial \phi_2}{\partial x} = \frac{\phi_1\phi_2}{\mu_c}\left(P_2 - P_1 - f(\phi_2)\right) \qquad (C.3)$$

Here the subscript "1" represents the fluid phase and the subscript "2" represents the solid phase. Equations (C.1) and (C.2) are the momentum equations for the fluid and solid phases, respectively. Equation (C.3) is the dynamic compaction equation. Density is represented by ρ, volume fraction by ϕ, velocity by u, pressure by P, drag coefficient by δ, gravitational acceleration by g, compaction viscosity by μ_c, and static pore collapse function by f, assumed to be a function of only the solid volume fraction, ϕ_2. For $\kappa = 0$ these equations describe the Nunziato-Baer formulation, for $\kappa = 1$, the Butler-Krier formulation.

The following equations partially describe the initial state in the vertical settling problem:

$$\phi_2(x,0) = h(x) \qquad (C.4)$$

$$u_1(x,0) = u_2(x,0) = 0 \qquad (C.5)$$

Here, it is assumed that there is an initial distribution of particles given by a general function h(x). It is further assumed that both particles and fluid are at rest.

It would seem that a basic test for any model of this problem is that the model should predict that the mixture stays at rest; thus at this initial state, the equations should predict that no variables change with respect to time. To insure that no volume changes are predicted, a condition on the relation between P_2, P_1 and ϕ_2 is obtained from Equation (C.3):

$$P_2 = P_1 + f\left[h(x)\right] \tag{C.6}$$

An equilibrium condition is also obtained from the fluid momentum equation (C.1) by using the initial conditions (C.4, 5). For no fluid motion to be predicted, the following condition must hold:

$$\frac{\partial P_1}{\partial x} = \kappa \frac{P_1}{1-h}\frac{dh}{dx} - \rho_1 g \tag{C.7}$$

For $\kappa = 0$, a result identical from one-phase fluid statics is recovered. It has been argued [68] that this limit must also be recovered from a two-phase model and that this is a sufficient reason to take $\kappa = 0$. However, it is still not clear whether this familiar result should extend to the two-phase situation.

When the solid momentum equation (C.2) is considered, it is seen that both formulations have difficulty describing an equilibrium configuration. By substituting the initial conditions (C.4, 5), the compaction equation condition (C.6), and the fluid pressure gradient condition (C.7) into Equation (C.2), the following condition is obtained for no solid acceleration:

$$\left(\rho_1/\rho_2 - 1\right) g - \frac{1}{\rho_2 h}\frac{d}{dx}\left[h\, f\left(h(x)\right)\right] - \kappa \frac{P_1}{\rho_2 h}\frac{1}{1-h}\frac{dh}{dx} = 0 \tag{C.8}$$

This equation raises questions regarding equilibrium in the presence of gravitational forces and initial volume fraction gradients.. Consider two limiting cases for the Nunziato-Baer model ($\kappa = 0$). In the first case consider a situation in which there is no intragranular stress; the particles are in contact but are not exerting a force on each other. This would correspond to the condition $f = 0$. In this limit, equation (C.8) predicts equilibrium only when the fluid density is equal to the solid density, which in general is not satisfied. (In this case it is questionable whether the state equations would allow Equation (C.6) to hold also.) In the second case consider the zero-gravity limit, $g \rightarrow 0$. In this limit for Equation (C.8) to be satisfied, the static pore collapse function f must be of the form f = constant / ϕ_2, a condition which is not enforced by the Nunziato-Baer model. The condition (C.8)

has not been enforced by the Butler-Krier model. It should be said that the Butler-Krier model never attempts to describe the situation in Figure C.1.

From this analysis, it is clear that both the Nunziato-Baer and Butler-Krier model equations are incapable of describing an equilibrium state in the presence of either a volume fraction gradient or gravity forces unless very restrictive conditions are placed on the constitutive relations. Neither of these models currently enforces such restrictions.

Energy Equations

Baer and Nunziato have included a term in their model which is intended to model experimentally-observed hot spots in granular explosives and the work associated with the local distortion of grains when a granular material is compacted. This term, called compaction work, appears in both the solid and gas phase energy equations. It is constructed such that when compaction work is predicted, energy is removed from the solid phase and deposited in the gas phase. This local energy deposition gives rise to a local hot spot which encourages a local acceleration of the reaction rate. It is shown by Baer and Nunziato that this compaction work term is consistent with but not required by the second law of thermodynamics.

Here, it will be shown that the presence of compaction work gives rise to a fundamental inconsistency in the limit of an inert mixture where the ratio of initial gas density to initial solid density is small. In this limit the steady-state mixture energy equation predicts a result inconsistent with the solid energy equation. It is shown that the solid energy equation in this limit gives rise to energy escaping from the system.

Consider the following equations, general equations which encompass the gas and solid energy equations of both models.

$$\frac{\partial}{\partial t}\left[\rho_1\phi_1\left(e_1+u_1^2/2\right)\right]+\frac{\partial}{\partial x}\left[\rho_1\phi_1u_1\left(e_1+u_1^2/2\right)+P_1\phi_1u_1\right]-\delta P_1u_2\frac{\partial\phi_1}{\partial x}=$$

$$-h(T_1-T_2)+\alpha(u_2-u_1)u_2-c_s^{+}\left(e_2+u_2^2/2\right)+\delta\frac{\phi_1\phi_2}{\mu_c}\left(P_2-P_1-f(\phi_2)\right)\left(P_2-f(\phi_2)\right) \quad (C.9)$$

$$\frac{\partial}{\partial t}\left[\rho_2\phi_2\left(e_2+u_2^2/2\right)\right]+\frac{\partial}{\partial x}\left[\rho_2\phi_2u_2\left(e_2+u_2^2/2\right)+P_2\phi_2u_2\right]+\delta P_1u_2\frac{\partial\phi_1}{\partial x}=$$

$$+h(T_1-T_2)-\alpha(u_2-u_1)u_2+c_s^+\left(e_2+u_2^2/2\right)-\delta\frac{\phi_1\phi_2}{\mu_c}\left(P_2-P_1-f(\phi_2)\right)\left(P_2-f(\phi_2)\right) \quad (C.10)$$

$$\delta = \begin{cases} 0 & \text{Model of this Work} \\ 1 & \text{Baer-Nunziato Model} \end{cases}$$

The new notation introduced here is that h is considered to be a general function specifying the heat transfer coefficient, likewise α is taken to be a general function specifying the drag coefficient, and c_s^+ is a general function specifying the combustion rate. The parameter δ is used to distinguish the two model formulations.

When Equations (C.10) and (C.11) are added, a homogeneous, unsteady mixture energy equation is obtained.

$$\frac{\partial}{\partial t}\left[\rho_1\phi_1\left(e_1+u_1^2/2\right)+\rho_2\phi_2\left(e_2+u_2^2/2\right)\right]+$$

$$\frac{\partial}{\partial x}\left[\rho_1\phi_1u_1\left(e_1+u_1^2/2\right)+P_1\phi_1u_1+\rho_2\phi_2u_2\left(e_2+u_2^2/2\right)+P_2\phi_2u_2\right]=0 \quad (C.11)$$

It is argued by Baer [45] that in the limit where material is inert ($c_s^+ = 0$) and where the effect of the gas phase is negligible that Equation (C.10) reduces to the following

$$\frac{\partial}{\partial t}\left[\rho_2\phi_2\left(e_2+u_2^2/2\right)\right]+\frac{\partial}{\partial x}\left[\rho_2\phi_2u_2\left(e_2+u_2^2/2\right)+P_2\phi_2u_2\right]=-\delta\frac{\phi_1\phi_2}{\mu_c}\left(P_2-f(\phi_2)\right)^2$$

(C.12)

If Equations (C.11) and (C.12) are transformed to steady dimensionless form and the limit of zero gas phase density is taken, the inconsistency becomes apparent. Using the same technique and nomenclature found in the main text for writing steady dimensionless equations, it is found that Equation (C.11) transforms to the following (equivalent to Equation (5.7))

$$\pi_5\rho_1\phi_1 v_1\left(e_1 + \frac{v_1^2}{2} + \frac{P_1}{\rho_1}\right) + \rho_2\phi_2 v_2\left(e_2 + \frac{v_2^2}{2} + \frac{P_2}{\rho_2}\right) =$$

$$\pi_5\pi_{11}(\pi_6\pi_{14} + 1/2 + \pi_{19}) + (1 - \pi_{11})(\pi_{14} + \pi_8 + \pi_{10} + 1/2 + \pi_{21}) \qquad (C.13)$$

In the limit of zero gas phase density, π_5 is zero. Thus in this limit the steady mixture equation (C.13) becomes

$$\rho_2\phi_2 v_2\left(e_2 + \frac{v_2^2}{2} + \frac{P_2}{\rho_2}\right) = (1 - \pi_{11})(\pi_{14} + \pi_8 + \pi_{10} + 1/2 + \pi_{21}) \qquad (C.14)$$

The steady dimensionless form of Equation (C.12) is

$$\frac{d}{d\xi}\left[\rho_2\phi_2 v_2\left(e_2 + \frac{v_2^2}{2}\right) + P_2\phi_2 v_2\right] = \delta\pi_9\phi_1\phi_2\left(P_2 - f(\phi_2)\right)^2 \qquad (C.15)$$

It is obvious that Equations (C.14) and (C.15) are consistent only when $\delta = 0$, that is when compaction work is ignored.

Inclusion of compaction work leads to violation of the conservation of energy in the zero-density gas phase limit. This is easily seen by considering the application of the unsteady energy equation (C.12) to the following problem (see Fig. C.2). Strike with a piston a constant area tube closed at one end containing a porous material. After a period of time bring the piston to rest. The piston motion induces a pressure imbalance in the porous material (i. e. $(P - f) > 0$). After the piston is brought to rest, a zero velocity boundary condition must be enforced at both ends of the tube. However the material inside the tube is not in a state of equilibrium.

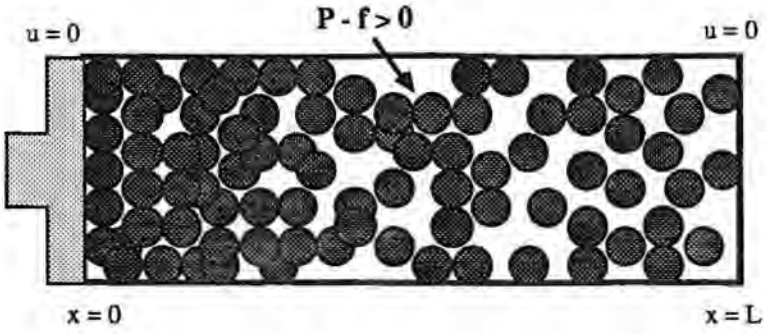

Figure C.2 Sketch of Piston Problem

By integrating the energy equation (C.12) from x = 0 to x = L, it is seen that for $\delta = 0$, the energy of the system is conserved and for $\delta = 1$, energy leaves the system as time progresses. The time rate of change of energy per unit cross-sectional area for this system is

$$\frac{\partial}{\partial t}\int_0^L \rho_2\phi_2\left(e_2 + u_2^2/2\right) dx = -\frac{\delta}{\mu_c}\int_0^L \phi_1\phi_2\left(P_2 - f(\phi_2)\right)^2 dx \qquad (C.16)$$

For $0 < \phi_2 \leq 1$, the integrand of the right hand side of the total energy equation is always positive; therefore, for $\delta = 1$, energy leaves this system, and for $\delta = 0$, energy is conserved. In order to preserve energy conservation in this limit, and in light of the fact that compaction work is not necessarily required by the second law of thermodynamics, compaction work is not included in this model.

It is concluded that though it may be important to model hot spot formation, the proposed mechanism of compaction work has an inherent flaw, and in order to model such phenomena another model must be proposed. To model hot spots in a granular material which arise from the material compaction is difficult in the context of a two-phase mixture model. One would need to devise a way to non-uniformly distribute the energy introduced to the system by the piston (P dV work) to the particles. The non-uniform distribution would allow some particles to have higher temperatures than others, thus giving rise to local "hot spots." It is unclear how this can be achieved with a two-phase mixture model which relies on averaged properties. In fact one of the strengths of two-phase modeling is that details of microstructure do not need to be considered as these local variations are eliminated in the averaging process. For this reason, it may be impossible to attempt to describe hot spots with a two-phase mixture model.

APPENDIX D. TWO-PHASE CJ DEFLAGRATIONS

It is possible in principle to use the two-phase model to study two-phase deflagrations, reactive waves which travel much slower than detonations and which have a much lower pressure, temperature, and density rise. Because of the more moderate changes in the state of the gas, the ideal gas state equation is appropriate for use in studying two-phase deflagrations. Understanding of two-phase deflagrations can be gained by studying the complete reaction two-phase Rayleigh line and Hugoniot equations (5.21, 22) in the P_1-$1/\rho_1$ plane (see Fig. D.1).

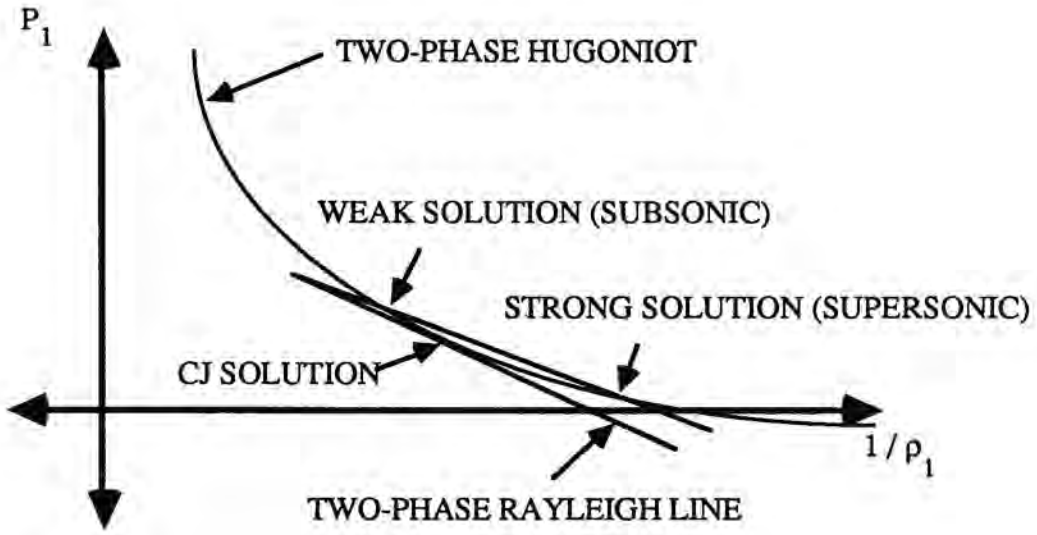

Figure D.1 Two-Phase Complete Reaction Deflagration Rayleigh Line and Hugoniot

Deflagration solutions are found at the intersection of these two curves at gas pressures lower than the initial apparent pressure P_a and gas densities lower than the initial apparent density ρ_a. It is possible to predict a maximum deflagration wave speed, called here the CJ deflagration speed. At the CJ deflagration state, the two-phase Rayleigh line is tangent to the two-phase Hugoniot. For wave speeds greater than the CJ deflagration speed, but less than the CJ detonation speed, there is no intersection of the two-phase Rayleigh line and Hugoniot and thus no solution. For wave speeds less than the CJ deflagration speed two solutions are obtained, a strong and weak deflagration solution.

For an ideal gas the complete reaction CJ wave speed is given exactly by the following equation using the nomenclature of Chapter 5.

$$D_{CJ}^2 = \frac{(2c_{v1}+R)\,Re_a - c_{v1}^2 P_a/\rho_a \pm \sqrt{(2c_{v1}+R)\left(e_a^2 R^2 (2c_{v1}+R) - (2e_a+P_a/\rho_a)c_{v1}^2 P_a R/\rho_a\right)}}{c_{v1}^2} \tag{D.1}$$

Here the plus branch of this equation corresponds to the CJ detonation state and the minus branch corresponds to the CJ deflagration state. When $P_a/(\rho_a e_a) << 1$, the CJ deflagration state simplifies considerably. In this limit, which is relevant for many physical systems including the HMX system studied in this thesis, the CJ deflagration state is approximated by the following equations.

$$D_{CJ} \cong \sqrt{\frac{\pi_7^2 e_a}{2(\pi_7^2 - 1)}\left(\frac{P_a}{\rho_a e_a}\right)} \tag{D.2}$$

$$P_{CJ} \cong \frac{1}{\pi_7 + 1} P_a \tag{D.3}$$

$$\rho_{CJ} \cong \frac{\pi_7}{2(\pi_7 - 1)}\left(\frac{P_a}{\rho_a e_a}\right)\rho_a \tag{D.4}$$

$$T_{CJ} \cong \frac{2}{\pi_7(\pi_7 + 1)}\frac{e_a}{c_{v1}} \tag{D.5}$$

$$e_{CJ} \cong \frac{2}{\pi_7(\pi_7 + 1)} e_a \tag{D.6}$$

$$v_{CJ} \cong u_{CJ} \cong -\sqrt{\frac{2(\pi_7 - 1)}{\pi_7 + 1} e_a} \tag{D.7}$$

It is important to stress that beyond describing the maximum speed two-phase deflagration wave the interpretation of Equations (D.2-5) is unclear. At this point it is not known whether a steady two-phase deflagration structure can be predicted by the model equations (5.1-15) and if such a structure could be predicted, what conditions would dictate whether a CJ, strong, or weak deflagration was obtained. A limited study was undertaken

to find steady deflagration structure with no success. This study included CJ deflagrations along with strong and weak deflagrations. Kuo and Summerfield have found steady two-phase deflagration structure using a similar model [37]. Also both the Kuo and Summerfield model and the model of this work have neglected diffusive processes such as heat conduction and viscous momentum transport which may be very important for the relatively slow deflagration waves.

APPENDIX E. DERIVATION OF UNCOUPLED EQUATIONS

This appendix will provide a detailed explanation of how the coupled set of differential-algebraic equations describing steady detonation structure (5.1-15) can be written as four differential equations in four unknowns and how in the zero heat transfer, zero compaction limits these equations can be further reduced to form the two-equation model (5.45-46). First, it will be shown how through an algebraic analysis the mixture equations (5.5-7) can be used to write gas phase quantities in terms of solid phase quantities. It is found that this process involves the solution of a cubic equation. Next the coupled differential equations (5.1-4) are uncoupled using linear algebra techniques. It is then shown how these equations reduce to the two-equation model.

The mixture equations (5.5-7), solid and gas caloric state equations (5.13, 10), and porosity definition (5.15) are rewritten here

$$\rho_1 \phi_1 v_1 + \frac{1}{\pi_5} \rho_2 \phi_2 v_2 = -\pi_{18} \tag{E.1}$$

$$\rho_1 \phi_1 v_1^2 + P_1 \phi_1 + \frac{1}{\pi_5}\left[\rho_2 \phi_2 v_2^2 + P_2 \phi_2\right] = \pi_{18} + \pi_{23} \tag{E.2}$$

$$\rho_1 \phi_1 v_1 \left[e_1 + \frac{v_1^2}{2} + \frac{P_1}{\rho_1}\right] + \frac{1}{\pi_5} \rho_2 \phi_2 v_2 \left[e_2 + \frac{v_2^2}{2} + \frac{P_2}{\rho_2}\right] = -\pi_{22} \tag{E.3}$$

$$e_2 = \frac{P_2 + \pi_{17}\pi_8}{(\pi_{17} - 1)\rho_2} + \pi_{10} \tag{E.4}$$

$$e_1 = \frac{P_1}{(\pi_7 - 1)\,\rho_1\,(1 + \pi_{13}\rho_1)} \tag{E.5}$$

$$\phi_1 + \phi_2 = 1 \tag{E.6}$$

By using Equations (E.4) and (E.5) to eliminate gas and solid energy in Equation (E.3) and Equation (E.6) to eliminate gas volume fraction in Equations (E.1-3), Equations (E.1-3) can be rewritten as follows

$$\rho_1 v_1 = A\left(\rho_2, \phi_2, v_2, P_2\right) \tag{E.7}$$

$$P_1 + \rho_1 v_1^2 = B\left(\rho_2, \phi_2, v_2, P_2\right) \tag{E.8}$$

$$\rho_1 v_1\left(\frac{P_1}{(\pi_7 - 1)\rho_1(1 + \pi_{13}\rho_1)} + \frac{v_1^2}{2} + \frac{P_1}{\rho_1}\right) = C\left(\rho_2, \phi_2, v_2, P_2\right) \tag{E.9}$$

where A, B, C, and D are functions of solid density, volume fraction, velocity, and pressure defined below

$$A\left(\rho_2, \phi_2, v_2, P_2\right) = \frac{-\pi_{18} - \frac{1}{\pi_5}\rho_2\phi_2 v_2}{1 - \phi_2} \tag{E.10}$$

$$B\left(\rho_2, \phi_2, v_2, P_2\right) = \frac{\pi_{18} + \pi_{23} - \frac{1}{\pi_5}\left(\rho_2\phi_2 v_2^2 + P_2\phi_2\right)}{1 - \phi_2} \tag{E.11}$$

$$C\left(\rho_2, \phi_2, v_2, P_2\right) = \frac{-\pi_{22} - \frac{1}{\pi_5}\rho_2\phi_2 v_2\left[\frac{P_2 + \pi_{17}\pi_8}{(\pi_{17} - 1)\rho_2} + \pi_{10} + \frac{v_2^2}{2} + \frac{P_2}{\rho_2}\right]}{1 - \phi_2} \tag{E.11}$$

Equations (E.7-9) can be combined to form a cubic equation for gas density. This is done by first using Equation (E.7) to express gas velocity as a function of gas density and solid variables. Then gas velocity may be eliminated from Equations (E.8) and (E.9). Thus modified, Equation (E.8) can be used to express gas pressure as a function of gas density and solid variables. This result is used to eliminate gas pressure from the modified energy equation (E.9). The resulting equation is a cubic equation for gas density whose coefficients are functions of the solid phase density, volume fraction, velocity, and pressure.

$$\left[-2(\pi_7 - 1)\pi_{13}C\right]\rho_1^3 + \left[2(\pi_7 - 1)(AB\pi_{13} - C)\right]\rho_1^2 + \left[2AB\pi_7 - (\pi_7 - 1)A^3\pi_{13}\right]\rho_1 - \left[(\pi_7 + 1)A^3\right] = 0 \qquad \text{(E.12)}$$

Equation (E.12) can be solved exactly for gas density in terms of solid phase variables and parameters. The solution is very lengthy and can be easily produced using the formula for solution to the general cubic equation. Three roots are found for Equation (E.12). One is associated with a shocked gas and is analogous to the strong branch of the ZND solution. Another is associated with an unshocked gas and is analogous to the weak branch of the ZND solution. The third predicts a negative density for all cases studied and is rejected as unphysical. This root is not present when non-ideal gas effects are absent. (It is seen from Equation (E.12) that for no non-ideal effects, $\pi_{13} = 0$, that the equation is quadratic, and only two roots are present.) It is possible for Equation (E.12) to predict a pair of imaginary roots under certain conditions. If such a condition was reached, the detonation structure must be rejected as unphysical. In addition to solving for the gas phase variables within the reaction zone, Equation (E.12) is used to determine the shock state of the gas.

With the gas density predicted from Equation (E.12) as a function of solid phase variables, all other gas phase variables can be expressed as functions of solid phase variables. The gas velocity is found by using Equation (E.7). The gas pressure can then be determined from Equation (E.8) and the energy from the state equation (E.5). The gas temperature and sound speed can then be found using Equations (5.9,11).

In the numerical code which predicts reaction zone structure, Equation (E.12) was solved using the IMSL subroutine ZRPOLY. Though one could use the exact cubic solution to determine the gas density, the numerical accuracy of the solution is higher when ZRPOLY is used. Given a general polynomial equation, the subroutine ZRPOLY determines all roots, real and complex.

Equations 5.1-4 can be expressed in the form

$$A_{ij}\frac{du_j}{d\xi} = B_i \qquad \text{(E.13)}$$

where $u_j = (\rho_2, \phi_2, v_2, P_2)$ and A_{ij} and B_i are functions of ρ_2, ϕ_2, v_2, and P_2. To put the equations in a form suitable for phase space analysis, explicit expressions for the

derivatives $du_j/d\xi$ must be obtained. This is done by multiplying both sides of Equation (E.13) by the inverse of A_{ij}.

$$\frac{du_i}{d\xi} = A_{ij}^{-1} B_j$$

One necessary step to express Equations (5.1-4) in this form is to use the solid caloric state equation (5.13) to determine an expression of the derivative of solid energy in terms of solid pressure and density. This derivative is given below:

$$\frac{de_2}{d\xi} = \frac{1}{(\pi_{17} - 1)\,\rho_2}\frac{dP_2}{d\xi} - \frac{P_2 + \pi_{17}\pi_8}{(\pi_{17} - 1)\,\rho_2^2}\frac{d\rho_2}{d\xi} \qquad \text{(E.14)}$$

Expanding the derivatives in Equations (5.1-4) and using Equation (E.14) allows a system in the form of Equation (E.13) to be written.

$$\begin{bmatrix} \phi_2 v_2 & \rho_2 v_2 & \rho_2 \phi_2 & 0 \\ 0 & P_2 & \rho_2 \phi_2 v_2 & \phi_2 \\ -\dfrac{P_2+\pi_{17}\pi_8}{(\pi_{17}-1)\rho_2} v_2 & 0 & P_2 & \dfrac{v_2}{(\pi_{17}-1)} \\ 0 & v_2 & 0 & 0 \end{bmatrix} \begin{bmatrix} \dfrac{d\rho_2}{d\xi} \\ \dfrac{d\phi_2}{d\xi} \\ \dfrac{dv_2}{d\xi} \\ \dfrac{dP_2}{d\xi} \end{bmatrix} = \begin{bmatrix} -\pi_1 \rho_2 \phi_2 P_1^{\pi_4}/r \\ -\pi_2 (v_2 - v_1)\phi_1 \phi_2 / r \\ -\pi_3 (\pi_6 T_2 - T_1)\phi_1 / r^{1/3} \\ \pi_9 \phi_1 \phi_2 (P_2 - \pi_5 P_1 - \pi_{15}\phi_2) - \pi_1 \phi_2 P_1^{\pi_4}/r \end{bmatrix} \qquad \text{(E.15)}$$

The left side of Equation (E.15) is expressed in terms of the fundamental variables ρ_2, ϕ_2, v_2, and P_2. The right hand side can also be expressed in terms of these variables. The method described earlier in this appendix can be used to write the gas phase variables v_1, P_1, and T_1 as functions of the fundamental variables. The number conservation equation

(5.8) and solid thermal state equation (5.12) can be used to express the radius r and solid temperature T_2 as a functions of the fundamental variables.

By multiplying both sides of Equation (E.15) by A_{ij}^{-1}, explicit expressions can be obtained for the derivatives of the fundamental variables.

$$\frac{d\rho_2}{d\xi} = \frac{D\left[\frac{\rho_2 v_2^2}{\pi_{17}-1} - P_2\right] - E\left[\frac{\rho_2 v_2}{\pi_{17}-1}\right] + F\left[\rho_2\right]}{\frac{\rho_2 v_2}{\pi_{17}-1}\left(v_2^2 - \pi_{17}\frac{P_2+\pi_8}{\rho_2}\right)} \tag{E.16}$$

$$\frac{d\phi_2}{d\xi} = \pi_9\frac{\phi_1\phi_2}{v_2}\left[P_2 - \pi_5 P_1 - \pi_{15}\phi_2\right] - \pi_1\frac{\phi_2 P_1^{\pi_4}}{v_2^r} \tag{E.17}$$

$$\frac{dv_2}{d\xi} = \frac{-D\left[\frac{P_2+\pi_{17}\pi_8}{(\pi_{17}-1)\rho_2}v_2\right] + E\left[\frac{v_2^2}{\pi_{17}-1}\right] - F\left[v_2\right]}{\frac{\rho_2 v_2}{\pi_{17}-1}\left(v_2^2 - \pi_{17}\frac{P_2+\pi_8}{\rho_2}\right)} \tag{E.18}$$

$$\frac{dP_2}{d\xi} = \frac{D\left[\frac{P_2+\pi_{17}\pi_8}{\pi_{17}-1}v_2^2\right] - E\left[P_2 v_2 + \frac{P_2+\pi_{17}\pi_8}{\pi_{17}-1}v_2\right] + F\left[\rho_2 v_2^2\right]}{\frac{\rho_2 v_2}{\pi_{17}-1}\left[v_2^2 - \pi_{17}\frac{P_2+\pi_8}{\rho_2}\right]} \tag{E.19}$$

where D, E, and F are defined as follows

$$D = \pi_9\rho_2\phi_1\left(P_2 - \pi_5 P_1 - \pi_{15}\phi_2\right) \tag{E.20}$$

$$E = -\pi_2(v_2 - v_1)\frac{\phi_1}{r} + \frac{P_2}{v_2}\left[\pi_1\frac{P_1^{\pi_4}}{r} - \pi_9\phi_1\left(P_2 - \pi_5 P_1 - \pi_{15}\phi_2\right)\right] \tag{E.21}$$

$$F = -\pi_3(\pi_6 T_2 - T_1)\frac{\phi_1}{r^{1/3}} \tag{E.22}$$

Equations (E.16, 18, 19) are singular when the following condition is met

$$v_2^2 = \pi_{17}\frac{P_2 + \pi_8}{\rho_2} \tag{E.23}$$

By using the solid thermal state equation (5.12) to eliminate solid pressure and density in favor of solid temperature and using the solid sound speed definition (5.14) it is seen that Equation (E.23) can be rewritten as

$$v_2^2 = c_2^2 \tag{E.24}$$

Thus when the velocity of the solid relative to the wave head is locally sonic, the system of equations (E.15) is singular. It is seen by examination of Equations (E.21-22) that the equations are also singular at the complete reaction state because the particle radius r appears in the denominator of the expressions for E and F.

The two-equation model can be derived form Equations (E.16-22). To derive the two-equation model, one must consider the zero-compaction, zero-heat transfer limit, corresponding to $\pi_9 \rightarrow 0$, $\pi_3 \rightarrow 0$. In this limit, Equations (E.20, 22) hold that D = F = 0. Then if Equation (E.16) is multiplied by solid velocity and added to the product of solid density and Equation (E.18), the following homogeneous equation is obtained.

$$v_2\frac{d\rho_2}{d\xi} + \rho_2\frac{dv_2}{d\xi} = 0 \tag{E.25}$$

This equation can be integrated to form the algebraic relation

$$\rho_2 v_2 = -1 \tag{E.26}$$

In applying the initial conditions when integrating this equation, it is unnecessary to specify whether the initial state is shocked or unshocked. This arises because Equation (E.26) is equivalent to the shock relation (5.29) when it is considered that porosity does not jump through the shock wave.

To determine a second algebraic relation, Equation (E.26) must first be used to eliminate solid velocity in favor of solid density in all remaining equations. Then if Equation (E.19) is multiplied by the factor

$$\frac{1}{\rho_2^{\pi_{17}}}$$

and added to the product of Equation (E.16) and the factor

$$-\pi_{17}\frac{P_2+\pi_8}{\rho_2^{\pi_{17}+1}}$$

the following homogeneous equation is obtained

$$\frac{1}{\rho_2^{\pi_{17}}}\frac{dP_2}{d\xi} - \pi_{17}\frac{P_2+\pi_8}{\rho_2^{\pi_{17}+1}}\frac{d\rho_2}{d\xi} = 0 \qquad \text{(E.27)}$$

This equation may be integrated to form an algebraic relation between solid pressure and density. The constant of integration for this expression is dependent on whether the initial state is shocked or unshocked.

$$P_2 = K\rho_2^{\pi_{17}} - \pi_8 \qquad \text{(E.28)}$$

with
$$K = \begin{cases} \dfrac{2-\pi_{14}\left(\pi_{17}-1\right)^2}{\pi_{17}+1}\left[\dfrac{(\pi_{17}-1)(1+2\pi_{14}\pi_{17})}{(\pi_{17}+1)}\right]^{\pi_{17}} & \text{shocked solid} \\ \pi_{21}+\pi_8 & \text{unshocked solid} \end{cases}$$

When Equations (E.26) and (E.28) are used to eliminate solid velocity and pressure from Equations (E.16) and (E.17), the two-equation model is found.

$$\frac{d\rho_2}{d\xi} = \frac{\pi_2(v_1-v_2)\rho_2^2\phi_1 - (K\rho_2^{\pi_{17}} - \pi_8)\pi_1\rho_2^3 P_1^{\pi_4}}{r\,(\pi_{17}K\rho_2^{\pi_{17}+1} - 1)} \tag{E.29}$$

$$\frac{d\phi_2}{d\xi} = \pi_1 \frac{\rho_2\phi_2 P_1^{\pi_4}}{r} \tag{E.30}$$

By multiplying the numerator and denominator of the right side of Equation (E.30) by the factor

$$\pi_{17}K\rho_2^{\pi_{17}+1} - 1$$

the form of Equations (5.45, 46) is found.

APPENDIX F. DERIVATION OF NUMBER CONSERVATION EQUATION

As the number conservation is not universally used in two-phase granular detonation theory, a derivation for the number conservation equation (3.7) along with Equation (3.16) is given here.

The volume fraction of particles ϕ_2 is defined as the ratio of the volume of particles to the total volume.

$$\phi_2 = \frac{\text{Volume Particles}}{\text{Total Volume}} \tag{F.1}$$

If it is assumed that the particles are spheres of radius r, then the volume of particles is equal to the product of the number of particles and the volume of a single particle. Based on this assumption Equation (F.1) is written as

$$\phi_2 = \frac{(\text{Number of Particles})\,\frac{4}{3}\pi r^3}{\text{Total Volume}} \tag{F.2}$$

If the number density n is defined as the number of particles per total volume, then Equation (F.2) can be used to determine an expression for number density as a function of particle radius and solid volume fraction.

$$n = \frac{3\phi_2}{4\pi r^3} \tag{F.3}$$

By performing a simple control volume analysis, an expression for the conservation of number density can be derived. The expression is

$$\frac{\partial n}{\partial t} + \frac{\partial}{\partial x}\left(u_2 n\right) = 0 \tag{F.4}$$

This equation could be modified to describe the agglomeration or splitting of particles by use replacing the zero on the right side of Equation (F.4) with a functional relation suitable to describe such a phenomenon.

Substituting the number density definition (F.3) into the number conservation equation (F.4), an equation identical to Equation (3.7) is derived.

$$\frac{\partial}{\partial t}\left(\phi_2 / r^3\right) + \frac{\partial}{\partial x}\left(u_2 \phi_2 / r^3\right) = 0 \qquad \text{(F.5)}$$

Using the Galilean transformation $\xi = x - Dt$, $v_2 = u_2 - D$ where D is the steady wave speed allows Equation (F.5) to be written in steady form.

$$\frac{d}{d\xi}\left(v_2 \phi_2 / r^3\right) = 0 \qquad \text{(F.6)}$$

Using the initial conditions from Chapter 3, Equation (F.6) may be integrated to provide the following algebraic expression for particle radius as a function of particle velocity and volume fraction

$$r = r_0 \sqrt[3]{\frac{- v_2 \phi_2}{D \phi_{20}}} \qquad \text{(F.7)}$$

To obtain an explicit equation for the particle radius evolution, Equation (F.5) can be expanded.

$$\frac{1}{r^3}\left[\frac{\partial \phi_2}{\partial t} + \frac{\partial}{\partial x}\left(u_2 \phi_2\right)\right] - \frac{3\phi_2}{r^4}\left[\frac{\partial r}{\partial t} + u_2 \frac{\partial r}{\partial x}\right] = 0 \qquad \text{(F.8)}$$

The solid mass equation (3.2) can be used to write an expression for the derivative of solid volume fraction.

$$\frac{\partial \phi_2}{\partial t} + \frac{\partial}{\partial x}\left(\phi_2 u_2\right) = -\frac{\phi_2}{\rho_2}\left[\frac{\partial \rho_2}{\partial t} + u_2 \frac{\partial \rho_2}{\partial x}\right] - \left(\frac{3}{r}\right)\phi_2 a P_1^m \qquad \text{(F.9)}$$

By using Equation (F.9) to eliminate the volume fraction derivative in Equation (F.8), an expression identical to Equation (3.16) for the evolution of particle radius is obtained.

$$\frac{\partial r}{\partial t} + u_2 \frac{\partial r}{\partial x} = -a P_1^m - \frac{r}{3\rho_2}\left(\frac{\partial \rho_2}{\partial t} + u_2 \frac{\partial \rho_2}{\partial x}\right) \qquad \text{(F.10)}$$

This equation states that the particle radius changes in response to combustion and compressibility effects. Equation (F.10) is inconsistent with the model equation used formerly by Krier and co-workers to determine the particle radius. As stated in Ref. 1, the particle burn law used in these works is (correcting for a sign error in the paper)

$$\frac{dr}{dt} = -a P_1^m \qquad \text{(F.11)}$$

In this equation the definition of the derivative d/dt is unclear as to whether or not convective terms are included. Regardless of this question, it is clear that Equation (F.11) does not account for compressibility effects in the particles. It must be concluded that since Equation (F.11) is inconsistent with Equation (F.10) that the model of Ref. 1 does not conserve number; thus, the physical motivation of Equation (F.11) is unclear.

VITA

Joseph Michael Powers was born on June 6, 1961, to Leo and Mary Powers. He was raised on a farm in the central Illinois town of Wapella and was educated in the local public schools. He was graduated as valedictorian from Wapella High School in 1979. In the fall of 1979 he entered the University of Illinois at Urbana-Champaign. He received his Bachelor of Science in Mechanical Engineering from the University of Illinois in May 1983 and was a recipient of the Bronze Tablet award. He began graduate studies at the University of Illinois in June 1983 and received a Master of Science in Mechanical Engineering in January 1985. While in graduate school he has been the recipient of a University Fellowship, various industrial fellowships, and a Department of Mechanical and Industrial Engineering Teaching Fellowship. He spent the summer of 1985 as a research scientist at the Naval Weapons Center in China Lake, California, and the spring of 1987 as a visiting student in the Theoretical and Applied Mechanics Department, Cornell University. Joe plans an academic career.